Investigation of the Velocity Field of Jets in Counter-Flow in the Vicinity of a Solid Wall

by

Mohammad Mahmoudi

A thesis submitted in partial fulfillment of the requirements for the degree of

Doctor of Philosophy

Department of Mechanical Engineering

University of Alberta

Abstract

This study presents experimental investigations showing the mean and fluctuating velocity field of a three dimensional round jet in counter-flow located in the vicinity of a solid wall. The jet to counter-flow velocity ratios ranged from 2.5 to 25 and the jet Reynolds numbers were from 1,000 to 10,000. The ratio of jet centerline distance from the wall over the jet diameter is changed from 0.5 to 4.3. The penetration of the flush mounted jet in counter-flow is measured and compared to the case in which there is no wall available. In addition, the penetration of the jet at various offset distances from the wall is measured and the effect of offset distance is analyzed. The results show that the flush mounted jet has the deepest penetration and as the jet offset distance increases, the penetration decreases to reach the penetration of a free jet in counter-flow. The jet offset distance creates a mechanism that controls the counter-flow entrainment into the jet.

The jet velocity decay and spreading rate are analyzed and the effect of offset ratio is discussed. It is found that as the offset ratio increases, the jet velocity decays faster and its spreading rate rises. In addition, the amplitude of random oscillations of the flow increases when the distance of the jets from the side wall increases.

The vortical structures of the flow are studied and their impact on the turbulence characteristics of the flow is explained. Two-point velocity correlation study shows that the size of turbulent structures of the flow becomes larger as the jet offset ratio increases. Also, the turbulent transport in the flow enhances dramatically as the jet gets higher distance from the side wall.

Preface

This research is an original work by Mohammad Mahmoudi. I designed and fabricated the jet system and performed the setup and calibration of the test rig. All of the experiments, data analysis, and writing of the thesis are my work. Dr Brian Fleck supervised the research. He studied the results and discussions and provided technical guidance as well as suggestions for composition of the thesis.

Chapter 2 of this thesis was presented at the 2nd International conference of Mechanical Engineering and Mechatronics, August 2013, Toronto, Canada. Later, It was selected to be published as *Mahmoudi, M., Nobes, D., and Fleck, B., "An experiment design for measuring the velocity field of a round wall jet in counter-flow." International Journal of Mechanical Engineering and Mechatronics (IJMEM), Vol. 2, (2014): 23-32.*I was responsible for designing the experimental setup, performing the experiments, data analysis and writing the paper. D. Nobes provided the PIV system and hints for running it, and B. Fleck provided supervisory guidance for the work.

Chapter 3 of this thesis is under review of the ASCE Journal of Hydraulic Engineering as: *Mahmoudi, M., and Fleck, B. "Experimental measurement of the velocity field of round wall jet in counter-flow.".* I was responsible for performing the experiments, data analysis and writing. B. Fleck was the supervisory author.

Chapter 4 of this thesis is under review of the International Journal of Heat and Fluid Flow as: *Mahmoudi, M., and Fleck, B. "Experimental study of round offset jets in counter-flow.".* I was responsible for performing the experiments, data analysis and writing. B. Fleck was the supervisory author.

This thesis is dedicated to

My Family

for their endless love and support

Acknowledgment

I would like to thank my supervisor Dr. Brian Fleck and the supervisory committee members, Dr. Morris Flynn and Dr. Sina Ghaemi for their support and productive feedbacks during my PhD study. The machine shop staff that helped me in manufacturing the test setup are also greatly appreciated. I acknowledge all my friends and colleagues who provided helps in conducting this research, in particular Miguel Balzan, Braden Rooke, Kevin Breton, Saleh Nabi, Alireza Setayeshgar, and Mathew Bussiere.

And finally, I sincerely thank my family and especially my wife, Narges, for their boundless love, support and encouragement that allowed me to follow my dreams in science and engineering.

Table of contents

List of tables

List of figures

List of symbols

D	Jet diameter
k	Constant coefficient
h, H	Slot jet height, vertical distance
m	Jet offset ratio
Lx_{uu}, Ly_{uu}	Streamwise and lateral extension of integral scales of flow
Re	Reynolds number
R_{uu}, R_{vv}	Auto correlation of velocity fluctuations
u, v	Mean velocity in x and y direction
u', v'	Velocity fluctuations in x and y direction
U_j	Jet average discharge velocity
U_{jm}	Maximum jet discharge velocity
U_m	Maximum axial velocity in local positions
U_R	Jet to counter-flow velocity ratio
U_0	Channel flow velocity
x, y	Axial and lateral coordinates
X_p, Y_p	Maximum jet penetration length in axial and lateral direction
X_r	The reattachment distance of the offset jet to the side wall
$y_{u=0}, y_{U_m}$	The height in which axial velocity is zero, and maximum
$y_{1/2}, y_{0.5}, z_{1/2}, z_{0.5}$	Jet half velocity width in lateral and spanwise direction

Greek symbols

δ Boundary layer height

Δ The discriminant of the characteristics equation of velocity gradient tensor

μ Dynamic viscosity

ν Kinematic viscosity

Abbreviations

HWA   Hot Wire Anemometry

LDA   Laser Doppler Anemometry

PIV   Particle Image Velocimetry

PLIF   Planar Laser Induced Fluorescence

TKE   Turbulent Kinetic Energy

Chapter 1: Introduction and background

1.1   Introduction

The jet in counter-flow configuration has potential applications in enhancing the mixing efficiency due to providing large recirculation regions in the flow. The jet penetrates in the counter-flow, loses its momentum gradually, and reaches to zero velocity at a stagnation area. Then, it gains negative momentum and return back with the counter-flow. Early investigators sought to apply this flow as an aerodynamic flame holder in after-burners of jet engines [1, 2]. The idea behind that was to replace the large bluff body flame holders by a series of inclined injectors on the perimeter of the afterburner and injecting the air and fuel mixture in the opposite direction of the main engine flow for increasing the thrust whenever needed. The intent was to reduce the engine losses created by permanently available solid flame holders. Using this flow configuration as a flame holder and a mixing enhancement device in laboratory scales was shown by McDannel et al. [3] in a cylindrical combustion chamber using premixed propane and air. A portion of the air and fuel mixture in their experiment was injected parallel and in the opposite direction of the main flow and provided a recirculation zone which had the functionality of a flame holder in providing sustained combustion.

Jets in counter-flow are also applied as a type of decelerator that some aircraft use during landing to reduce their speed quickly. A guide-vane is designed on the jet engine nacelle which can divert the jet flow in the same direction of aircraft velocity during the landing phase. A brief discussion on the application of jet in counter-flow for increasing the maneuverability of aircrafts is presented by Peck [4].

In another study, the capability of counter-flow jets are studied to control the flow separation and to enhance the performance of airfoils at high angle of attack. Traditionally near wall streams of high momentum air in the same direction of flow on the airfoil surface were used as a mechanism for energizing the boundary layer in order to prevent its separation [5]. However, Wake et al. [6] applied jet injection in the pressure surface and close to the leading edge of a Sikorsky SSCA09 airfoil at the opposite direction of the ambient free stream and found that the flow separation and the airfoil stall are postponed to higher angles of attack (4-5 degrees above the airfoil normal stall angle of attack). This was because the counter jet injection enhanced the near wall turbulence, transporting momentum from the high energy layers of the flow above the airfoil surface to the near wall regions in which the flow was slowing.

Volchkov et al. [7] studied the heat transfer rate from the side wall of a wind tunnel in the presence of a slot wall jet injected in the opposite direction of the wind tunnel flow of 12 m/s. The jet to counter-flow velocity ratio was varied up to $U_R=12$ in their study. The jet and counter-flow were injected at the same temperature and electrical heating elements were installed on the outer side of the wall to produce a constant heat source. The wall temperature distribution was recorded with a series of thermocouples. They found that in front of the wall jet injection port, there was a wide recirculation region, and the heat

transfer coefficient was much higher compared to the situation with no wall jet injection. Their analysis showed that with the injection of the wall jet in the opposite direction, the convective heat transfer coefficient is proportional to the jet to counter-flow velocity ratio. They concluded that counter-current wall jet injection can be used as an effective technique to control the heat transfer rate from the wall.

The other proven application of this flow is in increasing the mixing efficiency in liquid and gaseous streams by providing high turbulence and vortical structures due to the interaction of the jet and the opposed flow. This will be explained with more detail in the next chapters.

1.2   General remarks in turbulence

The research in turbulence has a history of more than a century. Yet still there is not a general solution or modelling approach available for accurate quantitative predictions of turbulent flow fields. The famous physicist Richard Feynman called turbulence as "the last great unsolved problem of classical physics".

Statistical methods of turbulence modeling like Reynolds Average Navier-Stokes (RANS) end up to a situation that the number of unknown parameters are higher than the number of equations. Therefore, ad hoc models are needed to close the system of equations and provide a solution for the flow [8].

Direct numerical simulation of turbulent flows is still restricted to very simple geometries and very low Reynolds number turbulent flows. The length and time scales of the smallest eddies (Kolmogrov micro scales) in a turbulent flow are proportional to $Re^{-3/4}$ and $Re^{-1/2}$, respectively. Consequently, as the Reynolds number increases, the length and time scale of the turbulent structures decreases sharply. Thus, very fine computational grid is needed to resolve the characteristics of these structures. This dramatically increases the required computational power for conducting the numerical simulation. Consequently, empirical data and experimental measurements of turbulent flows play the major role in studying and analyzing the flow field. Experimental data can also be used for tuning of the numerical models for better prediction of the turbulent flow fields. The next section presents a general overview of the effects of turbulence on the flow field.

1.2.1   Turbulent transport of momentum

The flow motion in every realization of the incompressible turbulent flow field obeys the

Navier-Stokes equation in the form of:

$$\frac{\partial U_i}{\partial t} + U_j \frac{\partial U_i}{\partial x_j} = -\frac{1}{\rho} \frac{\partial P}{\partial x_i} + \nu \frac{\partial^2 U_i}{\partial x_j \partial x_j} \qquad (1)$$

The continuity equation with the imposed incompressibility condition is:

$$\frac{\partial U_i}{\partial x_i} = 0 \qquad (2)$$

The turbulent flow can be considered as the ensemble of various solutions of the above

equation. By assuming that each flow realization is comprised of the mean plus the

fluctuation portion, one can write the velocity and pressure as:

$$U_i = \bar{U}_\iota + u_i \qquad (3)$$

$$P = \bar{P} + p \qquad (4)$$

Substituting the decomposed velocity and pressure into the Navier-Stokes equation,

assuming that the average product of a fluctuating parameter and an averaged quantity is

zero, and applying the continuity equation yields:

$$\frac{\partial \bar{U}_\iota}{\partial t} + \bar{U}_J \frac{\partial \bar{U}_\iota}{\partial x_j} + \overline{u_j \frac{\partial u_\iota}{\partial x_j}} = -\frac{1}{\rho} \frac{\partial \bar{P}}{\partial x_i} + \nu \frac{\partial^2 \bar{U}_\iota}{\partial x_j \partial x_j} \qquad (5)$$

Using continuity equation, the third term in the right hand side can be written as

$$u_j \frac{\partial u_i}{\partial x_j} = \frac{\partial}{\partial x_j}(\overline{u_\iota u_J}) \qquad (6)$$

The final form of the mean flow equation can be written as:

$$\frac{\partial \overline{U_\iota}}{\partial t} + \overline{U}_J \frac{\partial \overline{U_\iota}}{\partial x_j} = \frac{1}{\rho} \frac{\partial}{\partial x_j} \left\{ -\overline{P}\delta_{ij} + \mu \left(\frac{\partial \overline{U_\iota}}{\partial x_j} + \frac{\partial U_j}{\partial x_i} \right) - \rho \overline{u_\iota u_j} \right\} \qquad (7)$$

It can be seen from equation (7) that the average velocity fluctuation products appear as an additional stress tensor in the momentum transport equation. The term $-\rho \overline{u_\iota u_j}$ is called the Reynolds stress tensor and represents the average momentum flux into the flow field due to turbulent velocity fluctuations. The Reynolds stress tensor is one of the basic elements in the theory of turbulence and its divergence acts like a forcing function in the mean flow field. In fully developed turbulent flows, the Reynolds stress tensor can be as much as 500 times more than the viscous stress tensor [9].

$$\rho \left| u_i u_j \right| \gg \mu \left| \frac{\partial \overline{U_\iota}}{\partial x_j} + \frac{\partial \overline{U}_J}{\partial x_i} \right| \qquad (8)$$

Therefore, accurate prediction of the Reynolds stress tensor is a critical aspect in turbulent flow simulation and experimental data can be used as a validation tool for tuning of the turbulence models.

1.2   Thesis objectives

The main objective of this study is to contribute to the overall understanding of jets in counter-flow in the close proximity of solid walls. It should be emphasized that although the jets in counter-flow have interesting applications in engineering designs, they were not widely studied like other jet flow configurations. The current study is performed to understand the fundamental physics and the behavior of jets in counter-flow when they are located beside a wall. The quantitative measurements of the velocity field for this complex flow are presented and discussed for the first time.

In this thesis, chapter 2 provides a detailed review of the literatures related to jets in counter flow, wall jets, and offset jets. The purpose of this chapter is providing the necessary background for the study of jets in counter-flow near solid walls. Then, detailed aspects of the experimental setups, the measurement technique, the parameters that are studied and some preliminary results that gives a basic understanding of this flow are presented in chapter 3. In addition, chapter 3 includes the measurement of the velocity and major length scales of three dimensional wall jets in quiescent ambient flow and comparison of the results with available data in the literature. The aim of doing this was to provide a solid proof of the accuracy of the designed test setup and estimating the amount of bias error of the measurement system and the experimental setup.
Chapters 4 and 5 present the mean flow characteristics, the important velocity and length scales of the flow such as the decay rate, spreading rate, and the jet penetration length in the counter-flow. The parameters that have changed are the jet to counter-flow velocity ratio and the jet offset distance from the adjacent wall. In addition, critical point analysis of the velocity field, and two-point velocity correlation functions are used to investigate

the evolution and the behavior of vortical structures in the flow. Vortices have tremendous effects in flow fields and can dramatically change the momentum, mass, and heat transfer in the flow. In this study, the origin of the formation of vortical structures and their interaction with each other are discussed. Moreover, the impact of these vortices on enhancing the turbulence intensity of the flow in the stagnation region is explained. This information can provide important inputs into the design of flow control systems for the purpose of optimization in aerodynamics or mixing and heat transfer enhancement in process equipment. Finally, the profiles of Reynolds stresses and triple velocity fluctuation products are presented. These parameters represent the turbulent transport in the flow and are significantly important for efficient design of engineering systems that are using this flow configuration.

Chapter 6 provides a summary of findings of this study and introduces new research areas that can lead to better understanding of jets in counter-flow close to solid walls.

At the end, it must be noted again that the findings of this study can provide a solid basis for understanding the momentum transfer between the jets and the opposite flow. Although the laboratory scale experiments have lower operating Reynolds number compared to real world applications, they have a fundamental role in advancing the science of fluid dynamics and understanding the basic physics of the flow fields. Also, the results of these experiments can be used for the validation of numerical simulations that are essential tools in the design and optimization of industrial products in today's engineering world.

1.3 Thesis layout

The thesis is written in paper-based format and chapters 3, 4, and 5 are independent articles with all the required sections. Each article in the thesis has a brief literature review. However, to provide a more complete study of the available information about the jets in counter-flow, wall jets and offset jets, a comprehensive review on the previous related research is provided in chapter 2. Chapter 6 provides a summary of the major findings of the research and presents recommendations for future works. The outline of the thesis is described as the following sections.

Chapter 2: Literature review

This section of the thesis provides the required background and the available research results about free jets in counter-flow, wall jets in counter-flow, generic wall jets in quiescent flow, and offset jets.

Chapter 3: Experiment design for measuring the velocity field of wall jets in counter-flow

Chapter 3 is an article describes the experimental setup and preliminary tests for proving its capability to measure the velocity field of the jets in counter-flow. The test setup components and the PIV hardware are described in detail. The process of data acquisition, filtering, and data reduction are explained. In addition, the details of the calibration process and the estimation of errors and uncertainties are included. For the case in which the jet nozzle is flush mounted to the side wall, the jet discharge at various flow rates are analyzed in the absence of counter-flow. The velocity decay and the jet half-width slope are extracted. Then, the results are compared with other available data in the literatures for 3D round wall jets in quiescent ambient flow and compliance was

observed. This is considered as the proof for the validation of the test setup and the accuracy of the results.

Chapter 4: Experimental analysis of the velocity field of a round wall jet in counter-flow

The fourth chapter describes the velocity field of the flush mounted jet in counter-flow. The jet to counter-flow velocity ratio is varried in the range of $2.5 < U_R < 25$ and the jet Reynolds number is $1,000 < Re < 10,000$. The mean flow velocity contours and streamlines are extracted and discussed. The jet penetration distance versus jet to counter-flow velocity ratio is measured and compared with the case of free jet in counter-flow. In addition, the velocity decay and the spreading rate of the wall jet in counter-flow are calculated and the results were compared with the wall jets in quiescent ambient flow. The turbulent structures in the flow are analyzed and their interaction is discussed. Finally, the turbulence field of the flow including the second order and third order moments of the velocity fluctuations are described.

Chapter 5: Experimental study of the velocity field of round offset jets in counter-flow

In this chapter, the effect of jet distance from the side wall is discussed. The jet centerline distances from the wall are changed to four values of $1.5D$, $2.5D$, $3.3D$, and $4.3D$. The effects of offset ratio on the mean flow fields of the jets in counter-flow are explained. The jet penetration into the counter-flow at each offset ratio is extracted and compared with that of the free jets and wall jets in counter-flow. In addition, the velocity decay and half velocity width of the jets at each offset ratio are studied and the role of offset ratio is described. Turbulent structures of the flow at each offset ratio are studied and compared.

The turbulence statistics of the offset jets in counter-flow are analyzed and the effects of jet distance from the side wall are investigated.

Chapter 6: Conclusion and recommendations

In the last chapter, a summary of the results and recommendations for future works are presented.

References

[1] E. Filippi."La stabilizzazione della fiamma degliesorettori," L'aerotecnica, No. 1, (1958).

[2] Sekundov, A. N. "The propagation of a turbulent jet in an opposing stream." Turbulent jets of air, plasma and real gas (1969): 99-109.

[3] McDannel, M. D., P. R. Peterson, and G. S. Samuelsen. "Species concentration and temperature measurements in a lean, premixed flow stabilized by a reverse jet." Combustion Science and Technology 28, no. 5-6 (1982): 211-224.

[4] Peck, R.E. "Aerodynamics of a round jet in a counter-flowing wind," *Journal of Aircraft* 18, (1981): 61-62.

[5] Gad-el-Hak, M. "Flow Control: Passive, active and reactive flow management, 2000."

[6] Wake, Brian E., Gregory Tillman, Stuart S. Ochs, and J. Scott Kearney. "Control of high-reynolds-number turbulent boundary layer separation using counter-flow fluid injection." 3rd International AIAA Flow Control Conference. 2006.

[7] Volchkov, E. P., V. P. Lebedev, M. I. Nizovtsev, and V. I. Terekhov. "Heat transfer in a channel with a counter-current wall jet injection." International journal of heat and mass transfer 38, no. 14 (1995): 2677-2687.

[8] Tennekes, Hendrik, and John Leask Lumley. A first course in turbulence. MIT press, 1972.

[9] Mathieu, Jean, and Julian Scott. An introduction to turbulent flow. Cambridge

University Press, 2000.

Chapter 2: Literature review

2.1   Jet in counter-flow

The discharge of a jet flow in the opposite direction of the ambient flow is called jet in counter-flow. This flow configuration has many applications in enhancing the mixing efficiency of the fluids by providing large recirculation regions in the flow. The schematic of this flow is shown in Figure 2-1. The jet penetrates in the counter-flow and loses its momentum and finally reaches zero velocity at a stagnation point. It then gains negative momentum and return back with the counter-flow. The penetration of the jet in both the axial and the lateral directions (X_p and Y_p) was the subject of several studies. Beltaos and Rajaratnam [1] did a review of previous studies and used a systematic approach to analyze the velocity profiles of a round jet in a counter-flow. They conducted wind tunnel tests and found the mean velocity field by means of a Pitot-tube and used non-dimensional groups of variables to predict the penetration length of the jet in opposed flow. They found that the normalized axial penetration length of the jet has a linear relation with jet to counter-flow velocity ratio as:

$$X_p/D = k\, U_j/U_0 \qquad\qquad\qquad (1)$$

where k is a constant coefficient equal to 2.6 based on their experiments.
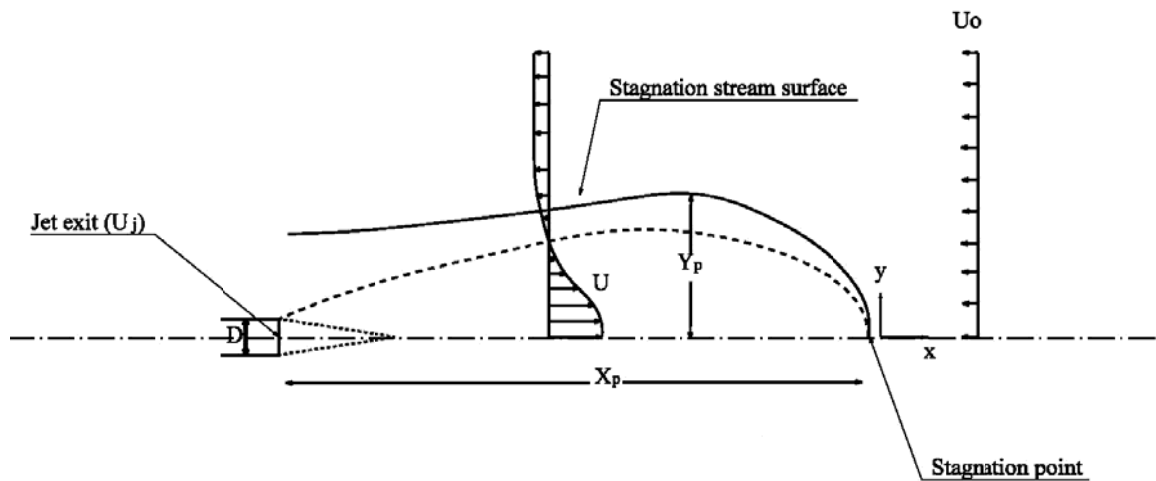
Figure 2-1: The schematic of the jet in counter-flow velocity profiles and major length scales.

The penetration of the jet in lateral direction did not show any clear relationship with the velocity ratio or the axial penetration length. They also combined the potential flow theory with their findings in an attempt to predict the shape of the stagnation stream surface though this was not successful.

Morgan and Brinkworth [2] showed that the penetration length of a jet in a confined region where the jet to counter-flow momentum ratio was relatively high was not linear. They used flow visualization for a jet in opposed flow in a pipe. The pipe diameter in their experiments was varied between 32 mm to 152 mm and the jet diameter was changed between 0.4 mm to 7 mm. They found the normalized penetration distance versus the momentum ratio of the jet to the counter-flow. They observed that the linear relation between the penetrating distance and the jet to counter-flow velocity ratio is valid when the momentum ratio of the jet and counter-flow was less than 0.25. In this situation they found the linear proportionality coefficient of $k = 2.5$. They also showed that there is

no significant change in the jet penetration length as long as the jet and counter-flow

Reynolds numbers were above 3×10^3 and 10^4, respectively.

Saghravani and Ramamurthy [3] studied the effect of confinement on the penetration

length as well. They analyzed the past research in this field and also conducted

experiments in a conduit for a round jet in uniform counter-flow up to velocity ratios of

70 using LDA. Their results showed that there is a critical value for the jet to counter-

flow velocity ratio as a function of the jet diameter and the conduit size which above that

the penetration length has a linear growth rate with velocity ratio.

Other researchers proposed linear penetration for the jet in counter-flow at low

momentum ratios. A survey of reported values for k from different research is shown in

Table 2-1. The values for k ranges between 2.4 to 2.8. This can be related to the

difference in jet exit momentum and the shape of velocity profile in each experiment as

well as uncertainty in the measurements.

Table 2-1: Summary of reported values for k from Equation 1.

Researcher	Jet exit geometry	Measurement method	k
Beltaos and Rajaratnam [1]	Contoured nozzle	Pitot tube	2.6
Morgan et al. [2]	Circular Pipe	Dye visualization	2.5
Koing and Fiedler [4]	Contoured nozzle	Smoke visualization	2.7
Lam and Chan (1995) [5]	Contoured nozzle	LIF visualization	2.4
Yoda and Fiedler [6]	Contoured nozzle	LIF visualization	2.8
Lam and Chan (1997) [7]	Contoured nozzle	LIF visualization	2.4
Lam and Chan (2002) [8]	Contoured nozzle	LDA	2.7
Tsudana and Saruta [9]	Contoured nozzle	PIV and PLIF	2.8

The whole velocity and scalar concentration field of the jet in counter-flow were also reported by some researchers [6-13]. They tried to find the extent of self-similarity of velocity and concentration profiles. Their analyses showed that up to 70% of the penetration length and in a limited radial distance from the centerline, the jet shows self-similar behavior.

Yoda and Fiedler [6] used PLIF in a water tunnel loop to investigate the scalar concentration field of a jet in counter-flow at velocity ratios of $1 < U_R < 10$. They found that up to 70% of the penetration length, the centerline concentration decay of the jet is inversely proportional to the axial distance and shows self-similar behavior for different values of velocity ratio. In addition, they found that using a scalar concentration of 40% of the jet inlet as the jet boundary, the radial profiles of concentration show self-similar behavior, too.

Bernero and Fiedler [10] employed PIV, PLIF, and LDA for a round jet with diameters between 2 to 10 mm in uniform counter- flow with velocity equal to $U_0 = 13$ cm/s. The velocity ratio in this research was up to $U_R = 50$. They reported that the decay of velocity and concentration in the jet centerline was 25% higher in comparison with a jet into quiescent ambient surroundings. In another study, Bernero and Fiedler [11] used PIV and PLIF simultaneously to study the flow of a round jet in counter-flow for velocity ratios up to $U_R = 20$. They found that the slope of the half-width lines for the jet velocity and concentration are more than that of the regular jets and self-similarity exists only in a limited zone in the central part of the jet.

Lam and Chan [8] performed an experimental analysis using LDA and PLIF to investigate the velocity and concentration field of a 10 mm diameter jet in counter-flow with 10 cm/s velocity. Their results showed higher decay of the velocity and concentration in the jet centre line. In addition, they observed self-similarity of excess velocity and concentration profiles in a limited core region of the flow up to 70% of the penetration distance.

Tsudana and Saruta [9] used PIV and PLIF in separate experiments and found the velocity and concentration field of a jet in counter-flow at the streamwise symmetry plane. The opposed flow velocity in their water channel was 0.21 m/s and they examined three velocity ratios of 2.9, 4, and 5.1. They reported the mean and fluctuating velocity and concentration field. In another experiment, Tsudana and Takei [12] investigated the concentration field in the lateral plane of a round jet in counter-flow at the same velocity ratios. They observed slightly higher scalar field dispersion compare to a jet in stagnant environment which was caused by higher radial fluctuations of the jet in counter-flow.

Torres et al. [13] used PLIF to investigate the scalar concentration field of a round jet in counter-flow at velocity ratios of $4 < U_R < 19$, which corresponded to the jet Reynolds numbers in the range of $1600 < Re < 5300$. They used fluorescein sodium salt as the tracer dye and employed a 2.1W argon ion laser to illuminate the flow. They used 5% concentration level as the boundary of the jet stagnation stream surface and employed different sets of length scales based on the geometrical parameters of the mean flow field to find self-similar profiles for the centerline and radial decay of the jet. In addition, they extracted empirical relations to predict the concentration decay in the jet centerline up to 70% of the penetration length.

The higher mixing efficiency of the jet in counter-flow which shows itself by a higher slope of half width concentration and velocity is a result of generation of high turbulence and large vortical structures in the flow. Koing and Fiedler [4] conducted wind tunnel tests for flow visualization of a 25 mm round jet in counter-flow at jet Reynolds number between 5,000 and 20,000. They found that for very low velocity ratios (U_R<1.4) the jet showed regular vortex shedding and stable behavior while for higher velocity ratios the jet had random fluctuations. They also employed a loud speaker in the jet discharge to provide axial and orbital excitation of the jet. The results showed that for the stable case these excitations have clear effects on the jet shape. However, in the unstable regime (U_R>1.4) no changes were observed in the penetration distance of the jet.

In another study Bernero and Fiedler [14] analyzed the main patterns in the flow of a round jet in a uniform counter-flow at two velocity ratios equal to U_R = 1.3 and U_R = 3.4. They found that for U_R = 3.4, the first mode of velocity vectors with the highest kinetic energy had a low frequency radial flapping while the second mode showed oscillation in the axial direction. For the case of U_R = 1.3, the first mode was oscillation in the axial direction and the second mode was radial flapping. In addition they found that the superposition of the first 20 modes reconstructs 70% of the energy of the flow. For a typical jet flow in quiescent ambient, usually the first 20 modes accounts for close to 95% of the energy of the flow. They concluded that the jet in counter-flow unlike other shear flows cannot be adequately described using a short collection of coherent structures due to its complex behavior.

2.2   Wall jet in counter-flow

The problem of a wall jet in counter-flow has been studied less than a free jet in counter-flow. Balachandar et al. [15] reported a qualitative investigation of the flow of a 2D slot wall jet in counter-flow at velocity ratios up to $U_R = 8$ using dye visualization in a water channel. They also recorded the wall pressure using an array of pressure transducers to find the flow behavior near the wall. Their results showed that for $U_R^2 > 10$ the radial and axial penetrations are of the same order.

Tanaka et al. [16] studied the velocity field of a slot wall jet in the opposed boundary layer of a flat plate. The wind tunnel which they used to carry their experiments had a cross section are of 450×270 mm^2 and the height of the slotted jet was $h = 5$mm. The jet was installed in the side wall of the wind tunnel. The velocity of the opposed flow in their experiment was set to be $U_0 = 20$ m/s and the jet to counter-flow velocity ratio was up to $U_R = 3$. A one dimensional tandem hot wire probe was used to find the mean and fluctuating velocity field. They found that for values of $U_R < 1.6$ the jet separates from the initial regions of the discharge point and it does not penetrate in the opposed stream. For $U_R > 2$ the jet at first penetrates and then separates from the wall. They provided a pattern of the stream functions and mean and fluctuation axial velocity. Also, for $U_R > 2$ they found an empirical relation that predicts the penetration length:

$$X_p/h = \ 9.5 U_R^{1.8} \tag{2}$$

To understand the physics of the wall jet and offset jet in counter-flow, it is required to know the behavior of a regular wall jet and offset jet in quiescent ambient. Therefore, the next section in this chapter is devoted to study the available information for the wall jet and offset jets in quiescent flow.

2.3   Wall jets

As described by Launder and Rodi [17] "the wall jet is a type of shear layer flow along a wall that due to its initial momentum, at any station, its streamwise velocity in some point is higher than the velocity of the external flow". Wall jets have numerous industrial applications such as boundary layer separation control in advanced aircrafts, film cooling of gas turbine combustion chambers and turbine blades, and air conditioning systems. A schematic of a three-dimensional wall jet velocity distribution is shown in Figure 2-2.
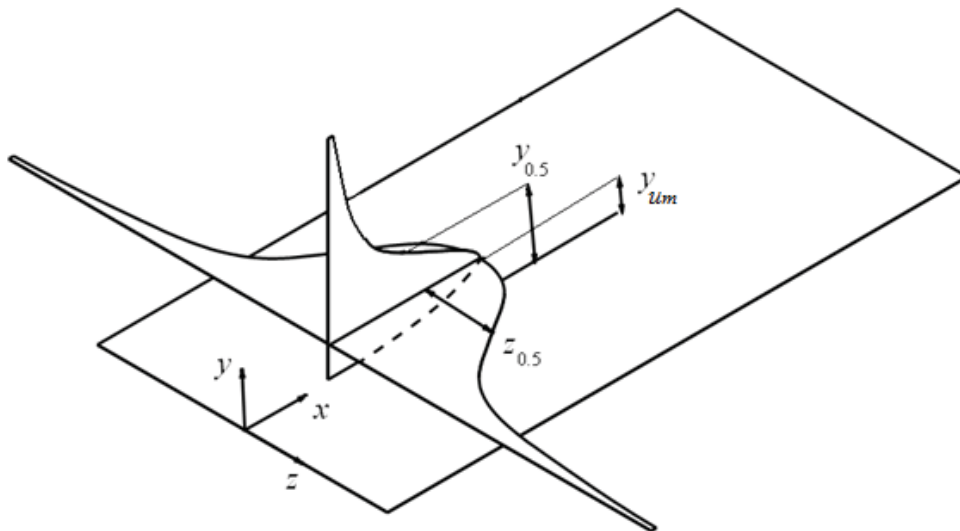
Figure 2-2: The velocity profiles in a three-dimensional wall jet.

The velocity profile shows a maximum axial velocity, U_m, which occurs at height of y_{u_m}. There are two different shear flows in the wall jet. The first one which starts from the wall and extends to the point of maximum velocity has typical characteristics of a boundary layer and traditionally is called the inner region. The second shear flow starts from the point of maximum velocity and extends to the other edge of the flow. It is called the outer region and has the characteristics of a free shear layer. The wall jets have been

studied extensively in the past decades. Launder and Rodi [17, 18] provided two comprehensive review papers and described the experimental studies and physical discussions that were available to date in this subject. The velocity decay rate and the slope of half velocity width (also called spreading rate) in streamwise ($dy_{0.5}/dx$) and lateral directions ($dz_{0.5}/dx$) were the major parameters that were investigated widely for various wall jet geometries and initial conditions. Launder and Rodi [17] proposed $dy_{0.5}/dx = 0.048$ and $dz_{0.5}/dx = 0.26$ for a three-dimensional wall jet. The most interesting feature of 3D wall jets is its higher spreading rate in lateral direction. As it is seen from the above values, the lateral spreading rate is almost 5.5 times larger than the streamwise rate of spreading. Table 2-2 shows a summary of the most recent investigations for three-dimensional wall jets that have been published after the review papers of Launder and Rodi [17, 18]. From Table 2-2, it can be seen that the velocity decay rate changes from -1.07 to -1.29, and the spreading rate in both streamwise and lateral directions varies in the range of 0.037 to 0.065 and 0.21 to 0.32, respectively.

The aforementioned data are for a wide range of jet Reynolds numbers and various types of exit geometries that change the initial momentum of the jet. This could be a major reason for the scattering of reported velocity decay and spreading rates in those studies. Another reason could be the uncertainty and errors and limitations in conducting the experiments that did not allow the wall jet to reach to fully developed state. In fact, a numerical investigation by Craft and Launder [19] revealed that 3D wall jets reach a fully developed state after long distances as high as $x > 400D$ from the discharge plane.

Table 2-2: Summary of research results for velocity field of 3D wall jets.

Researcher	Jet exit	Re ($\times 10^3$)	Zone of coverage	Decay rate	$dy_{0.5}/dx$	$dz_{0.5}/dx$
Davis and Winarto [20]	Nozzle	170	$0 < x/D < 65$	-1.15	0.037	0.32
Fujisawa and Shirai [21]	Square pipe	60	$50 < x/D < 150$	-1.2	0.052	0.25
Padmanabham and Gowda [22]	Orifice Segments	95	$0 < x/D < 100$	~ -1.15	~ 0.042	~ 0.23
Abrahamson et al. [23]	Nozzle	50 - 105	$50 < x/D < 90$	-1.29	0.065	0.32
Sun [24]	Pipe and nozzle	65 - 108	$0 < x/D < 90$	-1.14 -1.19	0.053 0.060	0.27 0.28
Law and Herlina [25]	Orifice	5.5 - 13.7	$0 < x/D < 50$	-1.07	0.042	0.21
Agelin-Chaab and Tachie [26]	pipe	5 - 20	$0 < x/D < 120$	-1.15	0.054	0.255

Different researchers have tried to find universal relations for the velocity and scalar concentration distribution in a wall jet. To this end, flow parameters from the outer region and/or inner region have been used to normalize the velocity and concentration of the wall jet to examine the self-similarity of the flow. In the inner region the wall jet is similar to a turbulent boundary layer. Thus, the friction velocity and wall units have been used for the scaling of the velocity profiles (e.g. Eriksson et al. [27], George et al. [28], and Tachie et al. [29]). In the outer region, the parameters which were traditionally used to find dimensionless scales for the velocity field are the maximum local velocity (U_m), and the height or width where the velocity becomes half of the maximum velocity (e.g. Law and Herlina [25], Agelin-Chaab and Tachie [26], and Verhoff [30]).

2.4.1 Turbulent characteristics of wall jets

Wall jets are complex since the turbulent structures in the flow are associated with two major instabilities. One is inflectional instability in the outer layer and the other is a viscous instability near the wall as mentioned by Han et al. [31]. The major effect of the outer layer on the inner layer is the shifting of zero point of Reynolds shear stress ($u'v'$) from the position of maximum velocity to a lower position near the wall (Launder and Rodi [17]). The turbulence intensity and Reynolds stresses of wall jets were the subject of several experimental investigations. The literature survey shows that for two-dimensional wall jets there are more data and with better spatial resolution available compared to three-dimensional ones. The turbulence stresses for 3D wall jets have higher values than those of the 2D wall jets. However, their general behavior is similar (Agelin-Chaab [32]). For two-dimensional wall jets, the axial component of the Reynolds stress ($\overline{u'^2}$) has two peaks. One peak happens in the near wall region due to the generation of turbulent eddies in the buffer layer. The second peak which has a higher magnitude than the first one occurs at the outer layer close to the inflection point of the velocity profile. The wall normal Reynolds stress component ($\overline{v'^2}$) shows a monotonic rise from zero at $y = 0$ and reaches to its maximum value around the peak location of $\overline{u'^2}$. The Reynolds shear stress ($\overline{u'v'}$) is negative in the close vicinity of the wall and grows steadily toward positive values to reach a maxima at almost the same height as $\overline{u'^2}$ and $\overline{v'^2}$ extrema. In order to know the quantitative values of the Reynolds stresses in two- and three-dimensional turbulent wall jets, some examples of available results are explained with more detail below.

Eriksson et al. [27] conducted a high resolution LDV test on a 2D slot wall jet with height of h=9.6 mm and Re_j= 9.6×10^3 (based on jet exit) in a water flume. In the range of 40 <x/h< 150 the normalized turbulence intensity with outer layer scaling parameters showed that $\overline{u'^2}/U_m^2$ had a small peak of 0.02 near the wall at $y/y_{0.5}$= 0.1. The second peak equal to 0.045 happened at $y/y_{0.5}$= 0.7. Also, $\overline{v'^2}/U_m^2$ increased monotonically to the maximum value of 0.025 at $y/y_{0.5}$ = 0.7 similar to the second peak of $\overline{u'^2}$. Frthermore, $\overline{u'v'}/U_m^2$ started from -0.005 close to the wall and reached to zero at $y/y_{0.5}$= 0.1; it then increased to a maximum value equal to 0.015 at $y/y_{0.5}$ = 0.8.

Abrahamsson et al. [23] performed hot-wire anemometry measurements to find the velocity field of a 3D round wall jet with diameter of D = 20 mm at jet Reynolds number equal to 53×10^3. Their results could not discern the first peak of streamwise turbulence intensity ($\overline{u'^2}/U_m^2$) due to poor spatial resolution, however, the second peak was equal to 0.07 and located at $y/y_{0.5}$= 0.5. The profiles of $\overline{v'^2}/U_m^2$ had a maximum value of 0.032 at $y/y_{0.5}$ = 0.4 and the exterma of $\overline{u'v'}/U_m^2$ happened at $y/y_{0.5}$ = 0.7 and its value was 0.019.

In another study, Agelin-Chaab and Tachie [26] conducted PIV experiments to investigate the turbulent characteristics of a round wall jet exiting from a long pipe with diameter of D =7 mm in a water tank. The jet Reynolds number was changed to three different values of 5×10^3, 10×10^3, and 20×10^3. The spatial resolution in this research was not good enough to realize the first peak in $\overline{u'^2}$ profiles. For the highest Reynolds number and at distance of x/D = 65, the peak values of $\overline{u'^2}/U_m^2$, $\overline{v'^2}/U_m^2$, and $\overline{u'v'}/U_m^2$ were 0.13, 0.063, and 0.027 and located at $y/y_{0.5}$= 0.5, 0.6, and 0.7, respectively.

2.4   Turbulent offset jets

The flow of a jet with some distance from an adjacent wall is called an "Offset Jet". The schematic of a 2D slot offset jet in streamwise plane is shown in Figure 2-3. It is seen that the jet flow bends toward the wall and attaches to it at the so called "reattachment point" (X_r). This phenomenon is called the "Coanda Effect" and happens due to the entrainment of the fluid elements between the wall and the jet wall-side boundary which reduces the pressure at this area and forces the jet to deflect toward the wall and attaches to it [33]. The flow field of a 2D offset jet can be divided into three zones as seen in Figure 2-3. The first zone is called the reverse flow region in which the near wall fluid elements undergo a spiral move due to shear forces of the lower boundary of the jet. The attachment area (zone II) is a transition region from the point of reattachment to the beginning of the wall jet zone (zone III). In the third zone, the flow has the behavior of a typical fully developed wall jet. The offset ratio (m) is defined as H/h in which H is the distance of the jet centerline from the bottom plate and h is the slot height. It is an important parameter for analyzing this type of jet flow.
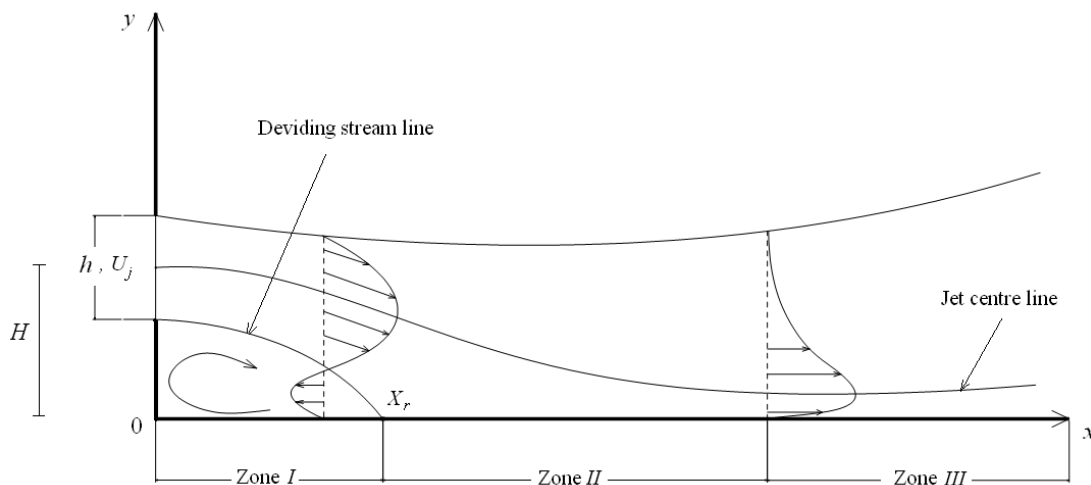
Figure 2-3: Schematic of 2D offset jet in streamwise plane.

Offset jets have been studied by fewer researchers compared to generic wall jets and the available data are mostly for two-dimensional slot jets. Nozaki et al. [34] investigated the flow field of a slot jet located close to a flat plate at offset ratios from 2 to 20 using hot-wire probes and pressure sensors mounted on the flat plate. They reported some data about the reattachment distance and also tried to modify the analytical solution of free slot jets for use in prediction of the reattachment length in offset jets. Their results show that this method is not successful for low offset ratios and with increasing the offset ratio its accuracy increases. For instance, at offset ratios of 4 and 10 their model over-predicted the reattachment length by 100% and 20%, respectively. They also changed the aspect ratio of the jet exit plane and found that the behavior of the offset jet in the symmetry plane changed considerably with the aspect ratio especially when it was lower than 3. They also discussed the effect of Reynolds number and found that for a 2D slot jet it has no effect while for 3D offset jets with aspect ratios lower than 8, the Reynolds number effects were quite visible.

In a similar experiment, Nozaki and Hatta [35] investigated the effects of the initial jet turbulence intensity on the offset jet flow field. They found that lowering the turbulence intensity increases the reattachment and development length of the flow.

Pelfrey and Liburdy [36, 37] studied the mean flow and turbulence characteristics of a two-dimensional slot offset jet in a wind tunnel by using wall mounted pressure taps and LDA. The offset ratio in their experiment was set to 7 and the jet Reynolds number was 15×10^3. The mean flow analysis in their experiments revealed that the reattachment point was located at x/h=13 and there was a recirculation region before the reattachment point. The centre of the swirling flow was consistent with the axial location of minimum wall

pressure. They analyzed the velocity fluctuations in the near field region of the offset jet and reported the velocity fluctuations. They observed that the upper jet boundary was more unstable and had higher turbulence intensity compared to the lower jet boundary.

Yoon et al. [38] performed extensive experiments and found the mean and fluctuating velocity field of a 2D offset jet using hot-wire anemometry and recording the wall pressure. The jet Reynolds number was 39×10^3 and the offset ratios were changed from 1 to 30 in their experiments. They reported the suction in the swirling flow region provided by the jet entrainment in the form of negative wall pressure coefficient. Also, they found that the wall minimum pressure coefficient is located in the centre of the recirculation zone and it jumps to its maxima at the reattachment point. The comparison of normalized Reynolds stresses in their research showed that the self-similarity for the offset jet profiles happened at farther distances from the jet exit compare to the regular wall jet case. In another investigation, Yoon et al. [39] studied the effect of surface roughness on the reattachment of the 2D offset jet in the same flow condition as described above. They found that roughness on the wall surface increased the reattachment length and the points of maximum velocity were located at higher elevation from the wall compared to the smooth wall situation. It also caused the mean and fluctuating velocity profiles self-similarity in a shorter distance compared to the smooth wall case.

Nasr and Lai [40, 41] analyzed the mean and fluctuating flow field of a 2D offset jet using LDA and measuring the wall pressure. The offset ratio and the jet Reynolds number were 2.1 and 11×10^3, respectively. They found that when the slot jet is bounded by side plates, the pressure is lower in the swirling region and the jet attaches to the wall at shorter distances from the exit plane. They also analyzed the previous available data

for the two dimensional offset jets and proposed an empirical relation for the reattachment length versus offset ratio in the form of:

$$X_r/h = 2.63(H/h)^{0.855} \qquad\qquad (3)$$

Agelin-Chaab and Tachie [42] reported the mean and fluctuating velocity fields of a 3D round offset jet at offset ratios of 1, 2, and 4. They employed PIV technique in a water tank and used a pipe with diameter of 7 mm to provide the jet flow at Reynolds numbers of 5×10^3, 10×10^3, and 20×10^3. They observed that there is no sustained recirculation area in the near wall region but a flow reversal exists due to the jet entrainment. However, this flow reversal was almost negligible compared to that of 2D offset jets. They found that the reattachment length is independent of Reynolds number and varied linearly with offset ratio. In addition, the reattachment length in their research was much shorter than previously reported 2D and rectangular nozzles offset jets. They attributed this observation to the differences between the jet profiles in the initial region which is caused by the nozzle geometry. The decay rate of the jet maximum velocity was in -1.17 based on their experiments which were very close to the decay rate of flush mounted jet in their research. In addition, far enough from the jet exit plane when the offset jet converted to a fully developed wall jet they reported the spreading rate of 0.055 and 0.25 in normal and lateral direction. Moreover, their results showed that the values of Reynolds stresses in their offset jet study were higher than the values previously reported for 3D wall jets.

In another report, Agelin-Chaab and Tachie [43] presented the two point correlation analysis of the velocity field for offset jets. They analyzed the inclination angle of the vortical structures in the inner region of the flow. They observed that the inclination angle of hairpin structures near the wall was about 11 degrees which was in good

29

agreement with reported values for turbulent boundary layers. They also reported the streamwise and wall normal extent of the turbulent structures of the flow in the inner layer.

The jet flows in quiescent ambient and near solid walls have been studied widely as shown above. When the jet discharges in a moving ambient with opposite flow direction, the transport and mixing in the flow field rises dramatically. This flow configuration can find applications in any engineering design that can takes advantage of higher mixing rate.

A survey of available literature shows that although the problem of free jets in counter-flow is investigated relatively well, there is not enough information available about the flow field of jets in counter-flow in the proximity of the solid walls. Round wall jets in counter-flows can be installed easily in pipelines, mixing chambers, heat exchangers, chemical reactors, and river beds to provide better mixing efficiency. The value of the jet to counter-flow velocity ratio and the offset distance of the jet from the wall can provide controlling mechanisms for altering the behavior of this flow. The aim of this research is to analyze the behavior of jets in counter-flow located beside solid walls.

References

 [1] Beltaos, S., and N. Rajaratnam. "Circular turbulent jet in an opposing infinite stream." (1973).

[2] Morgan, William D., Brian J. Brinkworth, and Gordon V. Evans. "Upstream penetration of an enclosed counterflowing jet." Industrial & Engineering Chemistry Fundamentals 15, no. 2 (1976): 125-127.

[3] Saghravani, S. F., and A. S. Ramamurthy. "Penetration length of confined counter flowing free jets." *Journal of Hydraulic Engineering* 136, no. 3 (2010): 179-182.

[4] König, O., and H. E. Fiedler. "The structure of round turbulent jets in counterflow: a flow visualization study." Advances in Turbulence *3*, pp. 61-66. Springer Berlin Heidelberg, 1991.

[5] Lam, K. M., and H. C. Chan. "Investigation of turbulent jets issuing into a counter-flowing stream using digital image processing." Experiments in Fluids 18, no. 3 (1995): 210-212.

[6] Yoda, M., and H. E. Fiedler. "The round jet in a uniform counterflow: flow visualization and mean concentration measurements." Experiments in Fluids 21, no. 6 (1996): 427-436.

[7] Lam, K. M., and H. C. Chan. "Round jet in ambient counterflowing stream." *Journal of Hydraulic Engineering* 123, no. 10 (1997): 895-903.

[8] Lam, K. M., and C. H. C. Chan. "Time-averaged mixing behavior of circular jet in counterflow: Velocity and concentration measurements." *Journal of Hydraulic Engineering* 128, no. 9 (2002): 861-865.

[9] Tsunoda, H., and M. Saruta. "Planar laser-induced fluorescence study on the diffusion field of a round jet in a uniform counter-flow." *Journal of Turbulence* 4, no. 1 (2003): 1-12.

[10] Bernero, S., and H. E. Fiedler. "Experimental investigations of a jet in counterflow." In Advances in Turbulence VII, pp. 35-38. Springer Netherlands, 1998.

[11] Bernero, Stefano, and Heinrich E. Fiedler. "Simultaneous PIV and LIF experiments on a round jet in counterflow." In *Proc.* 1st Int. Symp. on Turbulence and Shear Flow Phenomena (Santa Barbara), pp. 1053-8. 1999.

[12] Tsunoda, Hiroyuki, and Jun-Ichi Takei. "Statistical characteristics of the cross-sectional concentration field in a round counter jet." *Journal of Fluid Science and Technology* 1, no. 2 (2006): 105-113.

[13] Torres, Luis A., Mohammad Mahmoudi, Brian A. Fleck, David J. Wilson, and David Nobes. "Mean Concentration Field of a Jet in a Uniform Counter-Flow." *Journal of Fluids Engineering* 134, no. 1 (2012): 014502.

[14] Bernero, S., and H. E. Fiedler. "Application of particle image velocimetry and proper orthogonal decomposition to the study of a jet in a counterflow." Experiments in Fluids 29, no. 1 (2000): S274-S281.

[15] Balachandar, R., L. Robillard, and A. S. Ramamurthy. "Some characteristics of counter flowing wall jets." *Journal of Fluids Engineering* 114, no. 4 (1992): 554-558.

[16] Tanaka, E., Y. Inoue, and S. Yamashita. "An experimental study on the two-dimensional opposed wall jet in a turbulent boundary layer: Change in the flow pattern with velocity ratio." Experiments in Fluids 17, no. 4 (1994): 238-245.

 [17] Launder, B. E., and W. Rodi. "The turbulent wall jet measurements and modeling." Annual Review of Fluid Mechanics 15, no. 1 (1983): 429-459.

[18] Launder, B. E., and W. Rodi. "The turbulent wall jet." Progress in Aerospace Sciences 19 (1979): 81-128.

[19] Craft, T. J., and B. E. Launder. "On the spreading mechanism of the three-dimensional turbulent wall jet." *Journal of Fluid Mechanics* 435 (2001): 305-326.

[20] Davis, M. R., and H. Winarto. "Jet diffusion from a circular nozzle above a solid plane." *Journal of Fluid Mechanics* 101, no. 01 (1980): 201-221.

[21] Fujisawa, Nobuyuki, and Hiroyuki Shirai. "Mean flow and turbulence characteristics of three-dimensional wall jet along plane surface." Japan Society of Aeronautical Space Sciences Transactions 32 (1989): 35-46.

[22] Padmanabham, G., and BH LakshmanaGowda. "Mean and turbulence characteristics of a class of three-dimensional wall jets—part 1: mean flow characteristics." *Journal of Fluids Engineering* 113, no. 4 (1991): 620-628.

[23] Abrahamsson, H., Johansson, B., and Lofdahl L. "The turbulence field of a fully developed three dimensional wall jet. "*Internal Rep. No. 97/1*, Department of Thermo and Fluid Dynamics, Chalmers Univ. of Tech., Goteborg, Sweden. (1997)

[24] Sun, H. "Development of three-dimensional turbulent wall jet. " PhD thesis, McMaster University, Hamilton, Canada. (2002).

[25] Law, Adrian Wing-Keung, and Herlina. "An experimental study on turbulent circular wall jets." *Journal of Hydraulic Engineering* 128, no. 2 (2002): 161-174.

[26] Agelin-Chaab, M., and M. F. Tachie. "Characteristics of Turbulent Three-Dimensional Wall Jets." *Journal of Fluids Engineering* 133, no. 2 (2011): 021201.

[27] Eriksson, J. G., R. I. Karlsson, and J. Persson. "An experimental study of a two-dimensional plane turbulent wall jet." Experiments in fluids 25, no. 1 (1998): 50-60.

[28] George, William K., Hans Abrahamsson, Jan Eriksson, Rolf I. Karlsson, Lennart Löfdahl, and Martin Wosnik. "A similarity theory for the turbulent plane wall jet without external stream." *Journal of Fluid Mechanics* 425 (2000): 367-411.

[29] Tachie, M., R. Balachandar, and D. Bergstrom. "Scaling the inner region of turbulent plane wall jets." Experiments in Fluids 33, no. 2 (2002): 351-354.

[30] Verhoff, August. *The Two-dimensional, Turbulent Wall Jet With and Without an External Free Stream*. No. 626. PRINCETON UNIV NJ, 1963.

[31] Han, G., M. De Zhou, and I. Wygnanski. "On streamwise vortices and their role in the development of a curved wall jet." Physics of Fluids (1994-present) 18, no. 9 (2006): 095104.

[32] Agelin-Chaab, Martin. "Experimental study of three-dimensional offset jets and wall jets." PhD diss., University of Manitoba, 2010.

[33] Miozzi, M., F. Lalli, and G. P. Romano. "Experimental investigation of a free-surface turbulent jet with Coanda effect." Experiments in Fluids 49, no. 1 (2010): 341-353.

 [34]NOZAKI, Tsutomu, Keiji HATTA, Masahiro NAKASHIMA, and Hirohisa MATSUMURA. "Reattachment flow issuing from a finite width nozzle." Bulletin of JSME 22, no. 165 (1979): 340-347.

[35] NOZAKI, Tsutomu, Keiji HATTA, Norihide SATO, and Hirohisa MATSUMURA. "Reattachment Flow Issuing from a Finite Width Nozzle: Report 2, Effects of Initial Turbulence Intensity." Bulletin of JSME 24, no. 188 (1981): 363-369.

[36] Pelfrey, J. R. R., and J. A. Liburdy. "Mean flow characteristics of a turbulent offset jet." *Journal of Fluids Engineering* 108, no. 1 (1986): 82-88.

[37] Pelfrey, J. R. R., and J. A. Liburdy. "Effect of curvature on the turbulence of a two-dimensional jet." Experiments in Fluids 4, no. 3 (1986): 143-149.

[38] Yoon, Soon Hyun, Kyung Chun Kim, DaeSeong Kim, and MyungKyoon Chung. "Comparative study of a turbulent wall-attaching offset jet and a plane wall jet." KSME Journal 7, no. 2 (1993): 101-112.

[39] Yoon, S. H., K. C. Kim, D. S. Kim, and M. K. Chung. "Effect of surface roughness on a turbulent wall-attaching offset jet." Experiments in Fluids 19, no. 1 (1995): 38-42.

[40] Nasr, A., and J. C. S. Lai. "A turbulent plane offset jet with small offset ratio." Experiments in Fluids 24, no. 1 (1998): 47-57.

[41] Nasr, A., and J. C. S. Lai. "Comparison of flow characteristics in the near field of two parallel plane jets and an offset plane jet." Physics of Fluids (1994-present) 9, no. 10 (1997): 2919-2931.

[42] Agelin-Chaab, M., and M. F. Tachie. "Characteristics of Turbulent Three-Dimensional Offset Jets." *Journal of Fluids Engineering* 133, no. 5 (2011): 051203.

[43] Agelin-Chaab, M., and M. F. Tachie. "Characteristics and structure of turbulent 3D offset jets." International Journal of Heat and Fluid Flow 32, no. 3 (2011): 608-620.

Chapter 3: Experiment design for measuring the velocity field of wall jets in counter-flow[*]

Abstract - In this paper the wall jet, and the problem of jet in counter-flow are introduced briefly and an experimental method for finding the velocity field of a round wall jet in counter-flow is presented. The jet to counter-flow velocity ratio is changed from 2.5 to 25. The measuring technique is two component particle image velocimetry (PIV) by using 4 cameras which provides a large field of view to cover the whole penetration depth of the wall jet at all conditions. The details of the experimental procedure and data extraction are discussed. To validate the accuracy of the test setup, the velocity field of the wall jet in quiescent ambient is obtained in a range of Reynolds number up to 10,000 and is compared with available data in the literature. The mean velocity field and its main characteristics for the case of jet to counter-flow velocity ratio equal to 17.5 are discussed shortly.

3.1   Introduction

"The wall jet is a type of shear layer flow along a wall that due to its initial momentum, at any station, its streamwise velocity in some point is higher than the velocity of the external flow" [1]. Boundary layer control in advanced aircrafts, film cooling of combustion chambers and turbine blades, and air conditioning systems are typical examples for engineering applications of wall jets. The schematic of the velocity distribution of a wall jet with discharge velocity of U_j in a two-dimensional plane is shown in Fig. 3-1.
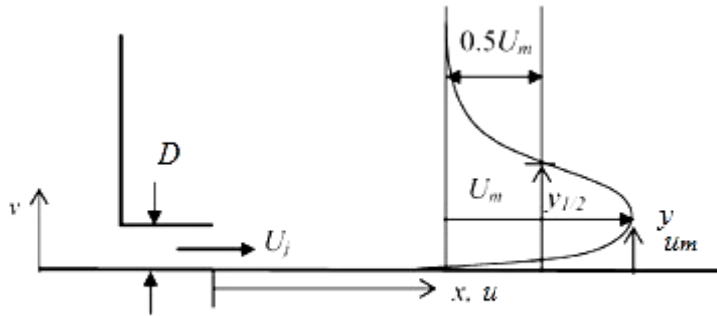
Figure 3-1: Streamwise velocity profile of a wall jet [1].

The velocity profile shows a maximum axial velocity, U_m, which occurs at height of y_{u_m} (see Fig. 3-1). There are two different shear flows in the wall jet. The first one which starts from the wall and extends to the point of maximum velocity has typical characteristics of a boundary layer and traditionally is called the inner region. The second shear flow starts from the point of maximum velocity and extends to the other edge of the flow. It is called the outer region and has the characteristics of a free shear layer. Different researchers have tried to find universal correlations for the velocity and scalar

concentration distribution in a wall jet. To this end, flow parameters from the outer region and/or inner region have been used to normalize the velocity and concentration field and to examine the self-similarity of the flow. The outer region parameters which are traditionally used to find dimension-less scales for the velocity field are the maximum local velocity (U_m), the height (y_{u_m}), and the height where the velocity becomes half of the maximum velocity ($y_{1/2}$).

Eriksson et al. [2] used two components laser Doppler anemometry (LDA) technique to investigate the velocity field of a two-dimensional slot wall jet in a water channel. The height and width of the slot were $h = 9.6$ mm and $w = 460$ mm, respectively. The Reynolds number of the jet based on the exit condition was 9.6×10^3. The measurements were done from a distance of 0.05 mm above the wall up to the outer region of the wall jet which allowed data acquisition in the viscous sub-layer with high spatial resolution. They used outer region scaling parameters and found that for the axial distances greater than 40 b, the streamwise velocity profiles showed self-similar behavior in the form of:

$$U / U_m = f(y / y_{1/2}) \qquad\qquad (1)$$

In addition to slot wall jets, the three dimensional wall jets were also investigated widely by other researchers. One of the important characteristics of a three dimensional wall jet is higher growth rate in spanwise direction compared to streamwise direction. The spreading rate of the velocity in the spanwise direction is about 5.5 times greater than that of the streamwise velocity [1]. Law and Herlina [3] reported the simultaneous measurement of the velocity and scalar concentration field for a round wall jet with diameter of $D = 5.5$ mm at three different jet Reynolds numbers equal to 5.5×10^3, 12.2×10^3, and 13.7×10^3. They used PIV and planar laser induced fluorescence (PLIF) at

the jet symmetry and lateral plane to find both the streamwise and spanwise mean flow characteristics up to the axial distance of 50D from the jet outlet. By using the outer region flow parameters for finding dimensionless velocity and concentration distribution, their results showed self-similar velocity and concentration profiles after an axial distance of 25D from the jet exit.

Investigation of flow characteristics of jets issuing in non-stagnant ambient flow can find application in many engineering problems. Co-flowing jets, jets in cross-flow and jets in counter flow are examples of this flow configuration. The efficient dilutions of effluents and mixing enhancement in combustion chambers have been important topics of research for many years. The jet in counter flow has higher mixing efficiency compared to other configurations and it has a great potential to be used in different industrial applications such as combustion chambers and chemical reactors as previously shown by Yoda and Fiedler [4], Chan and Lam [5] and Torres et al [6]. The dynamics of this flow and its response to harmonic excitation was studied by Koing and Fiedler [7]. They conducted a flow visualization study of a 25 mm round jet in counter-flow in a wind tunnel. For low values of jet to counter-flow velocity ratios (U_R< 1.4) they saw a regular vortex shedding and stable behavior of the jet, while for greater velocity ratios random fluctuations were observed. Flow excitation could not provide coherency or a change in the penetration length based on their experiments.

Figure 3-2 shows the schematic of a wall jet in counter-flow. The wall jet with exiting from an orifice with diameter of D and exit velocity of U_j is facing an opposing stream with mean velocity of U_0. Like other kind of jet flows, a potential core which has velocity and concentration equal to those of the jet discharge point forms in the beginning. The

length of this potential core is less than that of a jet in quiescent surroundings as shown

by Or et al [8]. As described by Torres et al [6], after the potential core, a transition

length exists for the jet to develop the well known self-similar velocity patterns. The

region of the potential core and transition to the self-similar area is called the zone of

flow establishment (Z.F.E.). The jet penetrates into the opposed flow up to axial and

radial penetration lengths of X_p and Y_p which are dependent on the jet to counter-flow

velocity ratio (U_R). The behavior of the jet up to the point where it reaches to the

maximum penetration height is similar to a wall jet flowing into quiescent ambient

surroundings. The region between the zone of flow establishment and the point of

maximum penetration height is called the established flow zone (E.F.Z.). Finally the jet

loses its momentum and ends in a stagnation point and is carried back with the opposing

flow. This happens in the mixing zone area (M.Z.).
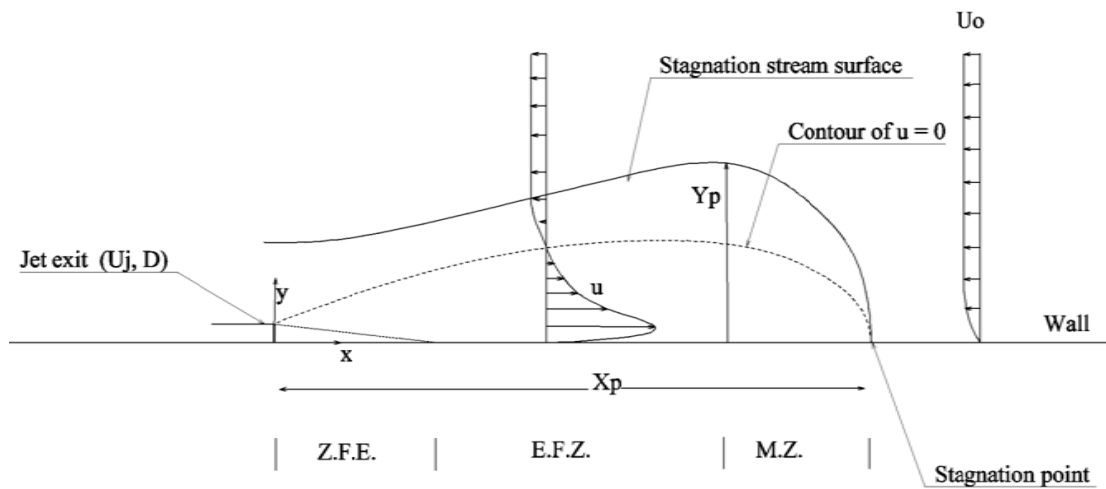
Figure 3-2: The schematic of a wall jet in counter-flow.

The formation of large scale vortical structures due to the strong shear layers between the

jet and opposed flow creates random oscillations with large amplitudes which cause

higher spreading rates compared to other jet configurations like co-flow and cross-flow jets. Although there are many publications related to the discharge of a simple round jet in a uniform counter flow, the problem of a jet in counter flow near solid walls has not been investigated completely. This flow configuration can have potential application in mixing of fluids and cooling of the heated walls in combustion chambers. The objective of this research is measuring and studying of the flow field of a round jet in counter flow in the proximity of wall surface. For this purpose, a test setup is designed and a series of experiments were conducted to find the velocity field of the wall jet in counter flow using PIV. The test setup is validated with available data in the literature for the wall jet flow in quiescent environment. The experimental procedure, data analysis and preliminary results are discussed.

3.2   Experimental setup

The experiments were done in the water channel facility at mechanical engineering department at the University of Alberta. The size of the water channel cross section was 680×480 mm^2 and its total test section length was about 5000 mm. It had a closed loop circuit and two pumps returned the water from the end plenum chamber to the front one. The schematic of the test setup is shown in Fig. 3-3.
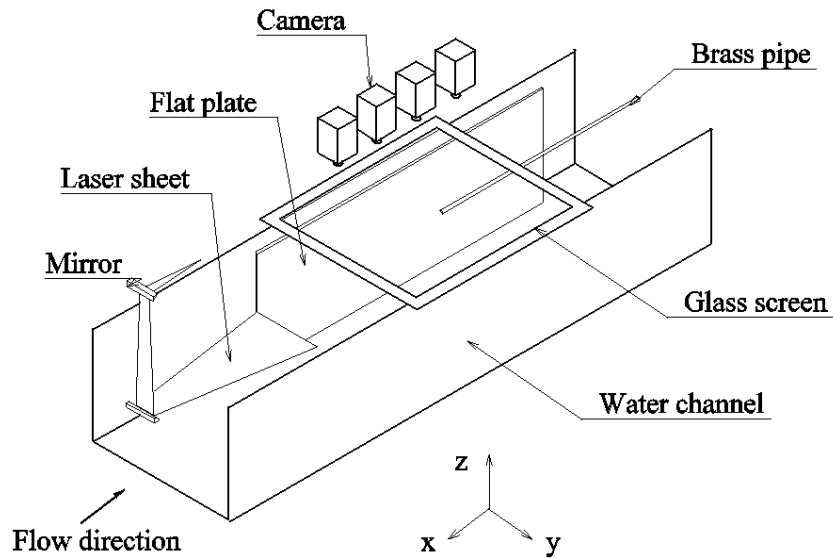
Figure 3-3: The schematic of the test setup.

The volume flow rate in the water channel was adjusted by means of two valves located after each pump. It was also possible to change the height of water in the channel by adjusting the angle of a gate located at the end of the channel. These two mechanisms were used to adjust the velocity of the flow. The water flowed from the upstream plenum chamber through an S shape nozzle with a contraction ratio of two and after passing from

a flow straightener entered the channel. The flow straightener width was 90 mm which was made from thin copper sheet and had a mesh size of about 20×20 mm². A grid turbulence generator was located about 150 mm in front of the flow straightener. It was made from stainless steel bars with width of 20 mm and thickness of 4 mm and had a mesh size of about 55×55 mm².

A periscope located after the grid turbulence generator was used to reflect the laser sheet in the channel from the upstream. In this experiment the channel flow velocity was set to U_0= 4cm/s and the turbulence intensity (TI) was measured about 3.5 % following:

$$TI = \sqrt{\frac{1}{3}(\overline{u'^2} + 2\overline{v'^2})}/U_0 \qquad (2)$$

where u' and v' are velocity fluctuations in axial and lateral direction.

A flat plate made from acrylic with size of 400×2000 mm² was installed in the side wall of the channel far from the channel boundary layer. The distance of the flat plate leading edge was about 2m from the beginning of the channel test section and had a chamfer upstream to minimize the stagnation area. A trip strip was glued on the wall surface at upstream to ensure a turbulent boundary layer with a set leading edge. The plate was equipped with a brass pipe with inner diameter equal to D= 8.84 mm and thickness of 0.1 mm to provide the jet flow in opposite direction of the channel flow, as shown in Figure 3-4. The length of the pipe was 920 mm (104D) which provided a fully developed flow in the pipe end. The brass pipe was held parallel to the flat plate and in the middle height by a simple supporting bar. The pipe holder had the ability to adjust the jet centerline distance from the flat plate to change the jet offset ratio (*m*). The jet offset ratio in this

study was changed from 0 to 4.3. The offset ratio of zero represents the flush mounted wall jet. The distance of the jet exit plane from the leading edge of the flat plate was 1200 mm. The jet discharge plane was about 40 cm far from the anchoring point to the pipe holder unit. Therefore, the interference effect of the pipe holder in the jet and opposed flow was negligible.
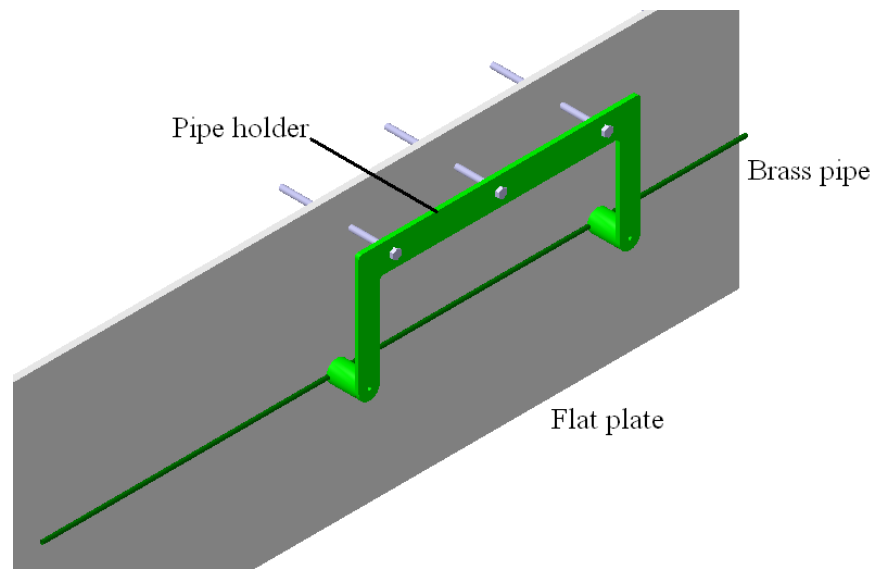
Figure 3-4: The flat plate and brass pipe.

The jet was fed by a pressurized stainless steel tank and the channel water was used to fill the tank during the experiments. The compressed air pressure in the tank was always about 350 kPa. At the beginning of the brass pipe a flow straightener was installed to suppress any secondary flow or vortices before entering the brass pipe. It consists of a set of straws with length of 120 mm and diameter of 2 mm located in a tube with diameter of 25 mm. this tube was connected to the brass pipe by a smooth converging nozzle. A flexible hose with approximate length of 5m and inner diameter of 25mm was used to connect the pressurized tank to the flow straightener.

A flow controller was installed on the jet feeding line to set the jet discharge velocity during the tests. That was a LCR-5LPM series of precise flow controllers made by AlicatScientific Company. In this study the range of variation for velocity ratio was $2.5 < U_R < 25$. The range of Reynolds number variation based on the jet diameter was about $1,000 < Re < 10,000$.

To find the velocity field, particle image velocimetry (PIV) was used. PIV is a non-intrusive technique for measuring the velocity field in a flow. It appeared about 30 years ago and is an essential measurement technique in fluid dynamics research. In PIV technique, the flow is seeded with small tracer particles which can follow the flow with the same velocity. A laser sheet is used for illuminating the particles in the desired region of the flow and one or more cameras are used to take images from that region. An accurate synchronizer is needed to control the triggering of the laser pulse and the cameras in order to provide a series of paired images taken immediately after each other. Statistical procedures like cross correlation algorithms are used to find the velocity field based on the light intensity distribution in each pair of images. This procedure is done by dividing the first and second image into small areas called interrogation windows and comparing each window in the first frame with the corresponding window in the second frame. A searching function will find the maximum correlation of intensities between these windows and therefore can find the average displacement vector of the group of particle images in each interrogation area. Dividing the displacement vector by the time step between the two frames will give the velocity vector in each window. The simple schematic of two interrogation windows in frame 1 and frame 2 and the resultant velocity vector is shown in Figure 3-5.
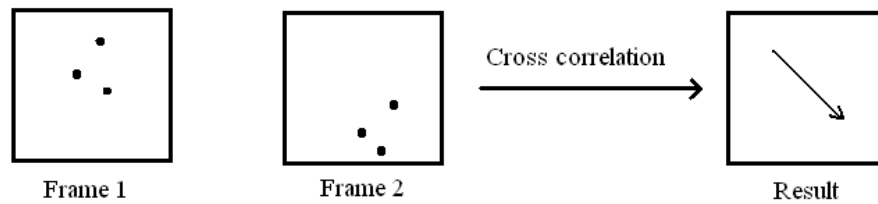
Figure 3-5: Schematic of interrogation windows and resultant velocity vector.

In this study four cameras were used and the resultant velocity field from them were combined to have a large field of view covering the whole penetrating length of the jet. The cameras were ImagerProX4M with data depth of 14 bits and resolution of 2048×2048 pixels equipped with Nikon AF NIKKOR lenses with focal length of 50 mm. They were located in a line such that their fields of view had about 15 mm overlap with each other, see Fig. 3-3. With the set of lenses were used in this study, the field of view for each camera was about 190×190 mm^2. Therefore, combining the images from these cameras provided a total effective field of view of 720×180 mm^2 which was large enough to cover the whole penetration region of the jet in counter-flow. A glass screen was installed on the water channel to have contact with the water surface to suppress the waves.

Illumination was provided by a dual cavity Nd:YAG laser with wave length of 532 nm. The laser was a Quanta Ray PIV- 400 series made by Spectra Physics and had a maximum energy of about 100 mJ in each pulse. The laser beam was transferred to the sheet generator with a laser guiding arm. The laser sheet with a thickness of about 1 mm

in the test section was generated by a cylindrical lens and was directed to the channel by means of a periscope, see Fig. 3-6.
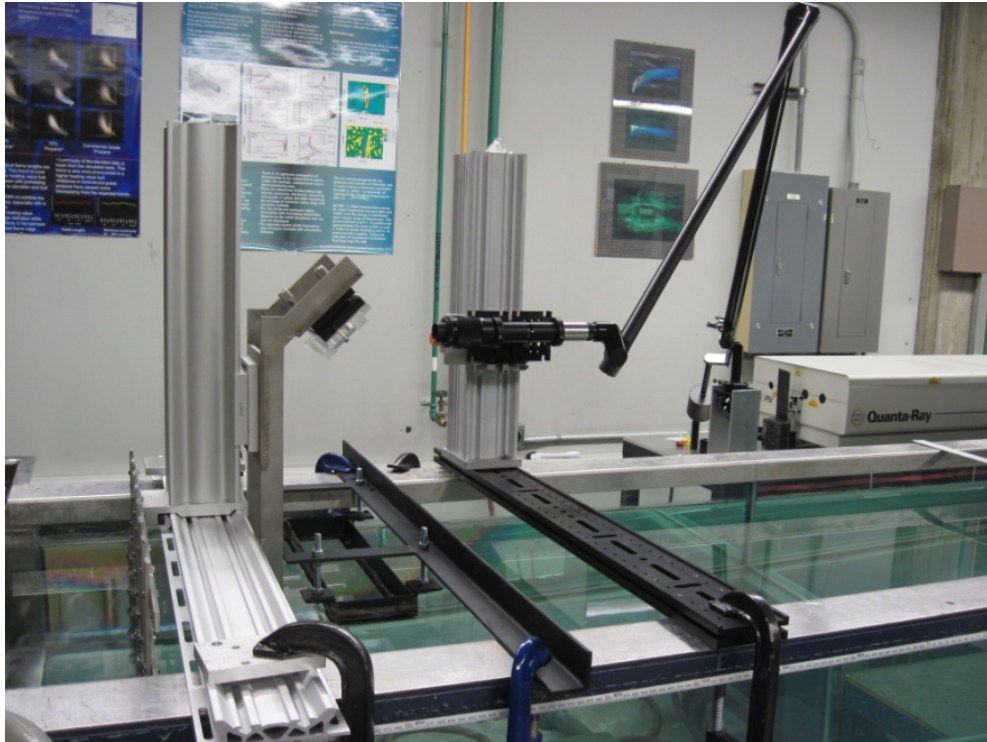
Figure 3-6: The laser, guiding arm, sheet generator, and periscope.

This should be noted that due to low velocity of the channel and very stiff and solid structure of the periscope and the mounting bars, no vibration observed in the laser sheet. The laser sheet was adjusted to be parallel to the channel floor and pass through the jet central plane. The channel flow was seeded by hollow glass spheres with mean diameter of 18 μm and to have a uniform seeding density the pressurized tank was fed by the channel flow. The PIV image recording and processing were done by Davis8.2 provided by LaVision Inc.

3.2.1   Data acquisition

When the camera's orientation and position were fixed and the test rig was ready with all components, the calibration of cameras was done to find the geometrical (spatial) mappings between the image space and the real coordinate system in the test setup. The printed calibration target which was used in this PIV study had a size of $740{\times}250$ mm^2 and was consisted of filled circles with diameter of 3 mm and centre to centre spacing of 15 mm. The calibration procedure for all four cameras was done simultaneously. A 3rd order polynomial fitting was selected for the calibration and the rms of fitting errors was less than 0.1%. For the PIV image acquisition, double frame and double exposure setting was selected.

In the statistical analysis of the physical phenomena with finite data series, the number of samples is an important factor to obtain the real and accurate properties of the problem. In this project, finding the average behavior of the flow of a wall jet in counter-flow was the main goal. Therefore, based on the initial tests which were done before the main tests, a simple analysis was done to find how many PIV images are enough to obtain this goal. The method was to examine the behavior of the average velocity versus number of images and the distribution of velocity data at several points in the velocity field. The points were selected to be close to the shear layers of the flat plate boundary layer and the interaction zone of the jet and opposed flow in the jet boundary. These points are shown schematically in Figure 3-7. The curve shows the loci of zero axial velocity.
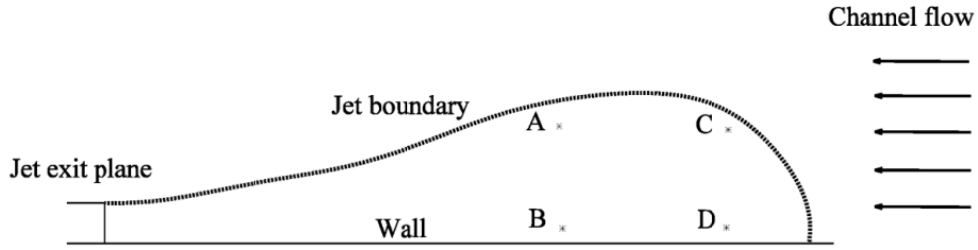
Figure 3-7: The schematic of the selected points for studying the statistical behavior of velocity.

The results for point D are shown in Figure 3-8 for the case where the jet to counter-flow velocity ratio was $U_R = 20$. It is seen that almost before 1000 images the average velocity approaches to a constant value or predictable behavior. Data distribution also showed that the recorded samples are acceptable since the major portion of them bouncing around the mean value. This trend was observed for points A, B, and C, too. Therefore, 1000 PIV images were recorded at each velocity ratio to obtain a valid average flow field of the jet in counter-flow.
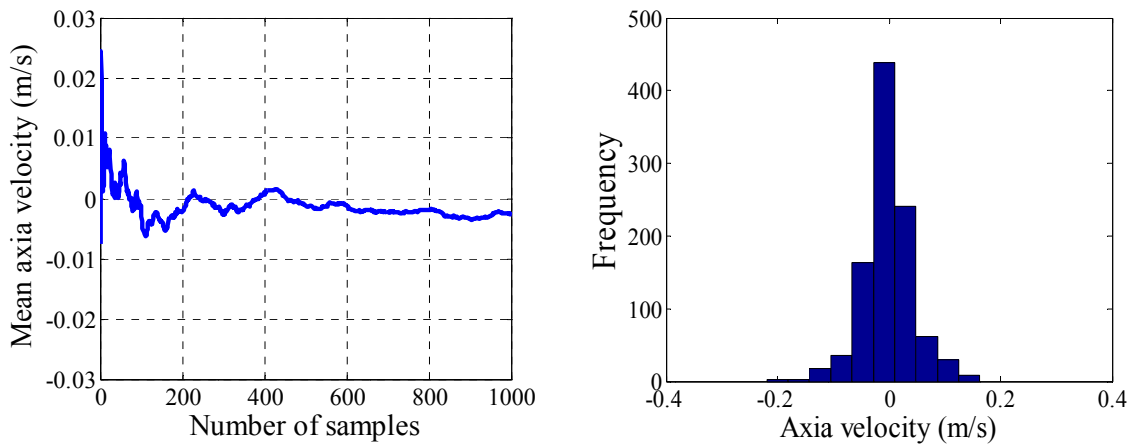
Figure 3-8: Variation of average velocity versus number of PIV images and data distribution at point D.

In PIV experiments, the setting of the time interval between the frames is an important issue which is depended on the physics of the flow and the processing scheme. Based on Davis manuals, the time difference between the images must be such that the displacement of identical particles in the image space is greater than 0.1 pixel and less than 25% of the interrogation window size. In the current experiments, the velocity field has areas with high velocity (e.g. at the jet discharge zone) and areas which the velocity vanishes (e.g. close to the wall or stagnation areas at the end of the jet penetration). Therefore, it was decided to do the experiments with one small time interval (~ 400 µs) suitable for the high velocity regions and one large time interval (3000 µs) to capture the velocity in low speed zones of the flow field. Then in the post processing of the data, these two velocity fields were combined with each other to find the whole velocity field.

3.2.2 Data processing

Data processing was done by Davis 8.2 on a graphics-processing unit (GPU) with total number of 1536 cores. Various schemes were selected and tested to find the most efficient and accurate scheme with lower amount of spurious vectors. Different multi-pass sequential cross correlations with decreasing window size were examined. Finally, the interrogation window size of 64×64 pixels with 50% overlap and 4 passes followed by a 16×16 pixels window size with 50% overlap and 3 passes was selected. With this processing scheme, it was found that the spatial resolution of the vector field is about 0.73×0.73 mm^2. This processing scheme was used to find the whole velocity field in this experimental study. In the vector post processing section, just a median filter was applied to get rid of the spurious vectors and fill the empty areas with the interpolation of neighbor vectors. Then, the average flow filed was found for each field of view.

The next step was stitching the flow fields of the cameras to each other to find the total flow field of the interaction of the jet and counter-flow. Since the field of view of the cameras had overlap with each other, this overlap was found and taken out during the stitching process. A simple schematic of the cameras field of view and their overlap is shown in Figure 3-9.
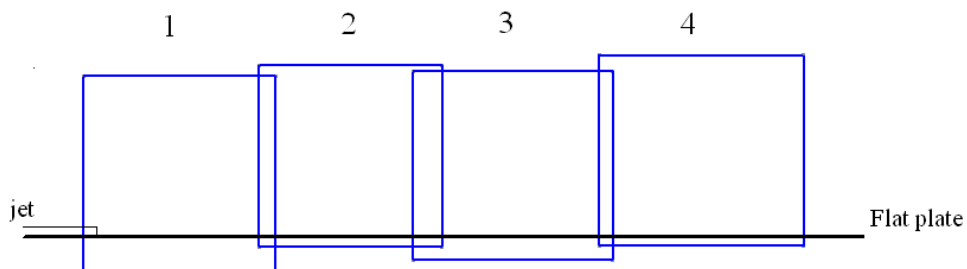
Figure 3-9: The schematic of cameras' field of view.

Camera 1
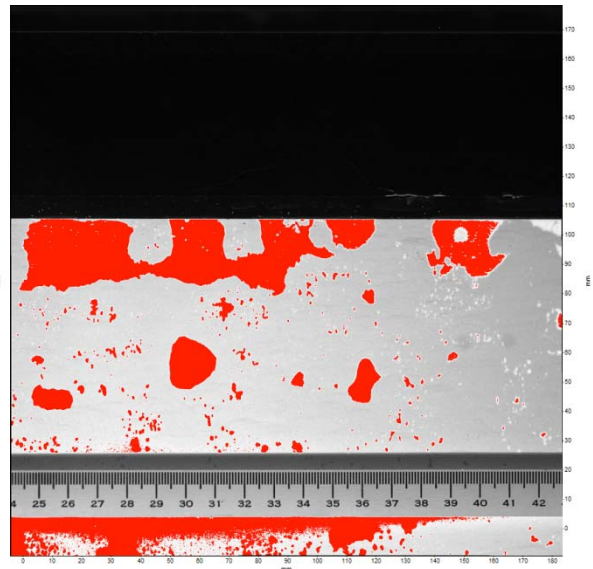
Camera 2
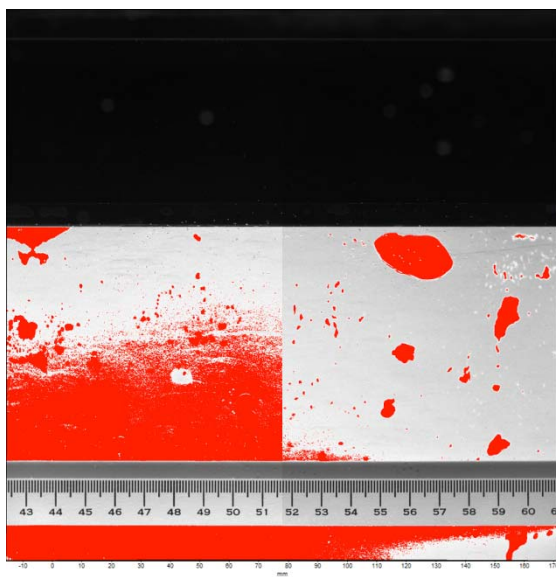
Camera 3
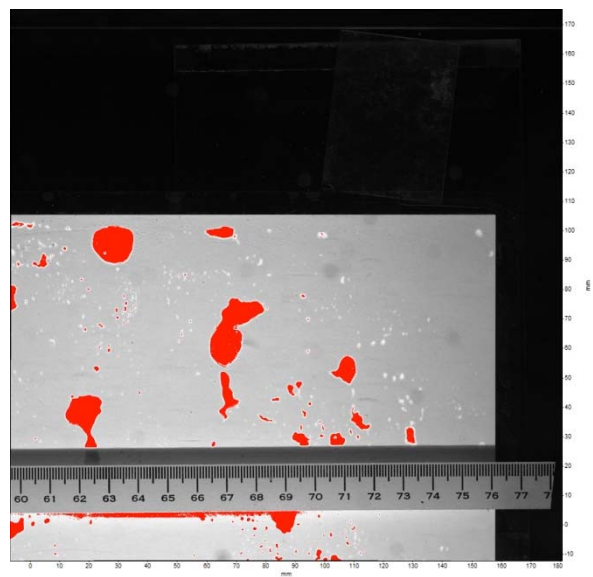
Camera 4

Figure 3-10: The cameras field of view and the measuring tape used for stitching the images.

The vector fields were imported to MATLAB for stitching and further post processing. The exact amount of the overlap of cameras was found by investigating the image of a measuring tape located in the same plane where PIV images were taken, see Fig. 3-10.

Searching was done on the images of the measuring tape from four cameras to find the common values. After finding the amount of overlaps, the images were cut with pixel accuracy to get rid of the common areas. This procedure was repeated for all velocity fields captured by each camera. So, for each data set the final velocity vector was extracted and used for further analysis.

The rules of thumb mentioned by Raffel et al. [9] were followed to reduce the bias error in the measurement system. These rules of thumb are to have between 5 to 8 particles in each interrogation window, and having particle images as big as 4-5 pixels. The total amount of bias error in the measurement of the velocity field was evaluated to be around 2%. More details about the uncertainty analysis in this study is presented in Appendix 1.

3.3 Results

An experiment is designed to measure the velocity field of a wall jet in counter-flow at different jet to counter-flow velocity ratios, up to $U_R = 25$. The main boundary conditions in this flow field are related to the counter-current flow, the boundary layer of the flat plate, and the jet outlet velocity. The flow condition of the channel was a uniform flow with the velocity of 4 cm/s and turbulence intensity of 3.5%. The boundary layer of the flat plate was tripped to be turbulent by a guitar string installed at a distance of 100 mm after the plate leading edge. The normalized velocity profile in the boundary layer of the plate at a distance of $x = 25D$ from the jet outlet plane is shown in Figure 3-11. The typical laminar and turbulent boundary layer profiles over flat plates described by Schlichting [10] are shown for comparison. It is clear that the current boundary layer velocity profile is similar to the turbulent profile; the discrepancy is due to the low Reynolds number artificially transitioned flow in these experiments.
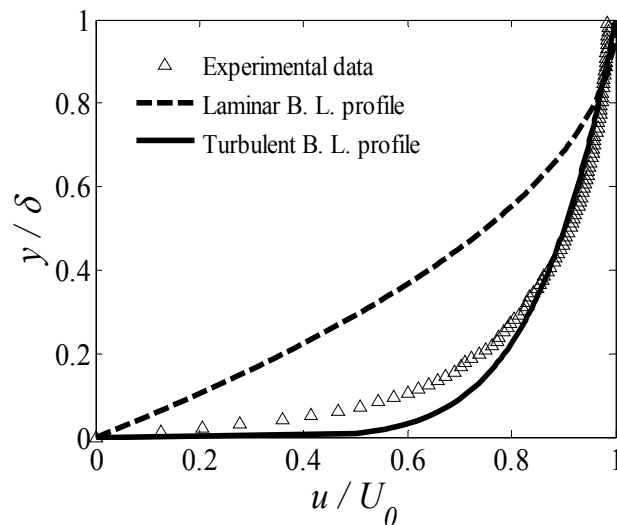
Figure 3-11: The boundary layer velocity profile of the flat plate at distance of 25D from the jet exit.

Detailed jet velocity profiles were obtained for the free jet exiting the brass pipe in the absence of the flat plate. Figure 3-12 shows the normalized mean axial velocity profiles at different Reynolds numbers based on the jet diameter at a distance of 0.4D from the outlet plane. It is seen that with increasing Reynolds number, the velocity profiles become fuller like a turbulent pipe flow and show minimal variation for $Re > 5,000$. It will be shown later that at low Reynolds number, the jet has a long laminar length and the jet velocity decay starts at a farther distance from the discharge plane.
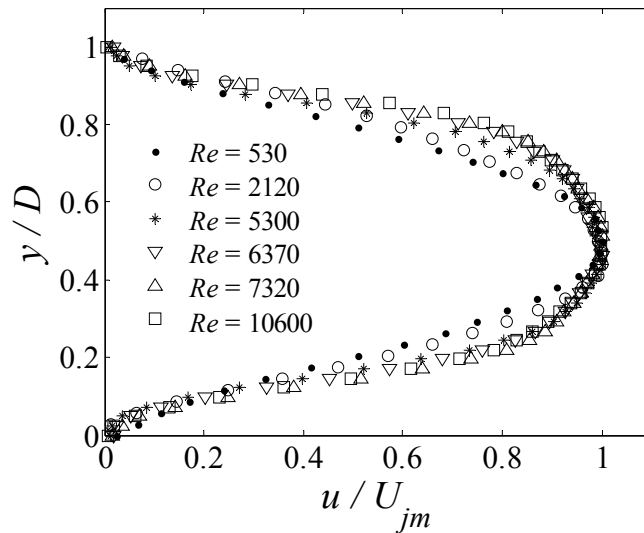
Figure 3-12: The jet outlet velocity profile at various Reynolds number and at distance of 0.4D from the discharge plane.

In order to ensure the capability and accuracy of this test setup, initial experiments were done to measure the velocity field of the wall jet when the water channel was not running. The results were then compared with the existing data in the literature for three dimensional round wall jets in quiescent ambient flow. Figure 3-13 shows a small portion of the axial velocity contours of the round wall jet at $Re = 1,000$ and $Re = 9,500$. It is seen

that at lower Reynolds number, the axial velocity decay is very slow and the jet shows laminar behavior in the initial regions. On the other hand, when the Reynolds number is high enough, the jet velocity decay starts immediately after the exit plane and the jet is completely turbulent.
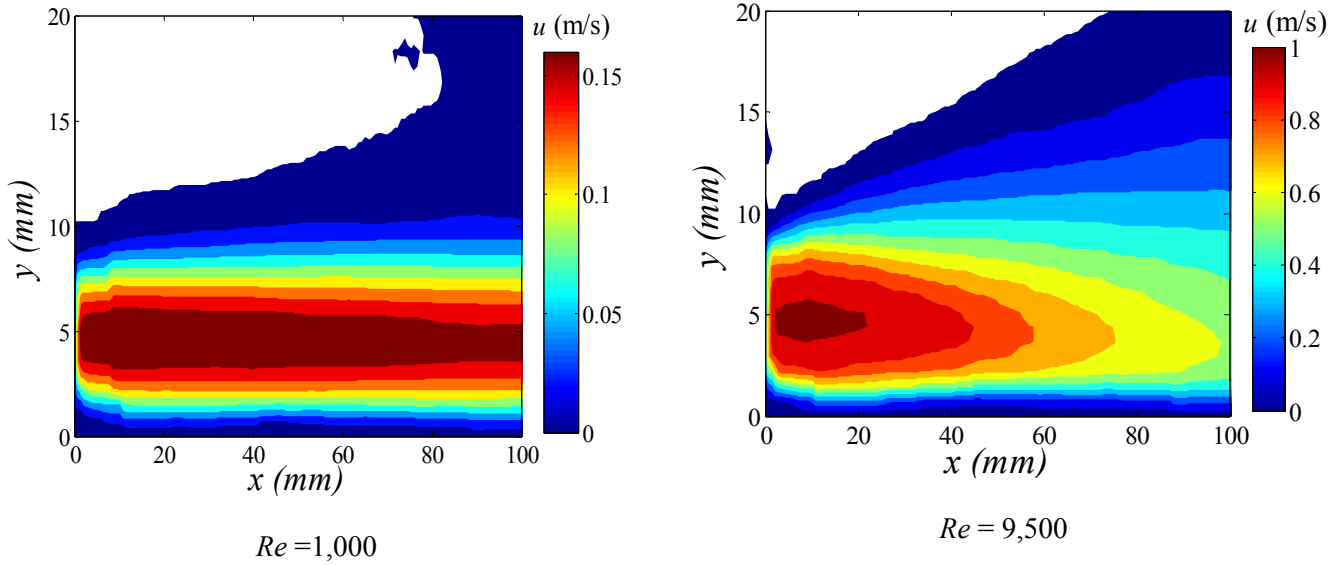
Figure 3-13: The axial velocity contour at low and high Reynolds number.

The normalized maximum velocity decay of the wall jet versus axial distance is shown in Figure 3-14. It is seen that for $Re > 7.3 \times 10^3$ the velocity profiles collapse on each other and show self-similar behavior. For axial distances of $x/D > 15$, a power law fit ($R^2 = 95\%$) can be used to represent the velocity distribution in the form of:

$$U_m / U_{jm} = 8.5 \, (x / D)^{-1.08} \tag{3}$$

where U_m is the maximum wall jet axial velocity, and U_{jm} is the maximum jet discharge velocity. This result has agreement with previous research of Law and Herlina [3] in which they found -1.07 power law fit for the velocity decay of a three dimensional wall jet provided by a round nozzle.
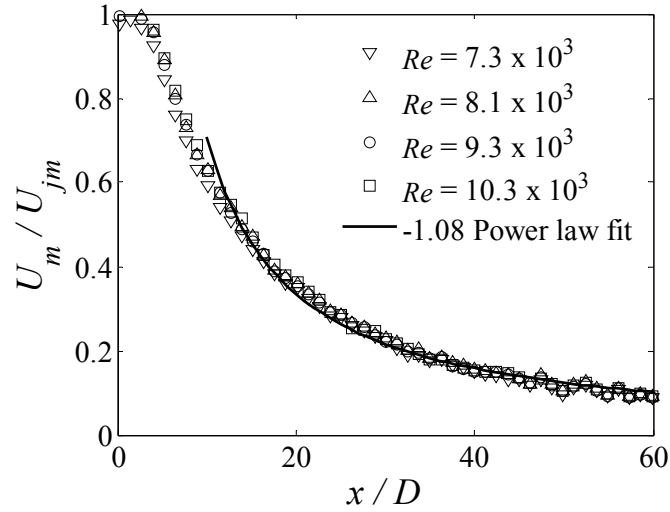
Figure 3-14: The normalized maximum velocity distribution.

Figure 3-15 shows the variation of half velocity width ($y_{1/2}$) of the round wall jet versus axial distance from the jet exit plane. For $x/D > 30$, it is seen that the variation of jet width is linear with slope of 0.04. Therefore, a linear fit ($R^2=95\%$) for the half width velocity of the round wall jet can be proposed as:

$$y_{1/2}/D = 0.5 + 0.04(x/D) \tag{4}$$
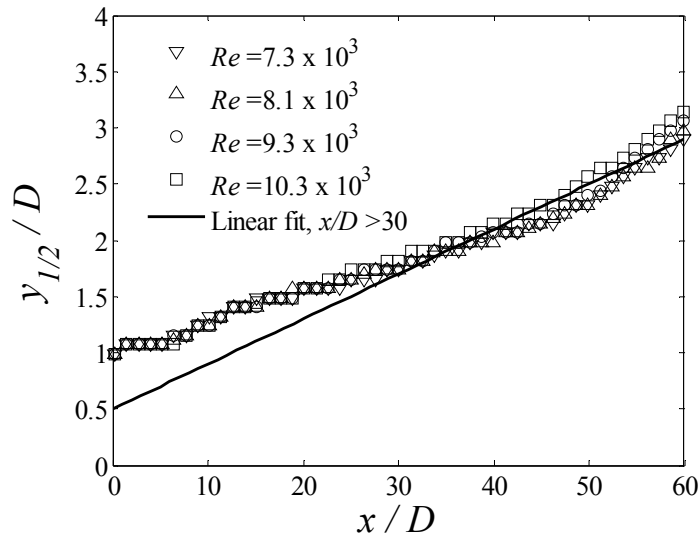
Figure 3-15: The variation of jet half velocity width in axial direction.

The normalized axial velocity distribution of the wall jet at two different Reynolds numbers and several distances downstream of the discharge plane is shown in Figure 2-16. The velocity profiles show self-similarity for $x/D > 30$. As Figure 3-16 shows, the velocity profile proposed by Verhoff [11] can completely fit to the current experimental data. This velocity profile is in the form of:

$$u/U_m = 1.48 \, (y/y_{1/2})^{1/7} \, [1\text{-erf} \, (0.68 \, (y/y_{1/2}))] \qquad (5)$$
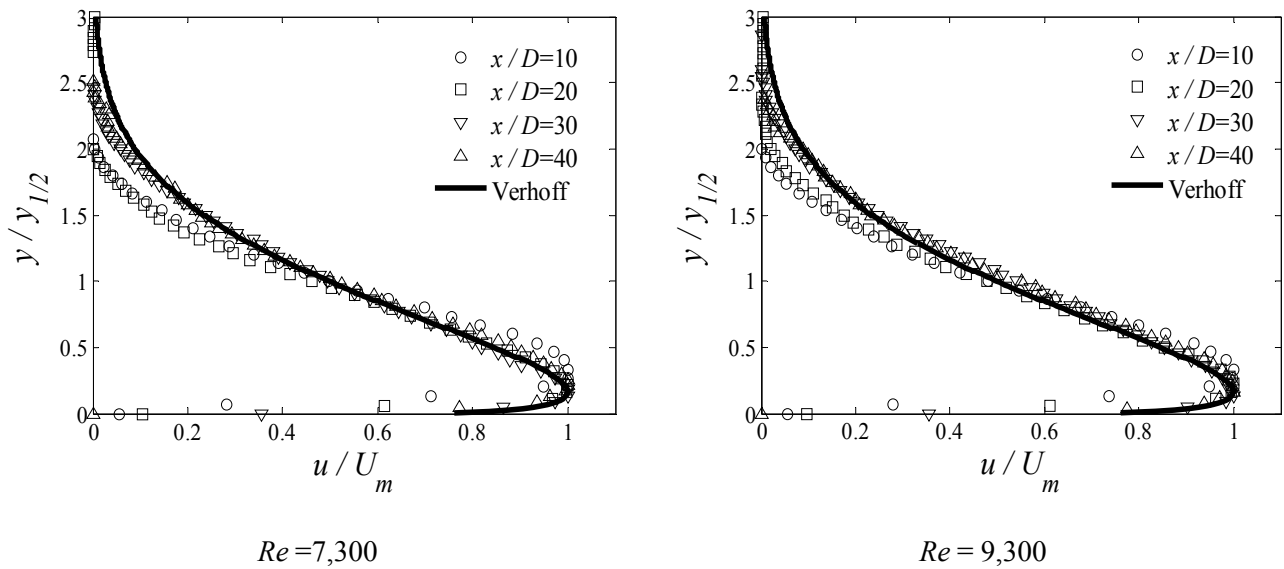
Figure 3-16: The normalized velocity profile at various distances.

From the above results one can conclude that the measured velocity field of the round wall jet in stagnant ambient has complete agreement with similar experiments done by other researchers. This proves the capabilities of the designed test setup for measuring the velocity field of the round wall jet with the presence of the counter-flowing stream in the water channel.

The whole flow field for the wall jet in counter-flow at U_R= 17.5 corresponding to jet

Reynolds number of Re =7,300 is shown in Figure 3-17. As it is seen, the jet penetrates

and exchange momentum with the counter-flow and finally reaches to zero velocity at

maximum penetration length of X_p = 64D.

Figure 3-18 shows a schematic of the stream lines in a 2D plane along with the loci of u =

0 regions. The zero axial velocity curve was found with a threshold of u > -0.0005 m/s.

Figure 3-18 clearly shows the path of fluid elements toward the stagnation area and their

turning. There is a recirculation region close to the stagnation area which contains a big

swirl located at x/D = 48. The axial velocity profiles at different positions are shown in

Figure 3-19. It is seen that the profiles have a typical shape of a wall jet flow at initial

regions. Then, the decay of axial velocity profile starts around x/D = 40 and continues to

reach to zero velocity at maximum penetration point. Different length scales of the flow

can be used to normalize these velocity profiles like what was done for a wall jet in

quiescent environment and will be discussed in next chapters.
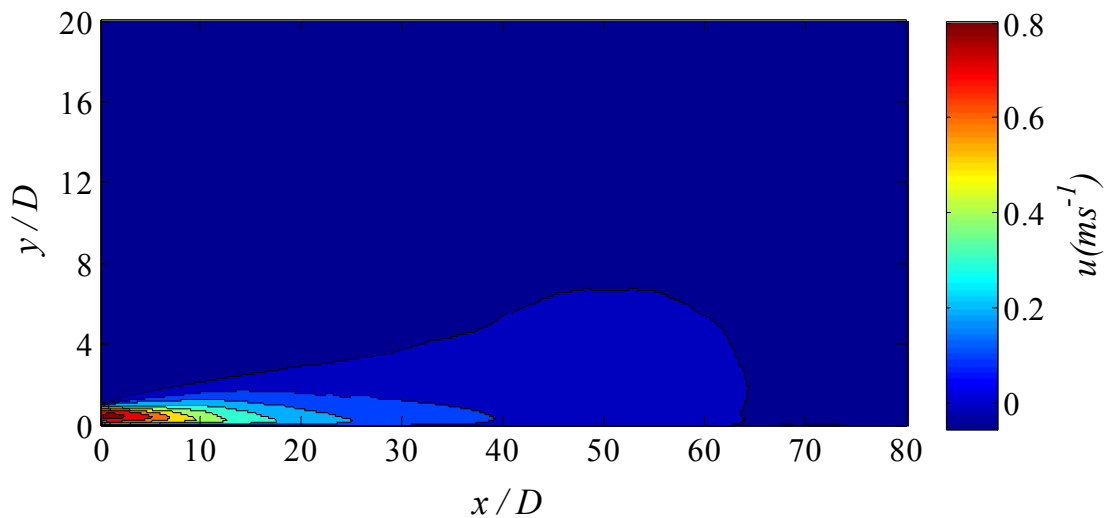
Figure 3-17: Contour of mean axial velocity at velocity ratio of U_R= 17.5.
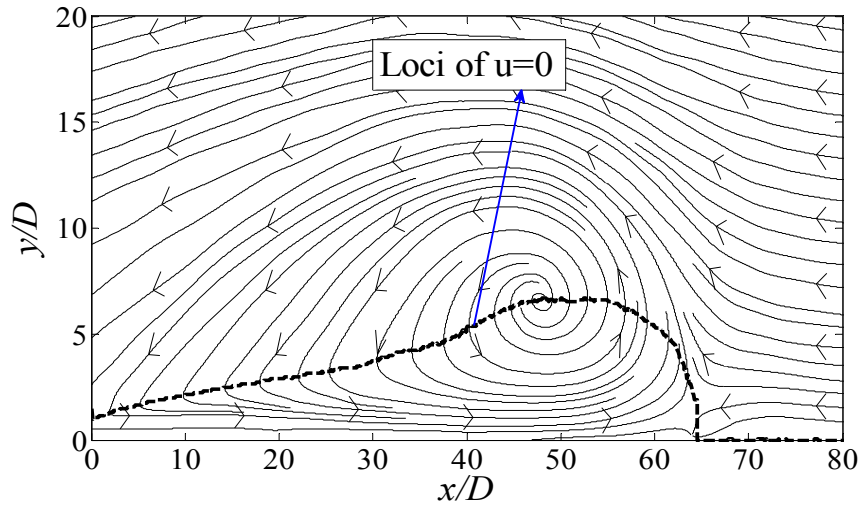
Figure 3-18: Streamlines and the loci of zero axial velocity at velocity ratio of $U_R = 17.5$.
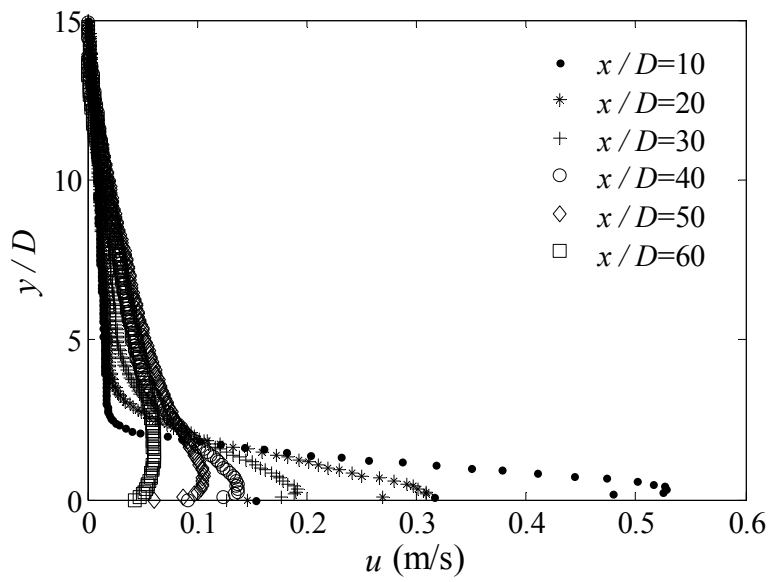
Figure 3-19: Normalized axial velocity profiles at different locations, $U_R = 17.5$.

3.4   Summary

The experimental procedure for studying the behavior of a round jet in counter-flow in the proximity of a solid wall were described. The wall jet and counter-flowing jet were defined and their typical applications were discussed briefly. The velocity field of a three dimensional round wall jet exiting from a pipe is analyzed at different Reynolds numbers ranging from 1000 to 10,000 in quiescent ambient and the agreement with previous investigations was proved. This proves the accuracy of the designed test setup for conducting the jet flow research. The self-similarity of velocity data was observed for Re>7,000. The maximum axial velocity decays with power of -1.08 versus the axial distance from the jet outlet. In addition, the normalized axial velocity profiles collapsed on each other for $x/D > 30$. The mean velocity field of the wall jet in the presence of counter-flowing stream at jet to counter-flow velocity ratio of U_R= 17.5 was analyzed shortly. It was found that the wall jet penetrates into the counter-flow and reached to zero velocity at axial distance equal to $64D$ from the jet exit plane. A large recirculation region was formed close to stagnation area that is an indication of higher mixing ratio of fluid elements.

References

[1] Lander, B. E., and Rodi, W., 1983, "The turbulent wall jet- Measurement and modeling," Ann. Rev. Fluid mech., 15, pp. 429-459.

[2] Eriksson, J. G., Karlsson, R. I., and Persson, J., 1998, "An experimental study of a two-dimensional plane turbulent wall jet," Experiments in Fluids, 25, pp. 50-60.

[3] Law, A. W., and Herlina, 2002, "An experimental study on turbulent circular wall jets," *Journal of Hydraulic Engineering*, 128, pp. 161-174.

[4] Yoda, M., Fiedler, H. E., (1996). "The Round Jet in a Uniform Counter-Flow: Flow Visualization and Mean Concentration Measurements," Experiments in Fluids, 21(6), pp. 427- 436.

[5] Chan, H.C., Lam, K.M., (1998). "Centerline Velocity Decay of a Circular Jet in a Counter-Flowing Stream," Physics of Fluids, 10(3), pp. 637-644.

[6] Torres, L.A., Mahmoudi, M., Fleck, B.A., Wilson, D.J., Nobes, D.S., (2012). "Mean Concentration Field of a Jet in a Uniform Counter-flow," *Journal of Fluid Engineering* 134, 14502-1 to 5.

[7] Konig, O. and Fiedler, H. E., 1991, "The Structure of Round Turbulent Jets in Counter-Flow: a Flow Visualization Study," Advances in turbulence 3, pp. 61-66.

[8] Or, C.M., Lam, K.M., Liu, P., (2011). "Potential core lengths of round jets in stagnant and moving environments" *Journal of Hydro-Environment Research* 5, pp. 81-91.

[9] Raffel, M., Willert, C. E. and Kompenhaus, J., "Particle Image Velocimetry: A Practical Guide," Springer Verlag, 1998.

[10] Schilichting, H., "Boundary Layer Theory," McGraw-Hill, 4th edition, 1962.

[11] Verhoff, A., 1963, "The two-dimensional turbulent wall jet with and without an external stream," Rep. No. 626, Princeton University, Princeton, N.J.

Chapter 4: Experimental analysis of the velocity field of a round wall jet in counter-flow

Abstract

Experimental investigations showing the mean and fluctuating velocity field of a three dimensional round wall jet in counter-flow are presented. The jet to counter-flow velocity ratios ranged from 2.5 to 25 and the jet Reynolds number were from 1,000 to 10,000. The jet penetration length was measured and scaled with a power law relation. The decay of the maximum jet velocity during its penetration into the oncoming flow was analyzed with proper scaling parameters. The results show that up to 70% of the wall jet penetration length, the velocity decay and the spreading rate are effectively identical to those of a wall jet in quiescent ambient flow. Above this distance, the velocity decay is linear and the jet spreading rate increases sharply. The mean axial velocity profiles show self-similarity between 25% and 80% of the penetration distance and are similar to the case with no counter-flow. The vortical structures from the jet and the opposed turbulent boundary layer interact in the stagnation area to provide a large recirculation region with stochastic oscillations which enhance the mixing of the wall jet and counter-flow. These interactions make a region with high turbulence intensity at the end of the wall jet penetration. The profiles of velocity fluctuations and their triple products are presented

and discussed. It was observed that the normalized velocity fluctuation profiles show

self-similarity in a shorter range between 30% and 70% of the wall jet penetration length.

4.1   Introduction

The flow of a jet in the opposite direction of a moving ambient flow can have many applications in industries. The jet penetrates in the counter-flow due to its higher local momentum, then, it stops, creates a large stagnation area and returns back with the counter-flow. Early studies were focused on its ability as an aerodynamic flame holder in after-burners to replace large bluff bodies in the jet engines providing a high amount of energy dissipation [1, 2]. Another application of a jet in counter-flow is the thrust reversing during landing of large commercial airplanes, increasing the capability of short take-off and landing aircraft in different maneuvers [3]. The other proven application of this flow is in increasing the mixing efficiency in liquid and gaseous streams [4] by providing high turbulence with interaction of the jet and the opposed flow.

Initial investigators sought to find theoretical and empirical models to predict the penetration length of a free round jet in a counter-flow. Beltaos and Rajaratnam [5] reviewed previous research and used a systematic approach to analyze the mean velocity profiles of a round jet in a counter-flow. They conducted wind tunnel tests and found the velocity field by means of a Pitot tube and used non-dimensional groups of variables to predict the penetration length of the jet in the opposed flow. They found that the normalized axial penetration length of the jet has a linear relation with jet to counter-flow velocity ratio as:

$$X_p/D = k\, U_j/U_0 \qquad\qquad\qquad (1)$$

where k is a constant coefficient equal to 2.6 based on their experiments. They also combined potential flow theory with their findings in an attempt to predict the shape of

the stagnation stream surface, though this was not in good agreement with the experiments.

Morgan and Brinkworth [6] used flow visualization in a transparent pipe and found an empirical relation for penetration distance versus the momentum ratio of the jet and the counter-flow. They observed a linear relation ($k = 2.5$) between the penetrating distance and the velocity ratio when the momentum ratio of jet and counter-flow was less than 0.25. For higher momentum ratios, the linear correlation was not valid and the penetration distance versus velocity ratio increased with a lower slope. They also showed that there is no significant change in the jet penetration length as long as the jet and counter-flow Reynolds numbers were above 3×10^3 and 10^4, respectively. Other researchers [7-9] reported a linear coefficient, k, between 2.5 to 2.8 for the jet axial penetration distance at low momentum ratios of jet and counter-flow. No universal relation for the penetration of the jet in the lateral direction has been reported.

Bernero and Fiedler [10] used PIV and PLIF simultaneously to study the flow of a round jet in a counter-flow for velocity ratios up to $U_R = 20$. They found that the slope of the half-width lines for the jet velocity and concentration are more than that of the regular jets and self-similarity of velocity and concentration profiles exists only in a limited zone in the central part of the jet. Lam and Chan [11] performed an experimental analysis to investigate the velocity and concentration field of a 10 mm diameter jet in a uniform counter-flow with 10 cm/s velocity. Their results showed higher decay of the velocity and concentration in the jet centre line compared to a free jet. In addition, they observed self-similarity of velocity and concentration profiles in a limited core region of the flow up to 70% of the penetration distance. Torres et al. [12] used PLIF to investigate the scalar

concentration field of a round jet in counter-flow at velocity ratios of $4 < U_R < 19$. They used different sets of length scales based on the geometrical parameters of the mean flow to find self-similar profiles for the centerline and lateral decay of the jet. In addition, they extracted empirical relations to predict the concentration decay of the jet in counter-flow up to 70% of the penetration distance.

The flow of a wall jet in an opposing stream has not been investigated completely and there are just a few qualitative studies about 2D slot wall jets in counter-flow in the literature. Balachandar et al. [13] studied a slot wall jet in counter-flow at velocity ratios up to $U_R = 8$ using dye visualization and wall pressure measurement in a water channel. Their results revealed that for low velocity ratios ($U_R^2 < 2$) the jet separates quickly from the wall and spreads in the lateral direction. For high velocity ratios ($U_R^2 > 10$), they observed that the radial and axial penetrations are of the same order of magnitude. In another research, Tanaka et al. [14] used hot-wire anemometry in a wind tunnel and reported the velocity patterns of a plane wall jet in the opposite direction of a turbulent boundary layer. The velocity of the opposed flow in their experiment was set to $U_0 = 20$ m/s and the jet to counter-flow velocity ratio was varied up to 3 corresponding to maximum jet Reynolds number of 19,500. For $U_R > 1.6$ they obtained an empirical power law relation that predicts the penetration length of the wall jet in counter-flow in the form of:

$$X_p/D = 9.5U_R^{1.8} \tag{2}$$

Clearly, the problem of a wall jet in a counter-flow, despite its wide potential applications, has not been studied thoroughly and there are few reports available in the literatures with the focus on qualitative mean flow characteristics. Round wall jets in

counter-flow can be easily produced and installed in pipelines, mixing chambers, heat exchangers, and chemical reactors to provide a controlling mechanism for better mixing efficiency. It also can be used as an effective flow control tool to alter and modify free shear layers and boundary layers. To the authors' knowledge, the velocity field of a three dimensional counter-flowing wall jet has not been investigated yet. The objective of this paper is to provide a quantitative velocity field measurement along with turbulence analysis of a round wall jet in counter-flow. In addition, a qualitative description of the vortical structures in the flow is provided.

4.2   Experimental setup

The experiments were conducted in the closed-loop water channel facility at Mechanical

Engineering Department at The University of Alberta. The size of the water channel cross

section is 680×480 mm² and its total length is 5000 mm. Figure 4-1 shows a schematic of

this test setup. A flat plate made from acrylic with size of 400×2000 mm² was installed in

the side wall of the channel far from the channel walls boundary layer. The plate had a

chamfer upstream to minimize the stagnation area and a trip strip was used to ensure a

turbulent boundary layer. A brass pipe with length of 920 mm and inner diameter equal

to $D = 8.84$ mm was installed in the mid-height of the plate to provide the wall jet flow.

The outlet plane of the brass pipe was 1000 mm from the leading edge of the flat plate.

The jet was fed by a pressurized tank and a precise flow controller was used in the feed

line to maintain constant jet discharge velocities during the tests.
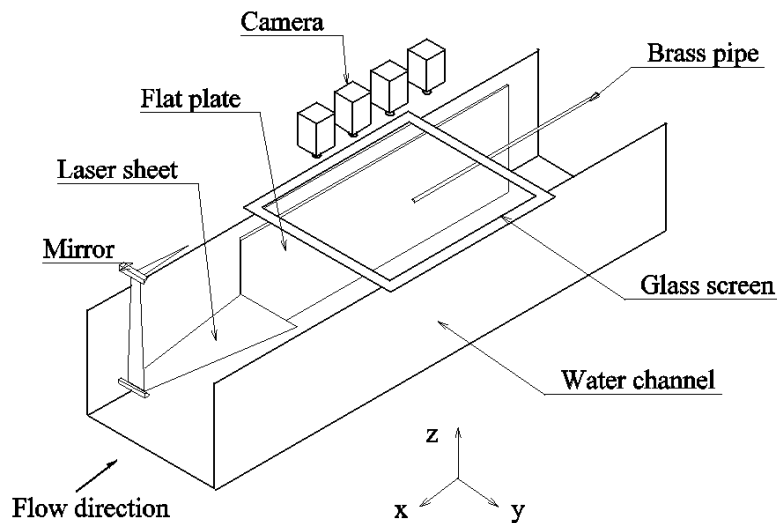
Figure 4-1: The schematic of experimental setup.

The velocity field was measured in the horizontal symmetry plane of the wall jet using Particle Image Velocimetry (PIV). In this work, four CCD cameras were used in tandem to provide a long field of view for capturing the 2D velocity field from injection to maximum penetration. The cameras were ImagerProX4M provided by LaVision Inc. and had data depth of 14 bits and resolution of 2048×2048 pixels. The cameras orientation was normal to the channel flow and their fields of view had about 15 mm overlap. Later in the data processing, the velocity fields provided from each camera were combined and stitched together to make a large aspect ratio velocity field covering the whole penetration length of the jet. With 50 mm Nikon lenses, the net dimension of the final velocity field was about 720×180 mm^2. Illumination was provided by a Quanta Ray PIV-400 Nd:YAG laser with wave length of 532 nm. The laser sheet was generated by a cylindrical lens and was directed to the test section from upstream by means of a small periscope. The periscope had two first-surface reflecting mirrors with 90 degree installation angle which were fixed on a thin stainless steel frame. The periscope structure was stiff and no vibration was observed in the laser sheet during the experiments. It was installed right after the grid turbulence generator in the channel entrance and had minimum blockage effect on the channel flow. The channel flow was seeded by hollow glass spheres with a mean diameter of 18 μm and to maintain a uniform seeding density, the pressurized tank was filled by the channel flow during the tests. The PIV image acquisition was done by DaVis 8.2 provided by LaVision Inc.

In all experiments, the height of water in the channel was 40 cm and its velocity was set to $U_0 = 4$ cm/s with a measured turbulence intensity equal to 3.5 %. The jet to counter-flow velocity ratio was varied from 2.5 to 25, corresponding to jet Reynolds number

variation of $10^3 < Re < 10^4$ based on the pipe diameter. With the chosen channel flow velocity and the jet discharge velocities, the maximum jet to counter-flow momentum ratio was measured to be about 0.14.

A glass screen was installed on the water surface in the imaging zone to prevent surface waves. When the test setup and all components were ready, calibration of the cameras was performed simultaneously with a large calibration target. Cumulative averaging of the velocity field at several points close to the stagnation zone of the wall jet in counter-flow was analyzed and it was found that 1000 images provide an accurate average velocity field in this complex flow. After all the settings were done for each velocity ratio, 1000 double frame and double exposure PIV images were recorded which took roughly 10 minutes. Data processing was done with DaVis 8.2 on a graphics processing unit (GPU) with total number of 1536 cores. The interrogation window size of 64×64 pixels with 50% overlap and 4 passes followed by a 16×16 pixels window size with 50% overlap and 3 passes was selected as the processing scheme. With this setting, the spatial resolution of the vector field was about 0.73×0.73 mm^2. In the vector post-processing, a median filter was applied to eliminate the spurious vectors and to fill the empty areas with the interpolation of neighboring vectors. The experiments were repeated several times for some velocity ratios and the repeatability of the results were proven. More details of the test setup along with the jet and boundary layer velocity profiles over the flat plate were described previously by Mahmoudi et al. [15]. The uncertainty estimation of the measured quantities is presented in Appendix 1.

4.3   Results and discussion

4.3.1   Mean flow

The velocity field of the wall jet in counter-flow was measured at different jet to counter-flow velocity ratios, up to $U_R = 25$. The wall jet in counter-flow velocity field showed random and large amplitude oscillations in both the axial and the lateral directions. This random oscillation is due to the generation of large vortical structures in the shear layers of the jet and opposed flow and will be discussed later with more detail. Figure 4-2 shows the average axial velocity contours and the streamlines for $U_R = 20$ in the jet central plane. The dashed thick line shows the location where the mean axial velocity is zero (loci of $u=0$). It is seen from the stream lines that the jet penetrates into the counter-flow and after reaching to a stagnation area, turns back with the oncoming flow. There is a large recirculation region close to the stagnation area which provides a mixing zone for the jet and the oncoming ambient flow. The jet reaches the mean axial stagnation point at around $x/D = 68$. The instantaneous penetration length oscillated randomly between x/D=60 to 80 which showed maximum 20% deviation from the mean penetration length. Yoda and Fiedler [10] reported a maximum instantaneous penetration length equal to 1.5 X_p for the free jet in counter-flow. So, the wall jet in counter-flow has a lower oscillation amplitude compared to the free jet; this is due to the stabilizing effects of the wall.
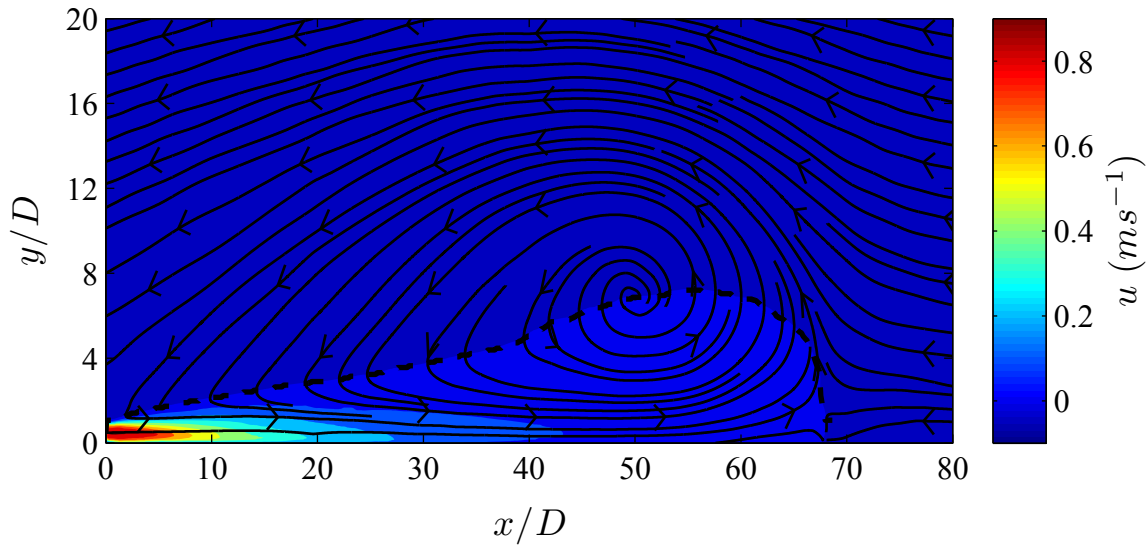
Figure 4-2: Mean axial velocity contours and streamlines for U_R=20.

At low momentum ratios, as previously mentioned, the penetration distance for a free jet in counter-flow varies linearly with velocity ratio. The normalized mean penetration distance in the axial direction versus velocity ratio for the 3D round wall jet in counter-flow is shown in Figure 4-3 along with the results reported for free jet and 2D slot wall jet. The best power law fit (R^2>98%) passing through current data points was found in the form of:

$$X_p/D = 14U_R^{0.53} \qquad\qquad (3)$$

It is seen from Fig. 4-3 that both the 2D and 3D type wall jets penetrate more than a free jet in counter-flow at the same velocity ratio and the friction from the wall side has negligible effect. As previously mentioned, since the wall jet is bounded on one side, it is more stable than a free jet in counter-flow. As a result, less ambient flow with negative momentum enters into the wall jet and the rate of its momentum loss is lower than a free jet in counter-flow. On the other hand, the penetration length of the 3D wall jet in

counter-flow is lower than that of the 2D slot wall jet in counter-flow reported by Balachandar et al. [13] and Tanaka et al. [14]. For the 3D wall jets, the momentum spreading rate in the lateral direction is much higher than in the streamwise direction [16]. So, most of the wall jet momentum spreads in lateral direction and leads to the lower penetration depth of the 3D wall jet in counter-flow compared to 2D case.
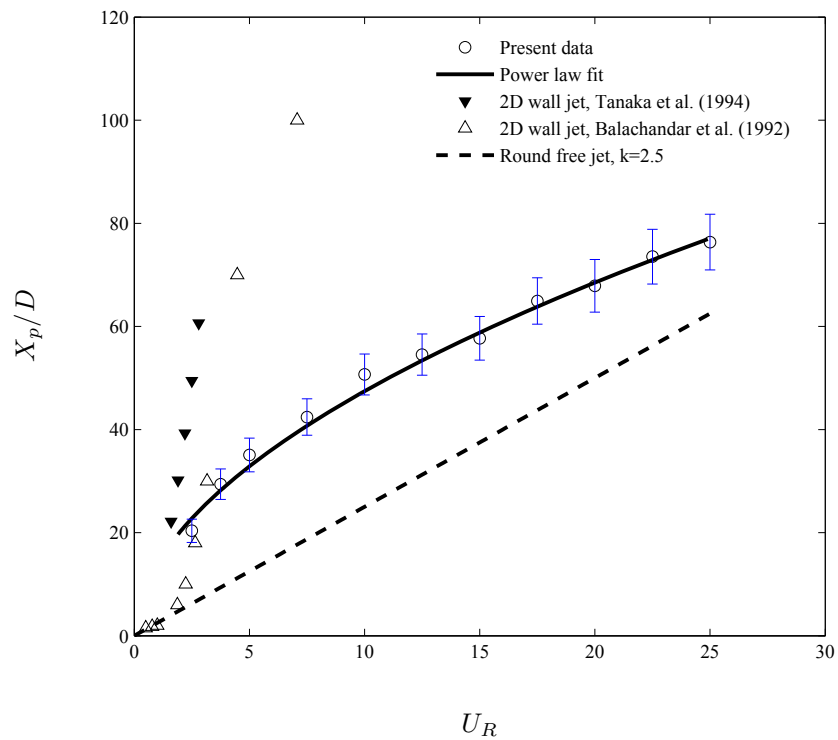
Figure 4-3: Mean penetration length versus velocity ratio, error bars are standard deviations.

The normalized maximum velocity decay of the wall jet as a function of penetration depth is shown in Figure 4-4 for jet to counter-flow velocity ratios of $U_R > 15$ corresponding to the jet Reynolds numbers above 6,000. It is seen from Figure 4 that these profiles completely collapse on each other for $x / X_p > 0.15$. For the range of

$0.15 < x / X_p < 0.7$, a power law curve with the same decay rate of -1.08 as previously

reported for the same wall jet in quiescent ambient [15] can be fitted to the data in the

form of:

$$U_m / U_{jm} \, X_p / D = 5.4 \, (x/X_p)^{-1.08} \qquad (4)$$

In the range of $0.7 < x / X_p < 0.8$ there is a transition region and the velocity decay profiles

change their behavior after an inflection point. Beyond $x / X_p = 0.8$, where the wall jet

loses its momentum and the counter-flow has the dominant role, the velocity decays

linearly with the slope of -25 and vanishes at $x / X_p = 1$.
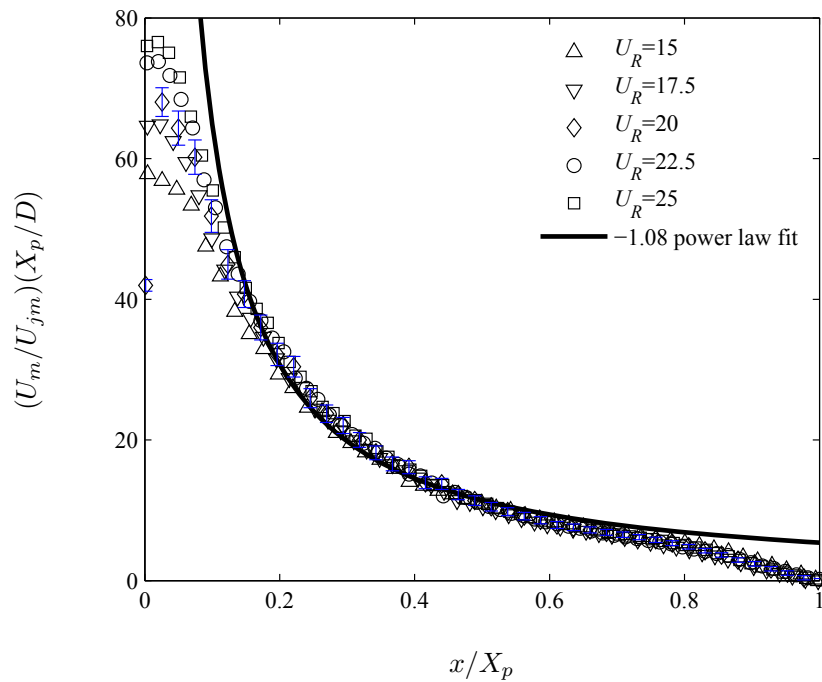
Figure 4-4: Maximum velocity profiles for the wall jet in counter-flow versus penetration length, (error bars are for U_R=20 but it is expected that error for other velocity ratios be similar).

Wall jets have traditionally been analyzed as a combination of two shear layers, with the first shear layer (also called inner layer) starting from the wall and ending at the point of maximum velocity (U_m) and the second layer (outer layer) beginning from the point of maximum velocity and continuing to infinity. The half velocity width ($y_{1/2}$) and maximum velocity were used frequently as the scaling parameters in wall jet studies [17, 18]. For the 3D wall jets in still ambient flow, the half velocity width grows linearly in the developed zone with its slope reported between 0.037 to 0.065 by different researchers [16]. In this study, with the current test setup and with no counter-flow, the slope of the half velocity width was estimated to be 0.04 as reported previously [15]. Figure 4-5 shows the variation of the half velocity width for various wall jet to counter-flow velocity ratios. Up to x/X_p=0.7, it varies linearly with the slope of 0.04 similar to a wall jet in still ambient fluid and then increases dramatically to reach a maximum at x/X_p= 0.9. After that, it decreases rapidly toward zero as the wall jet loses all its momentum and reaches the stagnation point. The half velocity width is an important length scale for jet flows and its slope indicates the spreading rate of the jet. The higher the slope, the higher the mixing rate. The spreading rate of the wall jet in counter-flow in the stagnation zone is higher due to the interaction between the vortical structures of the flow.
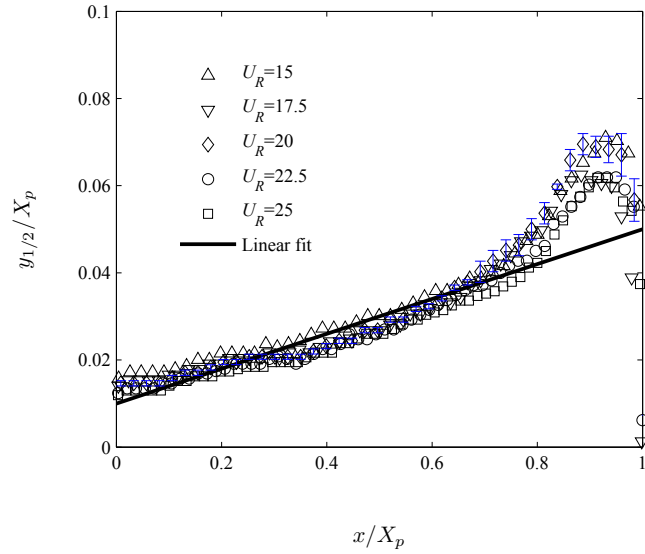
Figure 4-5: Variation of the half velocity width versus penetration length (error bars are for U_R=20 but it is expected that error for other velocity ratios be similar).

To study the self-similarity of the velocity profiles, the wall jet axial velocities were normalized at various locations using the outer layer scales. Figure 4-6 shows the resulting velocity profiles for the wall jet in counter-flow at a velocity ratio of $U_R = 20$.
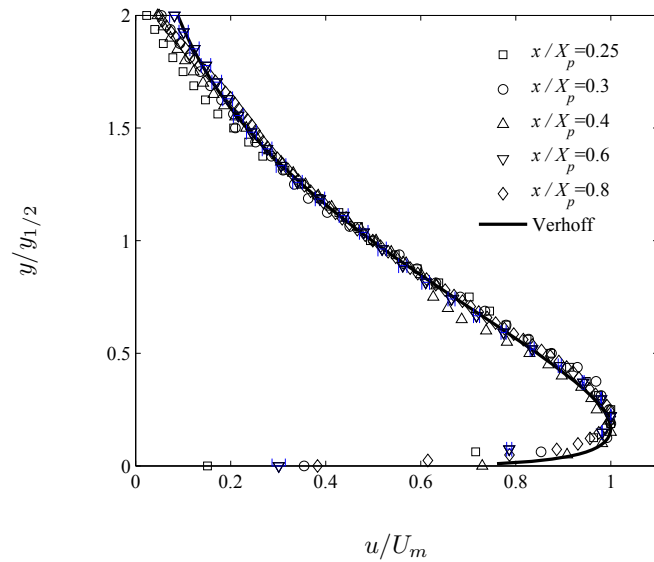
Figure 4-6: Normalized axial velocity profiles of the wall jet in counter-flow at U_R=20.

Self-similarity of the velocity profiles was observed in the range of $0.25 < x/X_p < 0.8$. The mean flow profiles are quite similar to the fully developed wall jet in still ambient fluid and collapse well onto each other up to $y/y_{1/2} = 2$, which is close to the height of $u=0$. The well-known velocity distribution for the wall jets proposed by Verhoff [19] is fitted quite well to the current data in the form of:

$$u/U_m = 1.48(y/y_{1/2})^{1/7}[1 - \text{erf}\,(0.68(y/y_{1/2}))] \qquad (5)$$

The maximum value of velocity profiles occurs at around $y/y_{1/2} = 0.2$ and the second derivative of the velocity profiles is zero (inflection) at around $y/y_{1/2} = 0.6$, see Fig. 4-6.

Figure 4-7 shows the variation of the two other scales of the flow, the height of maximum velocity (y_{U_m}) and the height of zero axial velocity ($y_{u=0}$) in which the jet streamwise velocity becomes zero due to interaction with the counter-flow. The maximum velocity height has a similar behavior of a wall jet in quiescent ambient up to $x/X_p = 0.8$ and then increases rapidly in the stagnation region, see Fig 4-7(a). The loci of zero axial velocities collapse well on each other and show a maximum value of 0.1 at $x/X_p=0.8$ as shown in Figure 4-7(b).
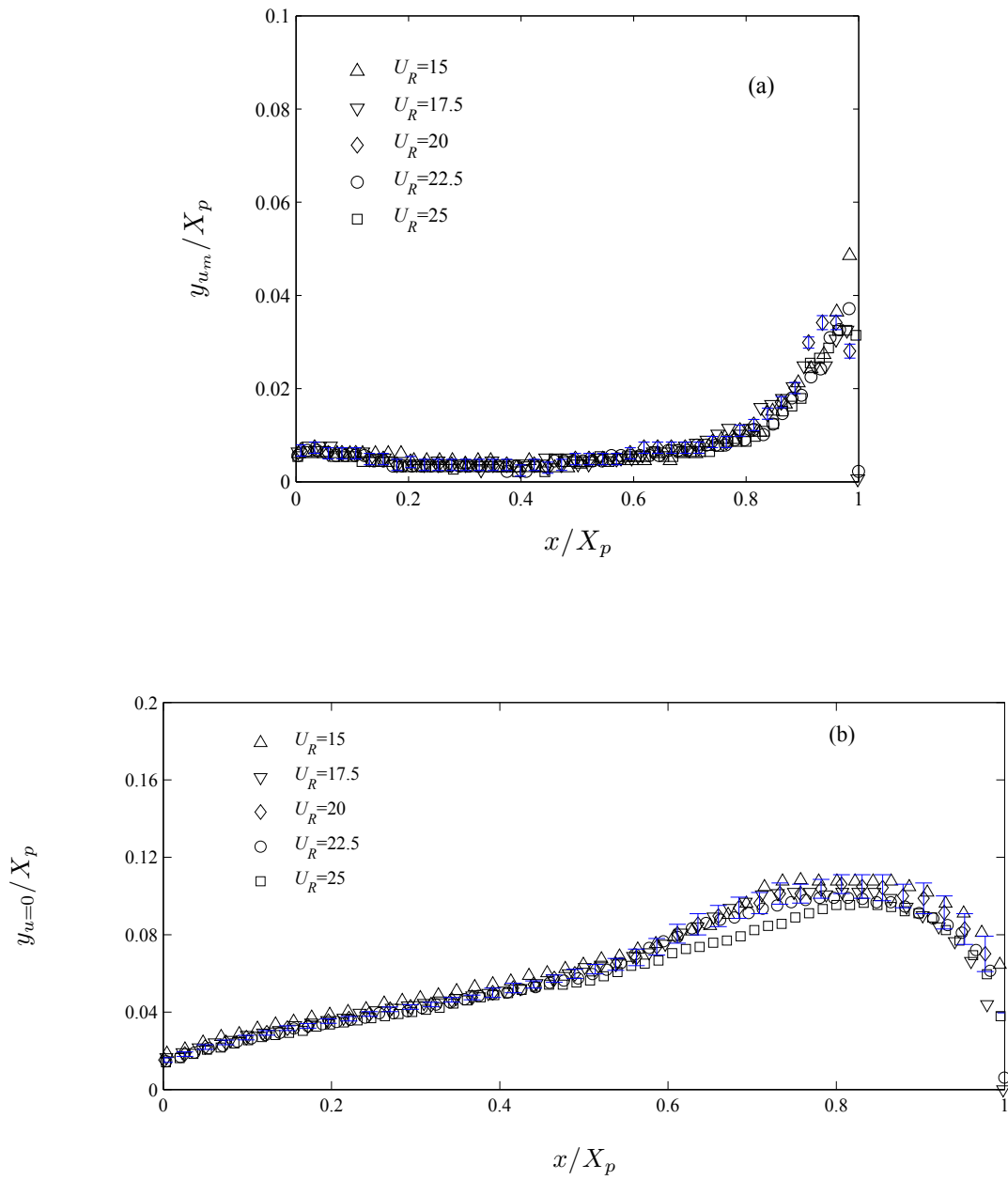
Figure 4-7: The variation of maximum velocity and zero velocity heights versus normalized axial distance (error bars are for U_R=20 but it is expected that error for other velocity ratios be similar).

4.3.2   Vortical structures

One of the interesting features of the jet in counter-flow is the creation of a large recirculation zone near the stagnation area. This phenomenon was studied in early developments of jet engines to be used as an aerodynamics flame holder by providing low velocity regions and trapping a portion of hot combustion products for maintaining sustained combustion. The interaction of the jet with the opposed flow creates vortical structures which enhance the mixing efficiency of the jet in counter-flow. Despite the fact that these structures are an important aspect of the jet in counter-flow, there is no study about their formation mechanism and their physical characteristics. In this section we try to study these vortices in more detail.

As mentioned by Kline and Robinson [20], "A vortex exists when instantaneous streamlines mapped onto a plane normal to the core exhibit a roughly circular or spiral pattern, when viewed in a reference frame moving with the centre of the vortex core". In simple flows with low shear, it is possible to capture the vortices and their physical characteristics by identifying isolated regions with high vorticity. However, in complex flow fields, vortices are usually masked by regions of high shear and the vorticity field analysis cannot reveal their characteristics [21].

In this study, critical point analysis of the velocity gradient tensor is used to identify and study the vortices and their interactions. This method works based on the definition of Kline and Robinson as described above. The critical point or phase plane analysis has been used in finding the solution trajectories of ordinary differential equations [22]. A general discussion about using this method in finding the topology of three-dimensional large structures in flow fields is reported by Chong et al [23]. They showed that the

82

solution trajectories of the fluid elements have spiral movement or closed circular shapes if the characteristics equation of the velocity gradient tensor had imaginary roots. This method has been applied widely as an effective tool for identifying large vortical structures in velocity fields from PIV studies [24].

For our analysis, the 2D velocity gradient tensor was obtained by central differencing of the velocity vector field resulting from 2D PIV experiments. In the boundaries, depending on the position, forward or backward difference schemes were applied. Following Vollmers [25] the discriminant of the characteristics equation of the 2D velocity gradient tensor is:

$$\Delta = (\partial u/\partial x + \partial v/\partial y)^2 - 4[(\partial u/\partial x)(\partial v/\partial y) - (\partial u/\partial y)(\partial v/\partial x)] \qquad (6)$$

The areas with negative discriminant (imaginary eigenvalues) represent vortices in the flow.

Figure 4-8 shows an instantaneous realization of the flow with the vortices and the schematic of streamlines in the central plane of the wall jet in counter-flow at U_R=20. The swirling direction of these structures was found by analyzing the vorticity sign at those locations. The red areas show positive (counter-clockwise) and the blue ones show negative (clockwise) vortices. The thick black curve shows the location of zero axial velocity of the mean flow (loci of u=0).

From Figure 4-8, it is seen that the backward facing wall jet provides a large turbulent region in the flow. The wall jet creates positive vortices in the outer layer and negative vortices in its inner layer. These structures penetrate to the opposed ambient flow, grow in size and finally reach a zero advection velocity as they approach the instantaneous

stagnation area. The positive vortices roll back on each other and merge together to provide a very large recirculation zone as observed in the mean velocity field as well, see Fig. 4-2.
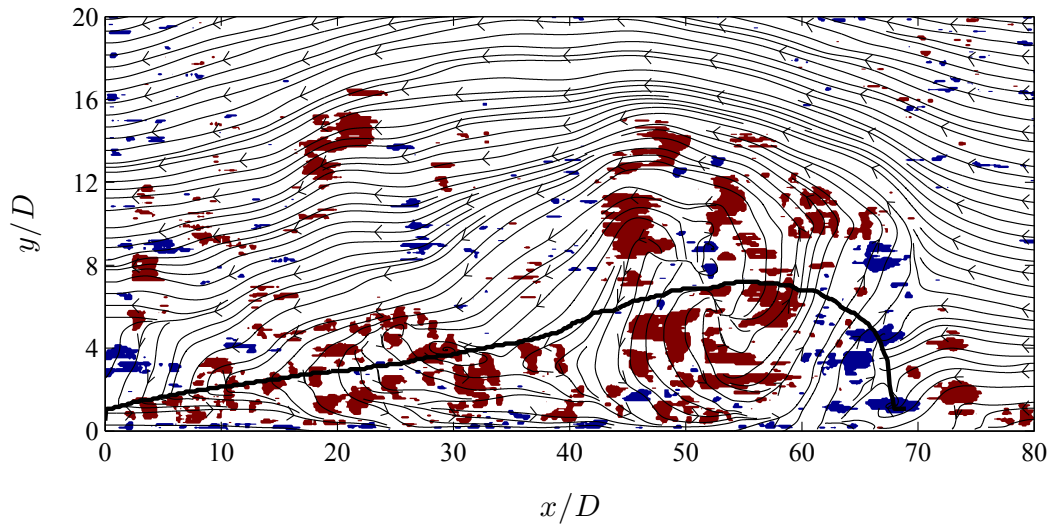
Figure 4-8: Vortical structures in an instantaneous realization of the velocity field, thick line indicates loci of zero axial velocity.

The negative vortices make a layer, separating counter-clockwise vortices coming from the wall jet and those left moving positive vortices generated by the counter-flow boundary layer on the flat plate. In the stagnation area while the axial momentum is almost zero, vortical structures play the dominant role in the mixing of the jet and counter-flow. Strong vortices (either positive or negative) drag the flow inside, circulate it and enhance the mixing by straining the fluid elements and increasing the contacting surface area of the jet and counter-flow. The induced velocity resulting from the combination of vortices creates random fluctuations of the flow which stimulates the mixing. As Figure 4-8 shows, a portion of vortices enter to the jet body due to the entrainment mechanism and some of them move back with the counter-flow and enhance

mixing downstream. However, much of the mixing process happens in the stagnation area as the population of vortices is higher there.

Two-point velocity correlation functions have been used widely in turbulent boundary layer analysis to investigate the average shape and size of large turbulent structures [26, 27]. In this study, the normalized spatial velocity correlation functions at a reference point (x_r, y_r) in the wall jet symmetry plane are evaluated in the form of:

$$R_{uu} = \frac{\overline{u'(x_r, y_r)u'(x_r + \Delta x, y_r + \Delta y)}}{\overline{u'^2(x_r, y_r)}}$$

and   (7)

$$R_{vv} = \frac{\overline{v'(x_r, y_r)v'(x_r + \Delta x, y_r + \Delta y)}}{\overline{v'^2(x_r, y_r)}}$$

where u' and v' are fluctuating velocity components in streamwise and wall-normal directions obtained by subtracting the mean velocity field from the instantaneous one and Δx and Δy are distances from the reference point.

Figure 4-9 shows the correlation contours of R_{uu} and R_{vv} at two reference points selected on $u=0$ line at 10% and 80% of the wall jet penetration distance for $U_R=20$. It is seen from Fig. 4-9 that the correlated regions of horizontal velocity fluctuations are larger than those of the vertical fluctuations which means the turbulent structures have more contribution in creating the streamwise portion of turbulent kinetic energy (TKE). The R_{vv} contours have almost circular shapes while the R_{uu} contours are elongated in x direction up to $x/X_P=0.8$. Following Christensen and Wu [28], twice the distance from each reference point to the location in which $R_{uu}=0.5$ is estimated to show the order of the size of integral scales of the turbulent flow passing through that point. Figure 4-10 shows the

variation in the size of the integral scales of the flow on the $u=0$ line versus jet

penetration up to $x/X_p=0.8$. In fact it can be interpreted as the average streamwise and

wall normal extent (Lx_{uu} and Ly_{uu}) of the vortical structures on the thick line indicated in

Figure 4-8. It is observed that the vortices are circular at regions very close to the jet exit

plane and they grow and change to elliptical shapes with axial to lateral length ratio of

about $Lx_{uu}/Ly_{uu}=2$ as they move forward. The vortices grow linearly as the jet penetrates

in the counter-flow. It is seen from Figure 4-10 that at $x/X_p=0.8$ the streamwise and lateral

extent of the large vortices are $8D$ and $4D$ which is consistent with the instantaneous

vortical patterns shown in Figure 4-8.
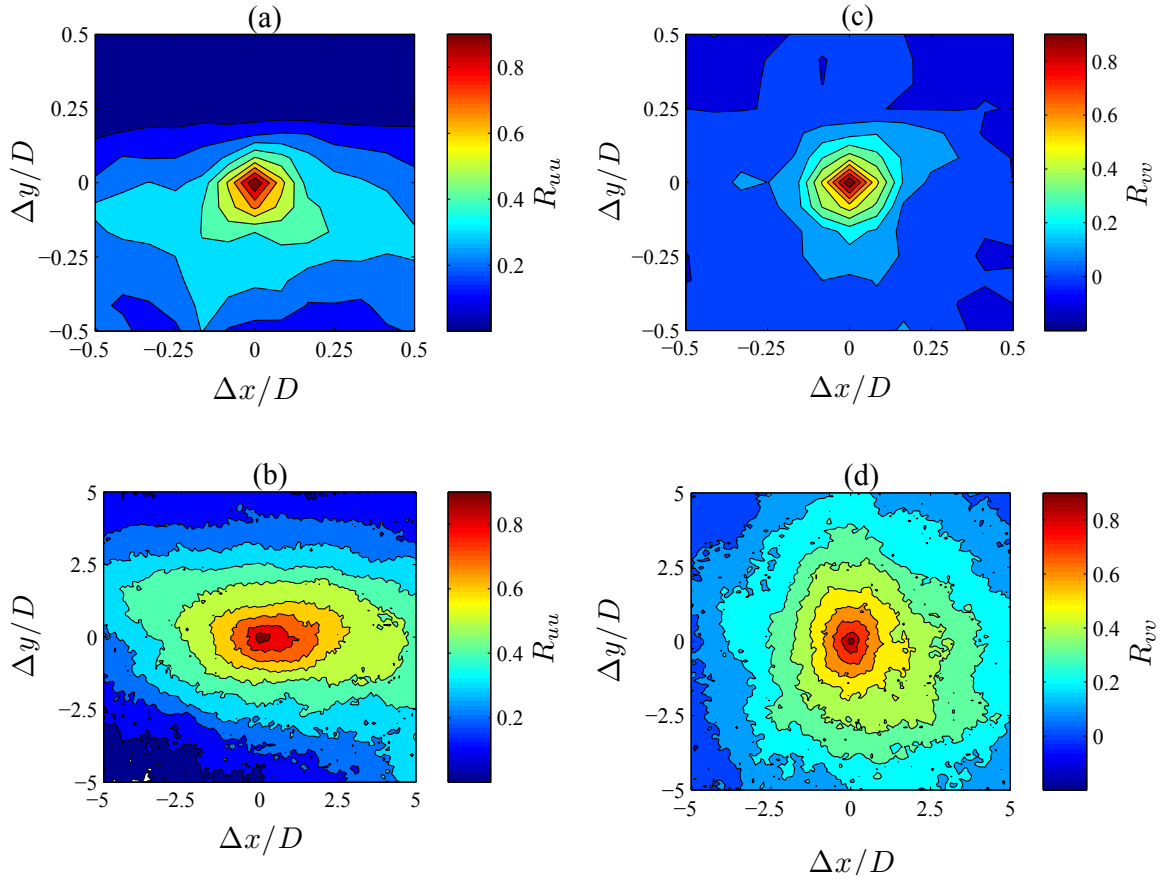
Figure 4-9: The contours of velocity correlations at 10% and 80% of the penetration length on the loci of zero axial velocity for U_R=20.
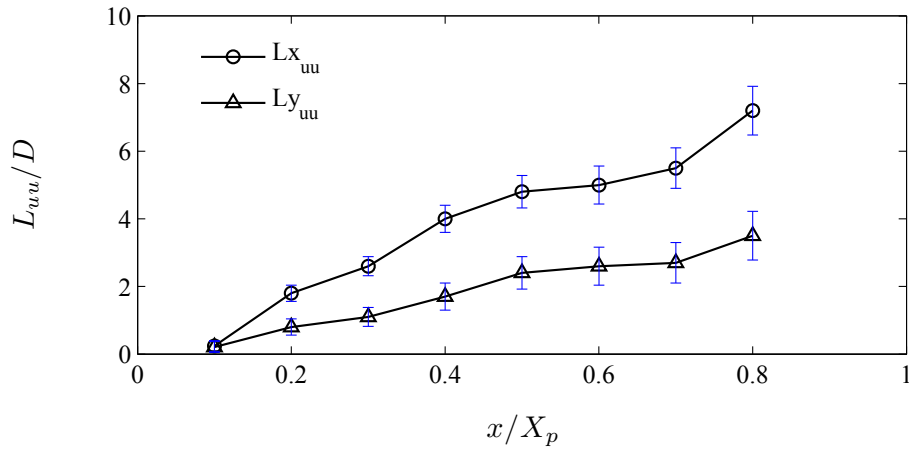
Figure 4-10: Streamwise and wall normal extent of vortical structures based on R_{uu}=0.5.

At the mixing stagnation zone where the flow retards to zero velocity, the elliptical autocorrelation distribution changes to a horizontal heart-shape structure, see Fig. 4-11. In this region the advection velocity of fluid elements is very low which causes a very long integral time scale of the flow. Therefore vortices coming from the jet and those that are returning back with the counter-flow have enough time to mix, showing a high correlation due to their slow advection.
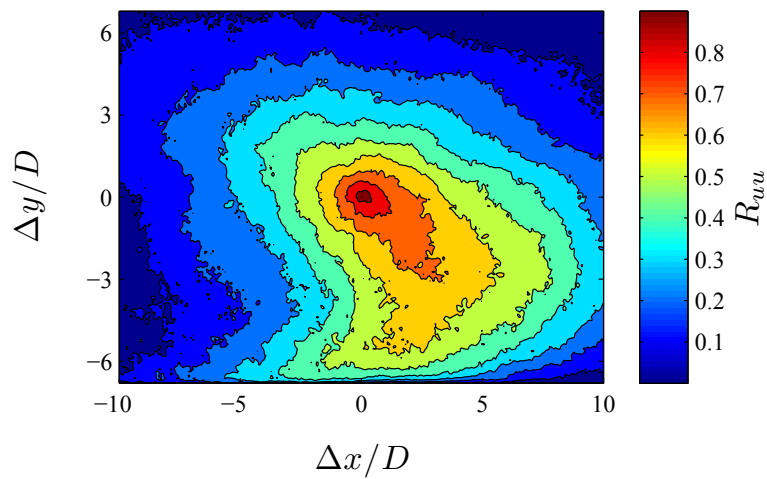
Figure 4-11: Contours of R_{uu} at 90% of the penetration length on the loci of zero axial velocity for U_R=20.

4.3.3   Turbulence statistics

 Studying the behavior of turbulent statistics of the wall jet in counter-flow is the last part of this experimental analysis. The normalized Reynolds stresses in the streamwise symmetry plane of the wall jet in counter-flow at U_R=20 and jet Reynolds number of Re_j= 8.1×10^3 are shown in Figure 4-12. Due to complexity of the flow field and lack of data in stagnating flows in the literature, the stagnation area is selected for in depth analysis. As seen from Figure 4-12, the streamwise Reynolds stress is dominant in the flow field. This is in agreement with larger the streamwise extent of R_{uu} correlations as discussed before.

It is observed from Figure 4-12 that close to the wall region, by approaching the stagnation area in horizontal direction, the magnitude of Reynolds stresses decrease and they reach a local minima at x/D =55, equivalent to 80% of the jet penetration length. This is consistent with decreasing the mean axial velocity of the flow approaching the stagnation area. In the vertical direction, as Figure 4-12 shows, up to x/D=55, the $\overline{u'^2}$ and $\overline{v'^2}$ stresses start from zero at the wall and grow in vertical direction to reach their absolute maximum value at y/D=1.5 and y/D=2 respectively. $\overline{u'v'}$ starts from negative values in the wall region and reach to maximum at y/D=2, similar to $\overline{v'^2}$.

An interesting phenomenon is the existence of a local maxima for the Reynolds stresses in the vicinity of the stagnation area which is more visible in Figure 4-12 (a) for $\overline{u'^2}$ contours. It is observed that after the local minima at x/D =55, the stresses increase again to reach to a maxima very close to the stagnation area where the mean axial velocity vanishes. It seems that the reason for this increase is the negative vortices which rise from the inner layer of the wall jet (blue vortices shown in Figure 4-8) and passing through this

region. These structures have stronger vorticity and induce a high level of fluctuations into the flow. They also entrain the counter-flow providing an effective mechanism for engulfing the kinetic energy of the ambient counter-flow and converting it to TKE in the stagnation area.

Figure 4-13 shows the distribution of Reynolds stresses normalized with jet local maximum velocity in vertical direction at several axial distances from the jet exit plane at U_R=20. It is observed that the profiles collapse onto each other and show self-similarity in the range of $0.3<x/X_p<0.7$. Beyond this range the profiles does not show a unique behavior as the turbulent flow field is not fully developed yet. Above the range the profiles show very high values as the normalizing factor in the denominator (U_m) goes to zero approaching the stagnation area (see for example the stress values for x/X_p=0.9 at Figure 4-13). The high Reynolds stresses in the stagnation zone creates higher mixing and heat transfer rate as previously reported by Volchov et al. [29].

The normalized streamwise Reynolds stress profiles show two peaks, one at $y/y_{1/2}$=0.1 and the second one at $y/y_{1/2}$=0.5, respectively. The second peak value is around 0.17 which is larger than the amount of 0.13 previously reported by Agelin-Chaab and Tachie [18] for a 3D round wall jet in still flow. The reason can be the adverse pressure gradient imposed by the stagnation area in the downstream of the wall jet in counter-flow which enhances the fluctuations and reduces the magnitude of mean flow. The wall normal stresses monotonically rise from zero at wall region and show maximum values of 0.06 at $y/y_{1/2}$=0.7. The normalized shear stresses start from negative values of about -0.01 very close to the wall and change sign at around $y/y_{1/2}$=0.07. The maximum value of shear stresses is almost equal to 0.03 and happens at $y/y_{1/2}$=0.7.
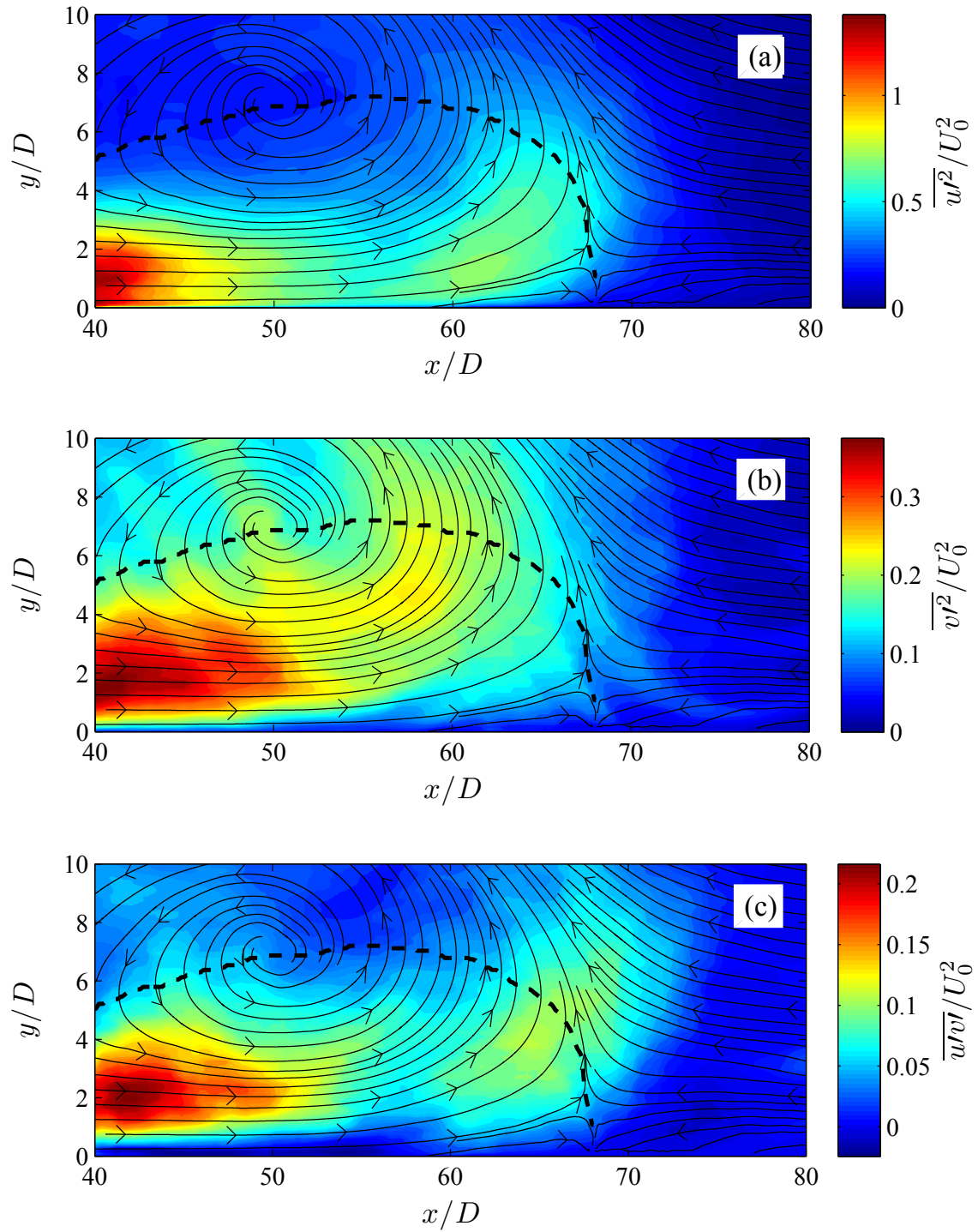
Figure 4-12: The contours of Reynolds stresses for U_R=20, dashed line is indicating loci of zero axial velocity.
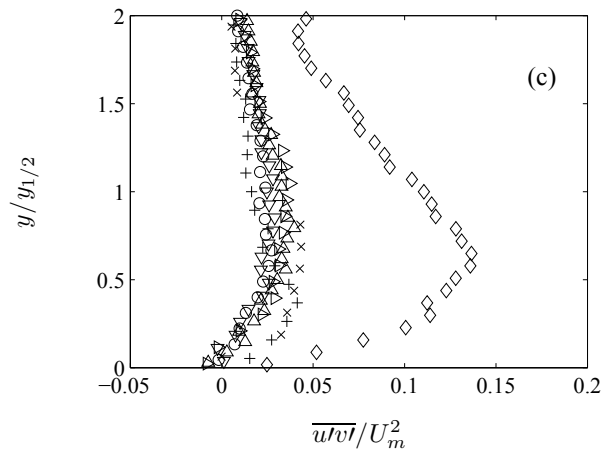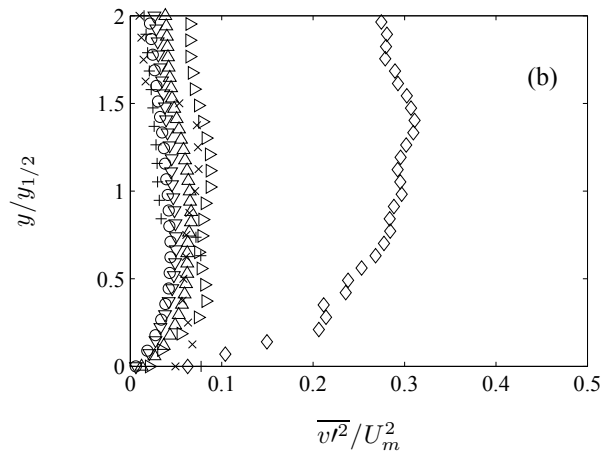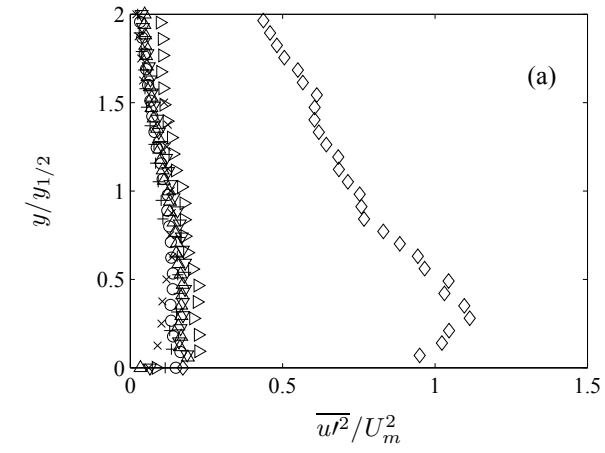
Figure 4-13: The normalized profiles of Reynolds stresses at U_R=20. The symbols ×, +, o, ∇, Δ, $\triangleright$, $\diamond$ represent x/X_p = 0.3 to 0.9 with steps equal to 0.1.

4.4   Conclusion

Extensive experiments were performed in a water channel facility to investigate the mean and fluctuating velocity field of a round wall jet in counter-flow. The jet to counter-flow velocity ratio was changed from 2.5 to 25 corresponds to the jet Reynolds number from 10^3 to 10^4. The critical point analysis and autocorrelation of the velocity field are used to analyze the qualitative physics of the vortical structures in the flow. The main findings are:

1) The wall jet in counter-flow has random oscillation but their amplitude is low compared to a free jet in counter-flow, due to the stabilizing effects of the wall. This causes lower entrainment of the ambient flow into the wall jet.

2) The penetration length of a round wall jet in counter-flow has a power law relation with the velocity ratio. It is higher than the penetration length of a free jet in counter-flow and lower than that of the 2D wall jet case.

3) The decay rate of the maximum velocity and the slope of half velocity width are similar to those of a wall jet in quiescent environment up to 70% of the penetration length. After that the velocity decays linearly and the jet width rises rapidly and reaches to a maxima at 90% of the penetration length.

4) The lateral distribution of the jet velocity is scaled and self-similarity of the profiles was observed between 25% to 80% of the penetration length.

5) The counter-clockwise vortices in the outer layer of the wall jet at the stagnation area merge together and make a large recirculation region. The interaction of the vortices provided by the wall jet and those created by the turbulent boundary layer of the counter-

flow enhances the mixing and momentum transfer in the stagnation zone. The induced velocity provided by these vortices plays the major role in random oscillation of the wall jet in counter-flow.

6) Two-point velocity correlation analysis showed that the vortical structures have more contribution in creating the streamwise component of the turbulence kinetic energy. These turbulent structures are elongated in the axial direction with a length to width ratio of two.

7) The turbulence statistics of the flow revealed that the streamwise velocity fluctuations are larger than the wall normal fluctuations. In the stagnation surface, the interaction of the jet and counter-flow provides a local region with high stresses. The profiles of normalized Reynolds stress show self-similarity in the range of $0.3 < x/X_p < 0.7$. Beyond this distance, in the mixing stagnation region, the profiles rise dramatically and lose their self-similarity. The values of normalized Reynolds stresses in the self-similarity region are larger than the reported values for the round wall jets in a quiescent ambient flow.

References

[1] Sekundov, A. N. "The propagation of a turbulent jet in an opposing stream." Turbulent jets of air, plasma and real gas (1969): 99-109.

[2] McDannel, M. D., P. R. Peterson, and G. S. Samuelsen. "Species concentration and temperature measurements in a lean, premixed flow stabilized by a reverse jet." Combustion Science and Technology 28, no. 5-6 (1982): 211-224.

[3] Peck, R.E. "Aerodynamics of a round jet in a counter-flowing wind," *Journal of Aircraft* 18, (1981): 61-62.

[4] Arendt, J., H. A. Babcock, and J. C. Schuster. "Penetration of a jet into counter-flow," Proc. ASCE Journal 82 (1956): 8-11.

[5] Beltaos, S. and Rajaratnam, N. "Circular Turbulent Jet in an Opposing Infinite Stream," Proc. First Canadian Hydraulics Conference, Edmonton, AB, (1973): 220-237.

[6] Morgan, William D., Brian J. Brinkworth, and Gordon V. Evans. "Upstream penetration of an enclosed counterflowing jet," Industrial & Engineering Chemistry Fundamentals 15, no. 2 (1976): 125-127.

[7] Lam, K. M., and H. C. Chan. "Round jet in ambient counterflowing stream," *Journal of Hydraulic Engineering* 123, no. 10 (1997): 895-903.

[8] Chan, C. H. C., and K. M. Lam. "Centerline velocity decay of a circular jet in a counterflowing stream," Physics of Fluids 10, no. 3 (1998): 637-644.

[9] Tsunoda, H., and M. Saruta. "Planar laser-induced fluorescence study on the diffusion field of a round jet in a uniform counter-flow," *Journal of Turbulence* 4, no. 1 (2003): 1-12.

[10] Yoda, M., and H. E. Fiedler. "The round jet in a uniform counterflow: flow visualization and mean concentration measurements," Experiments in Fluids 21, no. 6 (1996): 427-436.

[11] Lam, K. M., and C. H. C. Chan. "Time-averaged mixing behavior of circular jet in counterflow: Velocity and concentration measurements," *Journal of Hydraulic Engineering* 128, no. 9 (2002): 861-865.

[12] Torres, Luis A., Mohammad Mahmoudi, Brian A. Fleck, David J. Wilson, and David Nobes, "Mean concentration field of a jet in a uniform counterflow," *Journal of Fluids Engineering* 134, no. 1 (2012): 014502.

[13] Balachandar, R., L. Robillard, and A. S. Ramamurthy. "Some characteristics of counter flowing wall jets," *Journal of Fluids Engineering* 114, no. 4 (1992): 554-558.

[14] Tanaka, E., Y. Inoue, and S. Yamashita. "An experimental study on the two-dimensional opposed wall jet in a turbulent boundary layer: Change in the flow pattern with velocity ratio," Experiments in Fluids 17, no. 4 (1994): 238-245.

[15] Mahmoudi, M., Nobes, D., and Fleck, B. "An experiment design for measuring the velocity field of a round wall jet in counter-flow," International Journal of Mechanical Engineering and Mechatronics, Vol. 2, (2014): 23-32.

[16] Launder, B. E., and W. Rodi. "The turbulent wall jet measurements and modeling," Annual Review of Fluid Mechanics 15, no. 1 (1983): 429-459.

[17] Law, Adrian Wing-Keung, and Herlina. "An experimental study on turbulent circular wall jets," *Journal of Hydraulic Engineering* 128, no. 2 (2002): 161-174.

[18] Agelin-Chaab, M., and M. F. Tachie. "Characteristics of Turbulent Three-Dimensional Wall Jets," *Journal of Fluids Engineering* 133, no. 2 (2011): 021201.

[19] Verhoff, August. The Two-dimensional, Turbulent Wall Jet With and Without an External Free Stream. No. 626. PRINCETON UNIV NJ, 1963.

[20] Kline, S. J., and S. K. Robinson. "Quasi-coherent structures in the turbulent boundary layer. I-Status report on a community-wide summary of the data," Near-Wall Turbulence 1 (1990): 200-217.

[21] Adrian, R. J., K. T. Christensen, and Z-C. Liu. "Analysis and interpretation of instantaneous turbulent velocity fields," Experiments in Fluids 29, no. 3 (2000): 275-290.

[22] Kaplan, Wilfred. Ordinary Differential Equations. Reading, MA: Addison-Wesley, 1952.

[23] Chong, M. S., A. Eo Perry, and B. J. Cantwell. "A general classification of threedimensional flow fields," Physics of Fluids A: Fluid Dynamics (1989-1993) 2, no. 5 (1990): 765-777.

[24] Christensen, Kenneth T., and Yanhua Wu. "Visualization and characterization of small-scale spanwise vortices in turbulent channel flow," *Journal of Visualization* 8, no. 2 (2005): 177-185.

[25] Vollmers, Heinrich. "Detection of vortices and quantitative evaluation of their main parameters from experimental velocity data," Measurement Science and Technology 12, no. 8 (2001): 1199.

[26] Nakagawa, Shinji, and Thomas J. Hanratty. "Particle image velocimetry measurements of flow over a wavy wall," Physics of Fluids 13, no. 11 (2001): 3504-3507.

[27] Volino, R. J., M. P. Schultz, and K. A. Flack. "Turbulence structure in rough-and smooth-wall boundary layers," *Journal of Fluid Mechanics* 592 (2007): 263-293.

[28] Christensen, Kenneth T., and Yanhua Wu. "Characterization of vortex organization in the outer layer of wall turbulence," Proc. Fourth Intl Symp. On Turbulence and Shear Flow Phenomena, Williamsburg, Virginia, vol. 3, 1025-1030.

[29] Volchkov, E. P., V. P. Lebedev, M. I. Nizovtsev, and V. I. Terekhov. "Heat transfer in a channel with a counter-current wall jet injection." International journal of heat and mass transfer 38, no. 14 (1995): 2677-2687.

Chapter 5: Experimental study of the velocity field of round offset jets in counter-flow

Abstract

Experimental investigations showing the mean and fluctuating velocity field of three dimensional round offset jets in counter-flow are presented. The jet offset ratios are varied from 1.5 to 4.3 and the jet to counter-flow velocity ratios ranged from 2.5 to 20 and the jet Reynolds number were from 1,000 to 8,000. The penetration length of the jet in counter-flow at each offset ratio was measured and compared with the penetration of wall jets and free jets in counter-flow. The jet velocity decay and spreading rate were analyzed and the effect of offset ratio is discussed. The results show that as the offset ratio increases, the jet velocity decays faster and its spreading rate rises. Furthermore, the amplitude of random oscillations of the flow increases when the distance of the jets from the side wall becomes larger. The vortical structures of the flow are analyzed and their impact on the turbulence characteristics is explained. Two-point velocity correlation study shows that the turbulent structures grow as the offset ratio increases. Also, the turbulent transport in the flow amplifies dramatically when the jet has higher distance from the side wall.

5.1   Introduction

The flow of a jet with some distance from an adjacent wall is called "Offset Jet". In this flow configuration, the jet bends toward the wall and attaches to it at a so called "reattachment point" which is located at a distance of (X_r) from the jet exit plane. The tendency of a flow to attach to the nearby wall is called "Coanda Effect" [1]. It happens due to the entrainment of the fluid elements between the wall and the high momentum flow which reduces the pressure at this area and forces the flow to deflect toward the wall and attach to it. In case of an offset jet, after the reattachment distance, the jet passes a transitional state and finally shows the behavior of a wall jet. The offset ratio (m) is defined as the ratio of the jet centerline distance from the wall divided by the jet diameter.

In engineering applications it is typical that the jet flows are located near the walls due to the geometrical constraints or designs for heat transfer or boundary layer control. Offset jets have many applications in air conditioning devices, too. Due to their importance and complexity, offset jets have been studied widely by many researchers, however; most of these investigations were performed for 2D slot jets and in a quiescent ambient flow. Nozaki et al. [2] and Nozaki and Hatta [3] investigated the flow field of a slot jet located close to a flat plate at offset ratios from 2 to 20 using hot-wire probes and pressure sensors. They reported the reattachment distance and the effects of jet aspect ratio and initial turbulence intensity on the flow development. Based on their results, lower aspect ratio and jet turbulence intensity leads to a longer distance for the offset jet to attach the wall.

Pelfrey and Liburdy [4, 5] studied the mean flow and turbulence characteristics of a 2D slot offset jet with offset ratio of $m=7$ at a wind tunnel. The mean flow analysis in their experiments revealed that there was a recirculation region before the reattachment point. The centre of the recirculation zone was consistent with the axial location of minimum wall pressure. In addition, they observed that the upper jet boundary was more unstable and had higher turbulence intensity compared to the lower jet boundary.

Yoon et al. [6] on their experiments found the mean and fluctuating velocity field of a 2D offset jet using hot-wire anemometry and wall pressure measurement. They reported that the suction in the recirculation region provided by the jet entrainment in the form of negative wall pressure coefficient. Nasr and Lai [7, 8] analyzed the mean and fluctuating flow field of a slot offset jet using LDA and recording the wall pressure. The offset ratio and the jet Reynolds number in their experiments were 2.1 and 11×10^3, respectively. They also analyzed the previous available data for the two dimensional offset jets and proposed an empirical relation for the reattachment length versus offset ratio.

Agelin-Chaab and Tachie [9, 10] reported mean and fluctuating velocity field of a 3D round offset jet at offset ratios of 1, 2, and 4. They observed that there is no sustained recirculation area in the near wall region but a flow reversal exists due to the jet entrainment. However, this flow reversal was almost negligible compared to that of 2D offset jets. They found that the reattachment length varied linearly with offset ratio and it was much shorter than previously reported values for 2D and rectangular offset jets.

The survey of literature show that for an offset jet in counter-flowing ambient flow there is no information available. The flow of an offset jets in counter-flow can have many

applications in industries for enhancing mixing and heat transfer in engineering designs. The jet penetrates in the counter-flow due to its higher local momentum. Then, it stops, creates a large swirling area and returns back with the counter-flow. Early studies about jets in counter-flow were focused on their functionality as aerodynamic flame holders in after-burners to replace large bluff bodies in the jet engines [11, 12]. Another application of this flow configuration is the thrust reversing during landing of commercial airplanes that decreases the required runway lengths of short take-off and landing aircrafts [13].

Beltaos and Rajaratnam [14] used a semi-empirical approach to study the mean velocity profiles of a round jet in a counter-flow. They found that the normalized axial penetration length of the jet has a linear relation with jet to counter-flow velocity ratio as:

$$X_p/D = k \, U_j/U_0 \tag{1}$$

where k is a constant coefficient equal to 2.6 based on their experiments. They also combined potential flow theory with their findings in an attempt to predict the shape of the stagnation stream surface, though this was not in good agreement with the experiments.

Morgan and Brinkworth [15] applied flow visualization and found a relation for penetration distance versus the momentum ratio of the jet and the counter-flow. They observed a linear relation ($k = 2.5$) between the penetrating distance and the velocity ratio when the momentum ratio of jet and counter-flow was less than 0.25. Other researchers [16-18] reported a linear coefficient, k, between 2.5 to 2.8 for the jet axial penetration distance at low momentum ratios of jet and counter-flow.

The velocity and scalar concentration field of jets in counter-flow were also studied by several researchers. Bernero and Fiedler [19] used PIV and PLIF simultaneously to study the flow of a round jet in counter-flow for velocity ratios up to U_R =20. They found that the growth of the half-width for the jet velocity and concentration are greater than that of the jets in quiescent ambient and that the self-similarity of velocity and concentration profiles exists only in a limited zone in the central part of the jet. Torres et al. [20] studied the concentration field of a round jet in counter-flow using PLIF at velocity ratios of 4 <U_R<19. They applied different sets of the flow length scales to investigate the self-similarity of concentration profiles and extracted empirical relations to predict the dilution of the scalar concentration field of counter-flowing jets.

Some literature on wall jets in an opposing stream also exist but is more scant than for a free jet in counter-flow. Balachandar et al. [21] qualitatively analyzed a slot wall jet in counter-flow at velocity ratios up to U_R = 8 using dye visualization and wall pressure measurement in a water channel. In another study, Tanaka et al. [22] used hot-wire anemometry in a wind tunnel and reported the velocity patterns of a plane wall jet in the opposite direction of a turbulent boundary layer. The velocity of the opposed flow in their experiment was set to U_0 = 20 m/s and the jet to counter-flow velocity ratio was varied up to 3.

Recently Mahmoudi and Fleck [23] studied the flow field of a round wall jet in counter-flow at velocity ratios up to 25 using PIV. They found that the 3D wall jet in counter-flow penetrates more than a free jet in counter-flow at the same velocity ratios and reported an empirical relation for the penetration length of the wall jet as:

$$X_p/D = 14U_R^{0.53} \tag{2}$$

They observed that in the range of 0.25<x/X_p<0.8 the velocity profiles show self-similarity. In addition, they analyzed the vortical structures of the flow and their average shapes. The turbulence statistics such as the Reynolds stress profiles and triple products of velocity fluctuations were reported, too. Their study shows that the turbulent fluctuations rise in the stagnation region due to the accumulation of vortical structures and their interaction.

To the authors' knowledge the counter-flowing offset jets, despite their wide potential applications, have not been studied yet. Round offset jets in counter-flow can be installed in pipelines, mixing chambers, heat exchangers, and chemical reactors to provide a controlling mechanism to achieve better mixing efficiency. They also can be used as an effective device to alter near wall flows for controlling boundary layer separation. The objective of this paper is to provide a quantitative velocity field analysis along with turbulence measurement of jets in counter-flow at some distances from a solid wall and at different jet to counter-flow velocity ratios.

5.2 Experimental setup

The experiments were performed in the closed-loop water channel facility at Mechanical

Engineering Department at The University of Alberta. The test section of the water

channel has a cross section area of 680×480 mm^2 and its length is 5000 mm. A flat plate

made from acrylic with size of 400×2000 mm^2 was installed in the channel's side wall far

from its boundary layer. The plate had a chamfer upstream to minimize the stagnation

area and a trip strip was used to ensure a turbulent boundary layer. A brass pipe with

length of 920 mm and inner diameter equal to $D = 8.84$ mm was installed in the mid-

height of the plate to provide the jet flow. The outlet plane of the brass pipe was 1000

mm from the leading edge of the flat plate. The jet holder was designed to have the

capability of adjusting the distance of the jet centerline from the flat plate surface. The jet

was fed by a pressurized tank and a precise flow controller was used in the feed line to

maintain constant jet discharge velocities during the tests. Figure 5-1 shows the

schematic of this test setup.
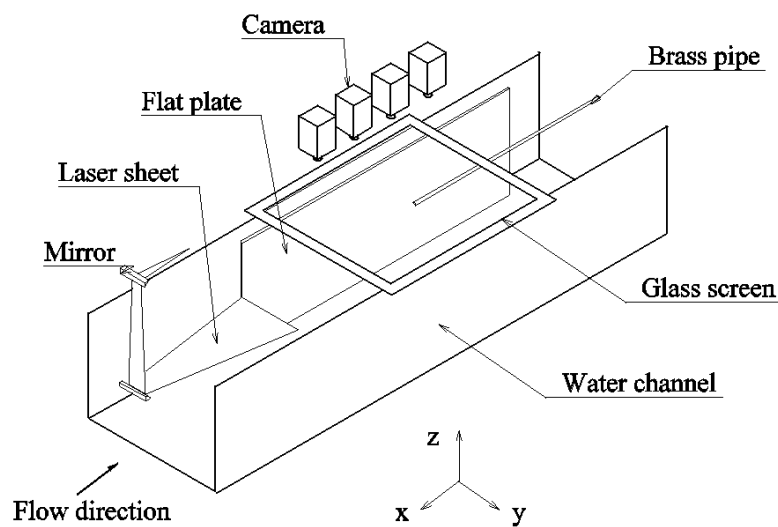
Figure 5-1: The schematic of experimental setup.

The velocity field was measured in the horizontal symmetry plane of the jet using Particle Image Velocimetry (PIV). In this work, four CCD cameras were used in tandem to provide a long field of view for capturing the 2D velocity field from injection to maximum penetration. The cameras were ImagerProX4M provided by LaVision Inc. and have data depth of 14 bits and resolution of 2048×2048 pixels. The cameras orientation was normal to the channel flow and their fields of view had about 15 mm overlap. Later in the data processing, the velocity fields provided from each camera were combined and stitched together to make a large aspect ratio velocity field covering the whole penetration length of the jet. With 50 mm Nikon lenses, the net dimension of the final velocity field was about 720×180 mm^2. Illumination was provided by a Quanta Ray PIV-400 Nd:YAG laser with wave length of 532 nm. The laser sheet was generated by a cylindrical lens and was directed to the test section from upstream by means of a small periscope. The periscope had two first-surface reflecting mirrors with 90 degree installation angle which were fixed on a thin stainless steel frame. The periscope structure was stiff and no vibration was observed in the laser sheet during the experiments. It was installed right after the grid turbulence generator in the channel entrance and had minimum blockage effect on the channel flow. The channel flow was seeded by hollow glass spheres with a mean diameter of 18 μm and to maintain a uniform seeding density, the pressurized tank was filled by the channel flow during the tests. The PIV image acquisition was done by DaVis 8.2 provided by LaVision Inc.

In all experiments, the height of water in the channel was 40 cm and its velocity was set to $U_0 = 4$ cm/s with a measured turbulence intensity equal to 3.5 %. The jet to counter-flow velocity ratio was varied from 2.5 to 20, corresponding to jet Reynolds number

variation of $10^3 < Re < 8 \times 10^3$ based on the pipe diameter. With the chosen channel flow velocity and the jet discharge velocities, the maximum jet to counter-flow momentum ratio was measured to be about 0.14. The jet offset ratio (the distance of the jet centerline from the wall surface divided by the jet diameter) was varied using four different values of 1.5, 2.5, 3.3, and 4.3.

A glass plate was installed on the water surface in the imaging zone to prevent surface waves. When the test setup and all components were ready, calibration of the cameras was performed simultaneously with a large calibration target. Cumulative averaging of the velocity field showed that 1000 images provide an accurate average velocity field in this complex flow. After all the settings were done for each velocity ratio (U_R) and offset ratio (m), 1000 double frame and double exposure PIV images were recorded which took roughly 10 minutes. Data processing was done with DaVis 8.2 on a graphics processing unit (GPU) with total number of 1536 cores. The interrogation window size of 64×64 pixels with 50% overlap and 4 passes followed by a 16×16 pixels window size with 50% overlap and 3 passes was selected as the processing scheme. With this setting, the spatial resolution of the vector field was about 0.73×0.73 mm^2. In the vector post-processing, a median filter was applied to eliminate the spurious vectors and to fill the empty areas with the interpolation of neighboring vectors. The experiments were repeated several times for some velocity ratios and the repeatability of the results were proven. More details of the test setup along with the jet and boundary layer velocity profiles over the flat plate were described previously by Mahmoudi et al. [24]. The uncertainty estimation of the measured quantities is presented in Appendix 1.

5.3   Results and discussion

5.3.1   Mean flow

Figure 5-2 shows the mean axial velocity of the offset jet in counter-flow at offset ratios

of 1.5, 2.5, 3.3, and 4.3 along with the streamlines in the jet symmetry plane normal to

the sidewall. The dashed line in Figure 5-2 shows the loci of zero axial velocity ($y_{u=0}$).

In all cases the jet to counter-flow velocity ratio is equal to 17.5, corresponding to jet

Reynolds number of $Re_j=7.1\times10^3$ based on the exit condition. The jet penetrates into the

upcoming flow, loses all its momentum and reaches a stagnation surface in which its

velocity vanishes. The jet fluid elements then gain negative momentum from the

oppositely moving ambient flow and return back with the counter-flow. The existence of

a large recirculation region is the common phenomena between all offset jets in counter-

flow at the aforementioned conditions. It happens due to the accumulation of counter-

clockwise vortices in the stagnation area and will be discussed with more detail in later

sections.

Jets in counter-flow typically show random oscillations with large amplitudes due to

existence of strong vortices in the flow which alter the jet boundary conditions. The

current study revealed that the amplitudes of the offset jet oscillation were larger compare

to that of the pure wall jet in counter-flow. In the previous study [23] it was observed that

the wall jet in counter-flow has maximum axial oscillation amplitude equal to 20% of the

mean penetration length. In the present experiments, it is found that the oscillation

amplitude for 1.5m and 2.5m offset jets are up to to 30% and 40% of the mean

penetration length, respectively. This value was found to be 45% for the m=3.3 offset jet

and 50% for the m=4.3 offset jet. In the former case, the maximum oscillation amplitude is equal to that of the free jet in counter-flow reported by Yoda and Fiedler [19].

As it is seen from Fig. 5-2, the average jet penetration distance into the counter-flow is different for each jet scenario. At an offset ratio of m=1.5, the jet shows the penetration of X_p=68D which is the largest value among other cases. For m=2.5, the offset jet penetration is X_p = 62D, showing about 10% decrease compare to m=1.5 case. For m=3.3 and 4.3 the penetration lengths are 55D and 47D, respectively. In all cases the velocity contours show non-symmetrical distribution after a short distance from the exit plane, indicating the jet is deflected toward the wall. This tendency for flows to adhere to the nearby wall is called Coanda effect [1]. It happens due to unbalanced fluid entrainment which causes a low pressure region in the wall side that forces the flow to attach to the wall [2, 3]. The normalized reattachment length of the jets into the wall are X_r/D= 3, 5, 7, and 8 for offset ratios of m=1.5, 2.5, 3.3, and 4.3, see Fig. 5-2.
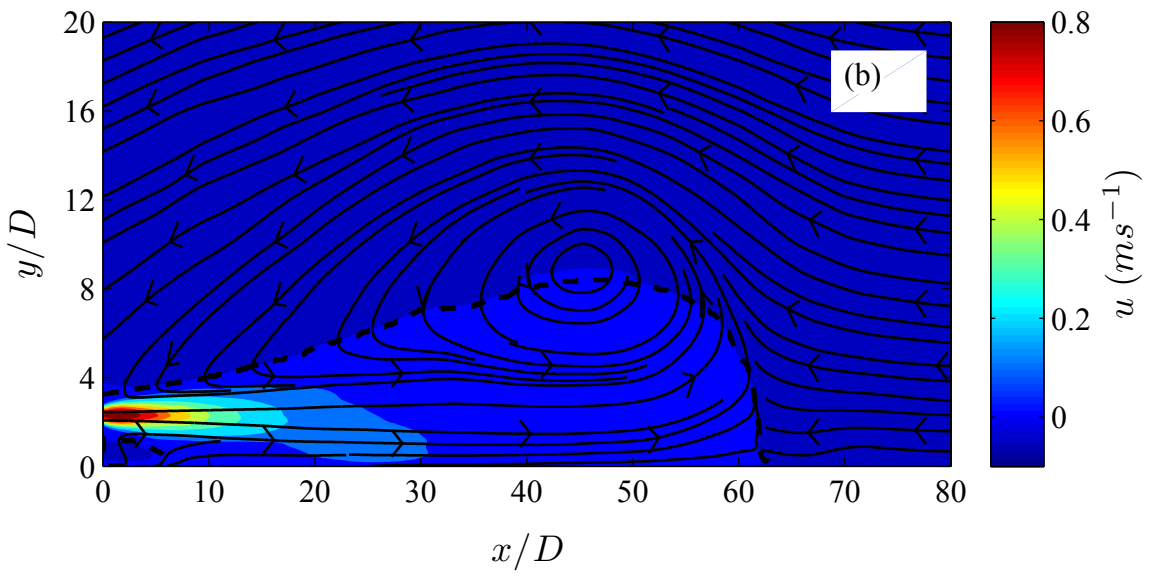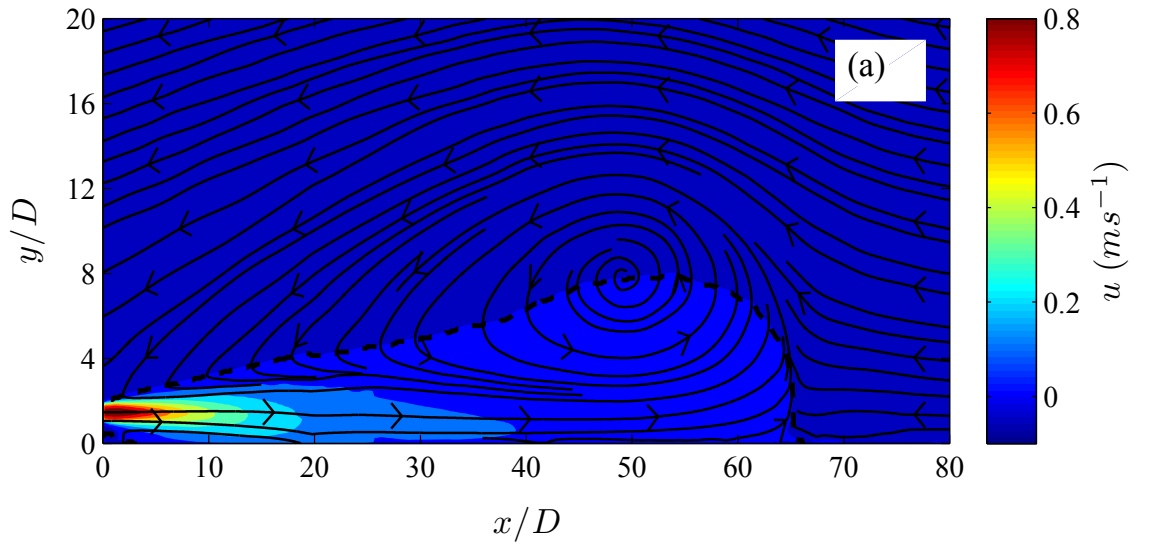
Figure 5-2(a, b), for caption see facing page.
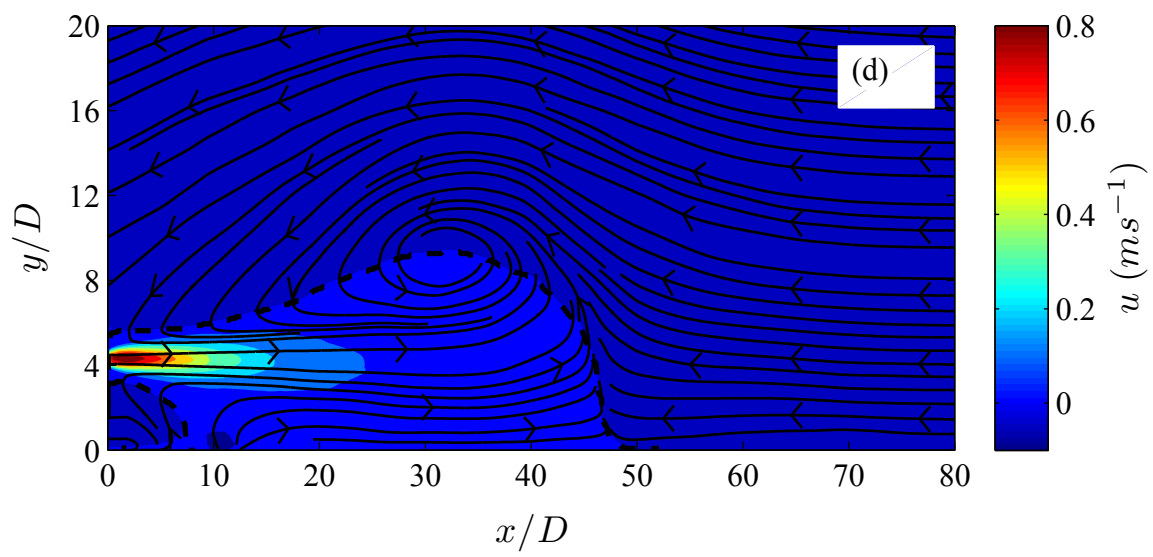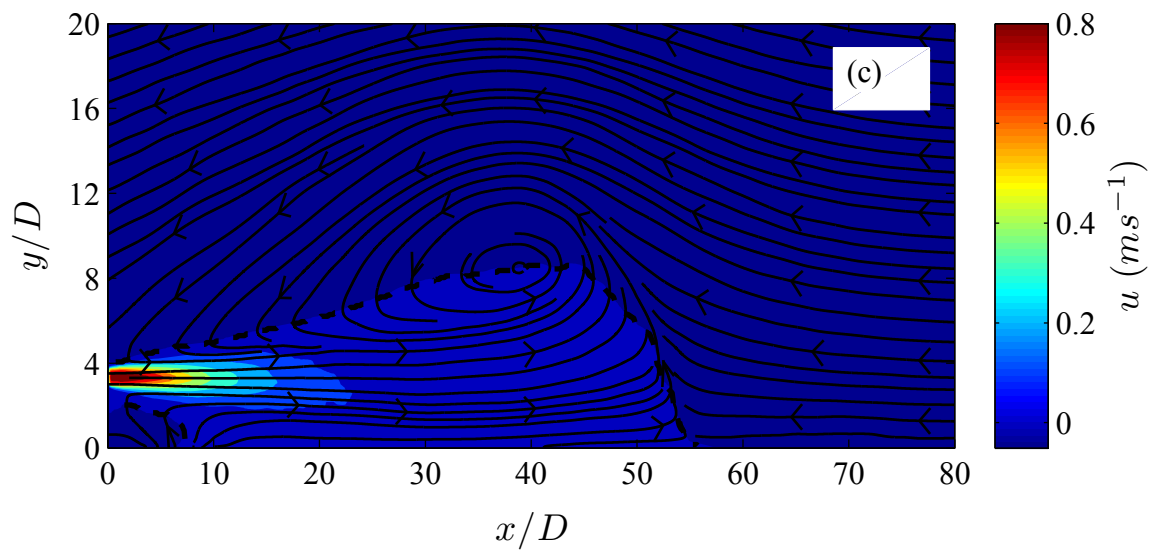
Figure 5-2: The mean axial velocity contours, stream lines, and loci of zero axial velocity for U_R=17.5 (a: offset ratio of 1.5, b: offset ratio of 2.5, c: offset ratio of 3.3, d: offset ratio of 4.3).

The normalized jet penetration distance versus jet to counter-flow velocity ratio is shown in Figure 5-3 for various offset distances. The penetration length of the flush mounted wall jet and free jet in counter-flow are also shown for comparison. It is observed from Fig. 5-3 that in general, the penetration distance of offset jets in counter-flow are located between the two extreme cases of wall jet and free jet in counter-flow. For jet to counter-flow velocity ratios less than 7.5 (U_R<7.5) the offset jet penetrations are entirely lower than that of the wall jet in counter-flow and greater than the penetration length of free jet in counter-flow. For instance at U_R=2.5, the penetration distance of the wall jet and the free jet in counter-flow are equal to 22D and 5D, respectively. The penetration of 1.5m and 2.5m offset jets are equal to 13D which is 140% higher than the penetration length of free jet and 40% lower than that of the wall jet in counter-flow. It is interesting that in the same situation, the penetration of 3.3m and 4.3m offset jets is about 10D, showing 30% lower penetration compared to 1.5m and 2.5m offset jets.

Furthermore, Figure 5-3 reveals that the penetration of the 1.5m offset jet becomes equal to the penetration of a wall jet at U_R=7.5 while this happens for the 2.5m offset jet at U_R=12.5. In the range of 7.5<U_R<20, the penetration of 1.5m and 2.5m offset jets approach to that of the wall jet in counter-flow. The penetration of 4.3m offset jet gets closer to that of the free jet in counter-flow and the penetration of 3.3m offset jet remains somewhere in the middle of free jet and wall jet case.
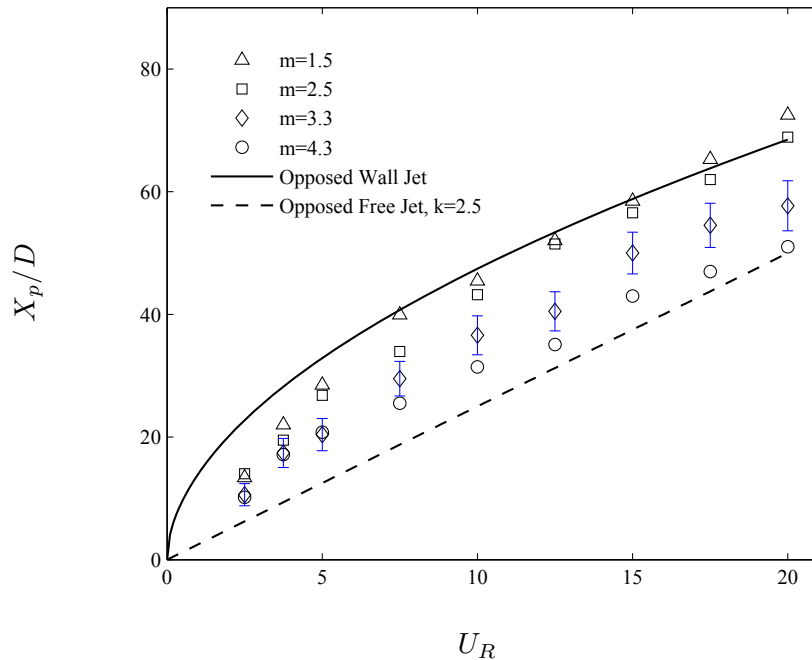
Figure 5-3: The mean penetration length of the jets in counter-flow for various offset ratio (error bars are for m=3.3 but it is expected that error for other offset ratios be similar).

The key factor in analyzing this complex behavior can be found by attention to the velocity contours and stream line patterns at low values of U_R in which the penetration length of the jets in the axial and wall normal direction are low and the effect of offset distance can be seen better. Figures 5-4a to 5-4d show the mean axial velocity contours and streamline patterns for U_R=3.75 and offset ratios of m=1.5, 2.5, 3.3, and 4.3, respectively.

Figure 5-4a shows that for m=1.5 the jet penetration distance is X_p=22.5D and the jet reattachment to the wall happens at X_r=5D. The streamline pattern shows only one recirculation region at the upper jet body thanks to the zero gap between the jet and the wall that eliminates the counter-flow entrainment into the jet from the lower section. For the case of m=2.5 as Figure 5-4b depicts, reattachment occurs at X_r=7D and the

113

penetration length is about 19D, showing a 15% reduction compared to the case of

m=1.5. An interesting phenomenon is observed at the end of the jet penetrating distance

for m=2.5 in which a secondary recirculation region is formed at the lower section

between the wall and the jet body. This small recirculation region indicates that the

entrainment of the counter-flow with negative momentum occurs in lower jet body in

addition to the entrainment from upper section. Thus, the total entrainment of the

counter-flow into the jet is increased compared to the case of 1.5m offset jet. This brings

more negative momentum from the counter-flow into the jet, causing lower penetration

distance for 2.5m offset jet.

Figures 5-4c and 5-4d show that the penetration length for 3.3m and 4.3m offset jets are

almost equal to 17.5D and the streamline patterns reveal two recirculation regions at the

top and bottom of the jet bodies. In these two cases, the counter-flow impact on the jets

limits their extension in axial direction; therefore, they do not attach to the sidewall. The

gap between the jets and the wall allows the counter-flow to easily pass in this region and

enter to the jets. The patterns of streamlines show that the entrainment is not completely

equal from the top side and the bottom side. As Figures 5-4c and 5-4d show, in the near

wall region, the centre of the recirculation regions are located farther from the jet exit

plane compared to the upper recirculation pattern. This indicates that interaction of the

counter-flow and its entrainment is higher in the top side of the jet compared to the

bottom side. In fact, in the wall side, due to the meandering of the jet, at a portion of

times the jet is attached to the wall which reduces the overall ambient flow entrainment.

This is completely visible in the 3.3m offset jet that shows an oscillatory reattachment to

the wall at x=7D, see Fig. 5-4c.

The above discussion reveals that the jet offset distance from the wall creates a controlling mechanism for adjusting the amount of ambient fluid entrainment into the jet in that alters its penetration distance. At lower offset ratios, the jet reattachment to the wall happens sooner with lower near wall loss of momentum. Therefore, the jet adhering to the side wall is stronger which shows more resistance to separation from the wall. As the jet offset distances increase, the jet has interaction from the wall and provides more entraining surface with the counter-flow. Moreover, closer proximity of the jet to the wall limits the jet oscillation amplitude in wall normal direction that causes more stability of the jet and reduces ambient flow entrainment. For $m=1.5$ and $m=2.5$ offset jets at high values of U_R , the jet bodies are attached to the wall for longer time and counter-flow entrainment from the wall side becomes negligible, with their penetration converging the penetration of the wall jet in counter-flow. The $m=3.3$ and $m=4.3$ offset jets have more entrainment from the wall side which leads to their lower penetration lengths in counter-flow compared to low offset ratio scenarios.
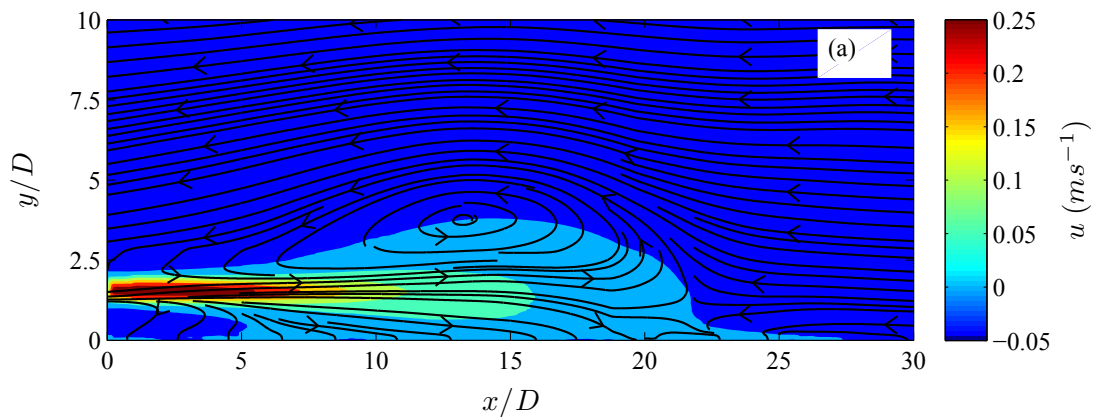
Figure 5-4 (a), for caption see facing page.
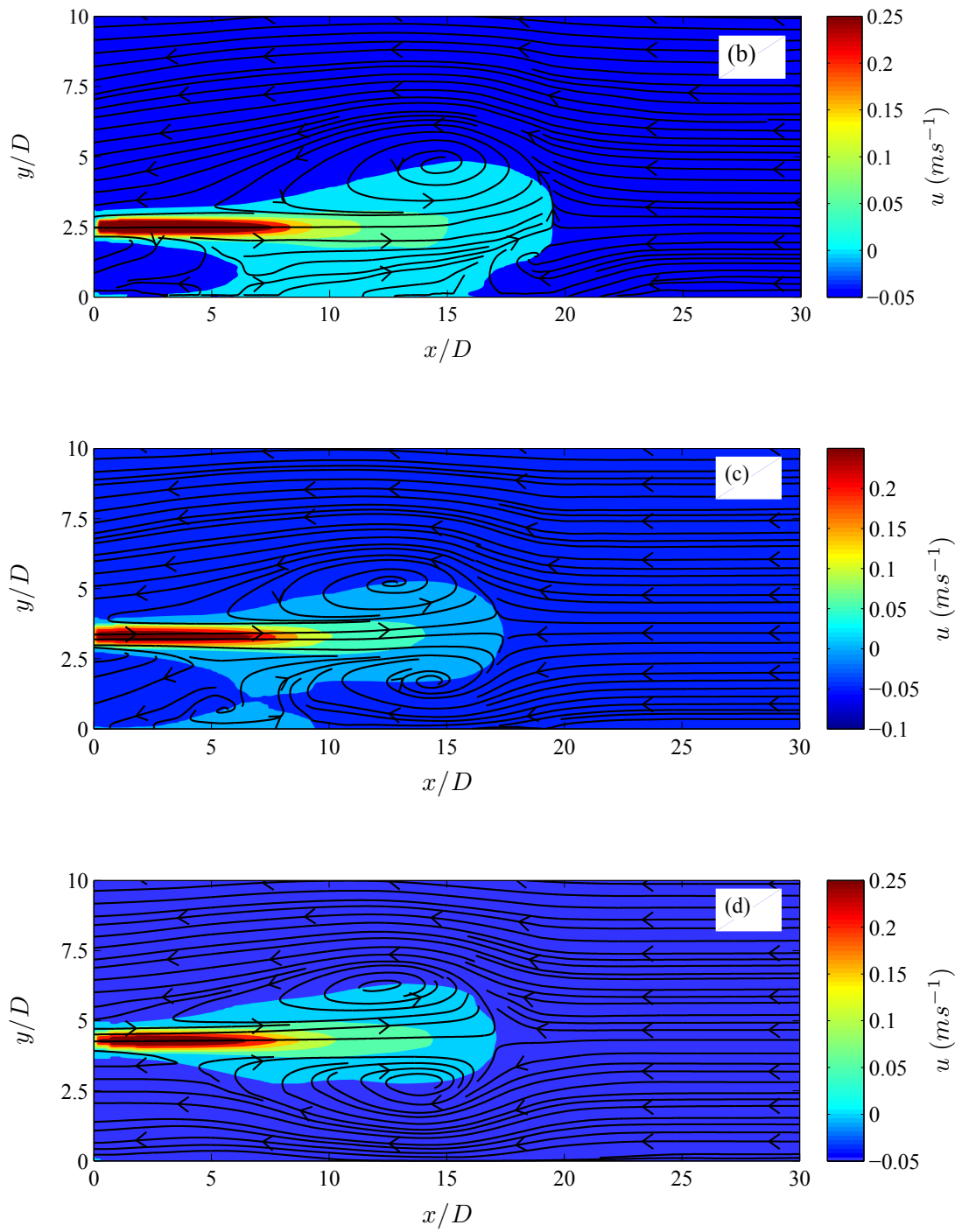
Figure 5-4: The mean axial velocity contours and streamlines for U_R=3.75 (a: offset ratio of 1.5, b: offset ratio of 2.5, c: offset ratio of 3.3, d: offset ratio of 4.3).

The normalized maximum velocity decay of the offset jets in counter-flow along the x axis are shown in Figures 5-5a to 5-5d for the velocity ratios in the range of $12.5 < U_R < 20$ and for offset ratios of m=1.5, 2.5, 3.3, and 4.3. The profiles collapse on each other and show self-similarity for $x/X_p > 0.15$. As is seen from Fig. 5-5, increasing the offset ratio increases the decay rate of the maximum velocity of the jets in counter-flow. This is due to the stronger interaction of the counter-flow with the jets that causes higher entrainment of the negative momentum from the ambient flow into the jet. In all cases the profiles show an inflection point at around x/X_p=0.8. Beyond this point the counter-flow has dominant effect and the jet flow terminates at a stagnation region. The velocity decays linearly between the inflection and the stagnation points. Power law equations are fitted for each case in the form of:

$$U_m / U_{jm} \, X_p/D = p \, (x/X_p)^q \qquad\qquad (3)$$

and the coefficients are shown in Table 5-1. Attempts were made to provide the best fits for the data in the range of $0.3 < x/X_p < 0.8$ in which the jet reattachments to the wall are completed and the effect of counter-flow over the jets is not dominant. For m=1.5, the velocity decay rate is very close to the amount of -1.08 that was reported previously for a generic wall jet in counter-flow [23]. In this particular case, the proposed power law curve collapses well onto the data points in the range of $0.15 < x/X_p < 0.8$ similar to the wall jet in counter-flow. As the offset ratio increases, the data points show more discrepancy from the power law curves in the initial regions which is due to the larger distance which the jet travels before attaching to the wall and reach to a fully developed established situation.

Table 5-1: The coefficients of the power law fit for the velocity decays.

m	1.5	2.5	3.3	4.3
p	3.8 ±0.05	2.7 ±0.08	1.6±0.05	1.2±0.05
q	-1.10 ±0.005	-1.36 ±0.005	-1.74±0.005	-2.05±0.005
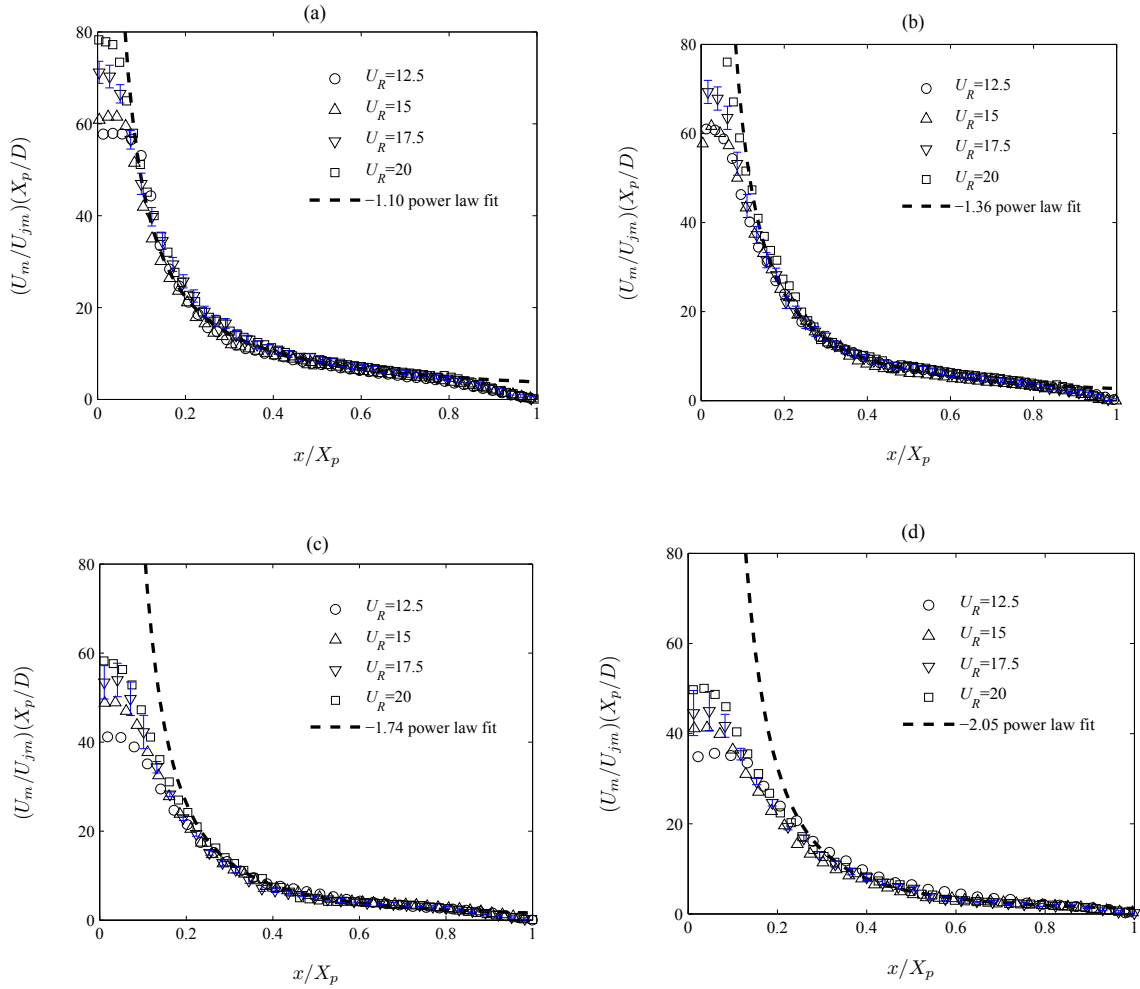
Figure 5-5: The maximum velocity decay of the offset jets in counter-flow, a: offset ratio of 1.5, b: offset ratio of 2.5, c: offset ratio of 3.3, d: offset ratio of 4.3 **(**error bars are for U_R=17.5 but it is expected that error for other velocity ratios be similar).

The other scales of the mean flow like the height of maximum velocity (y_{u_m}), the height of zero axial velocity ($y_{u=0}$), and the half velocity width of the jets ($y_{1/2}$) are investigated in order to analyze their behavior and to examine self-similarity.

The normalized height of maximum velocity versus axial distance from the jet exit plane are shown in Figures 5-6a to 5-6d for offset ratios of m=1.5, 2.5, 3.3, and 4.3. The tendency of the offset jets to be drawn to the adjacent wall is clearly visible from these Figures which show the downward trajectories of y_{u_m} profiles. The profiles remains close to the wall like a wall jet for a limited distance. After that, y_{u_m} rises and shows a peak in the mixing stagnation region ($0.8 < x/X_p < 1$). Figures 5-6 reveal that the range in which the jet has tendency to behave like a wall jet decreases with increasing the offset ratio. For example, Figure 5-6d depicts that the downward path of y_{u_m} is followed by an immediate rise, showing no near wall maximum velocity distribution.
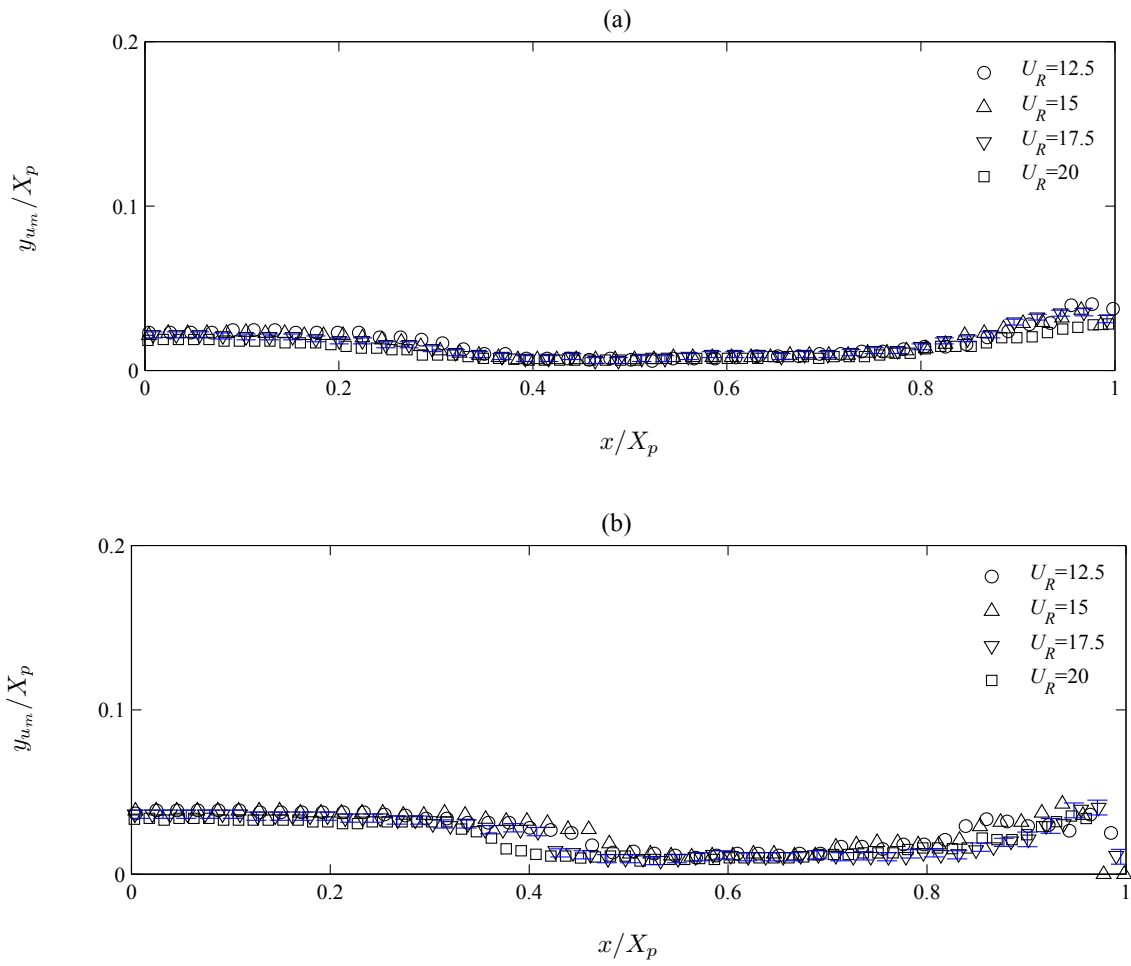
Figure 5-6 (a, b), for caption see facing page.

(c)

(d)
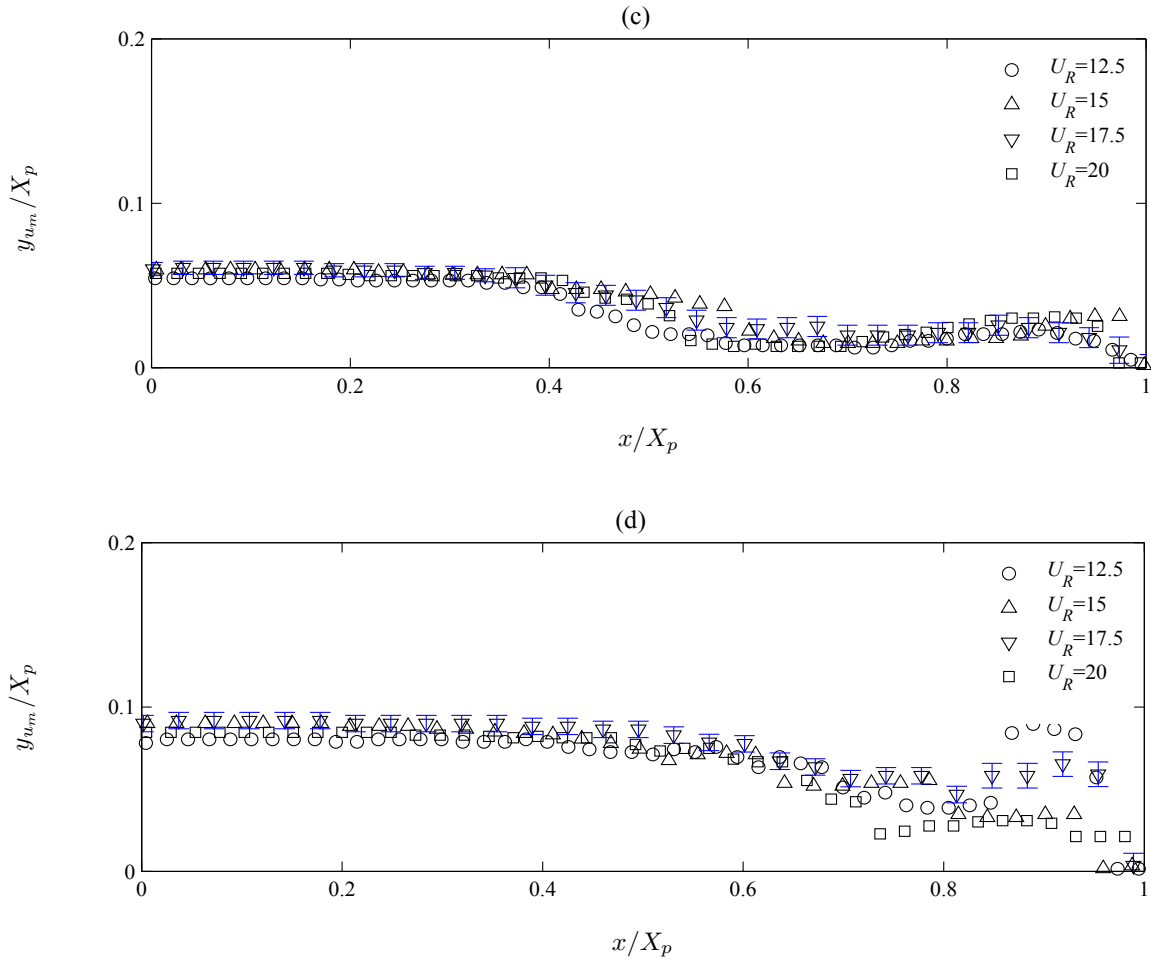
Figure 5-6: The normalized height of maximum velocity versus normalized axial distance, a: offset ratio of 1.5, b: offset ratio of 2.5, c: offset ratio of 3.3, d: offset ratio of 4.3, **(**error bars are for U_R=17.5 but it is expected that error for other velocity ratios be similar).

The normalized heights of zero axial velocity $(y_{u=0})$ for both the jet free side and wall side are shown in Figures 5-7a to 5-7d. The data at lower values of offset ratio show better collapse. On the jet upper side the profiles show monotonic rise and then after reaching to a maximum height, a sharp decline toward zero height at the stagnation point happens. The axial position of the maximum height moves toward the jet exit with an increase in the offset ratio. This means that increasing the offset, increases the effect of counter-flow on the jet.

On the underside of the jet, the intersection of the $y_{u=0}$ profiles with the x axis indicates the reattachment point of the offset jet to the wall. The stagnation area in the jet downstream causes wall normal growth of the jet and provides shorter reattachment compared to an offset jet in quiescent ambient flow. Figure 5-8 shows the variation of the reattachment distance (X_r) versus jet offset ratios. The reattachment distance increases with increasing the offset ratio. However, its rising declines as the jet distance increases from the side wall.
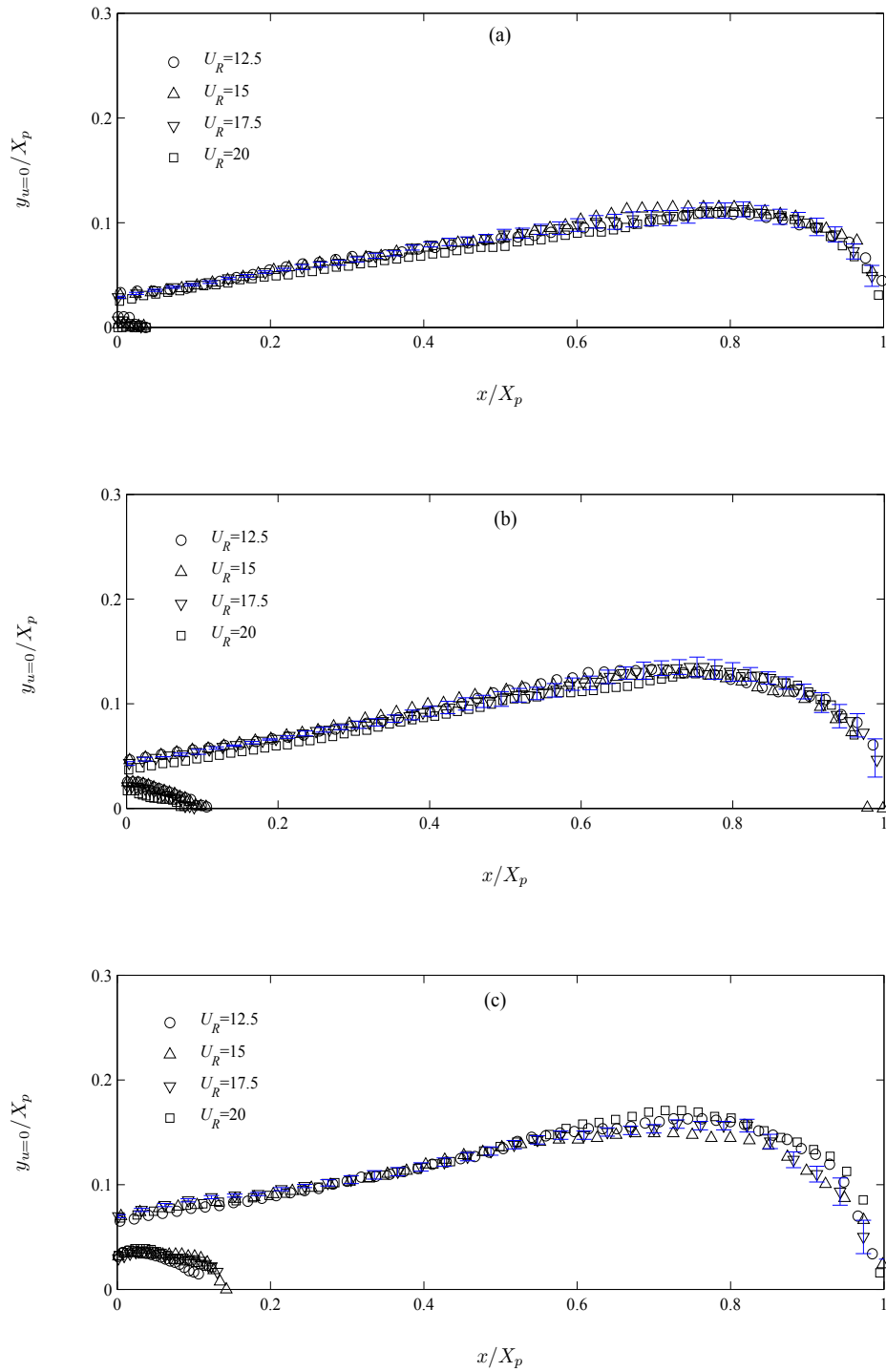
Figure 5-7 (a, b, c), for caption see facing page.

(d)
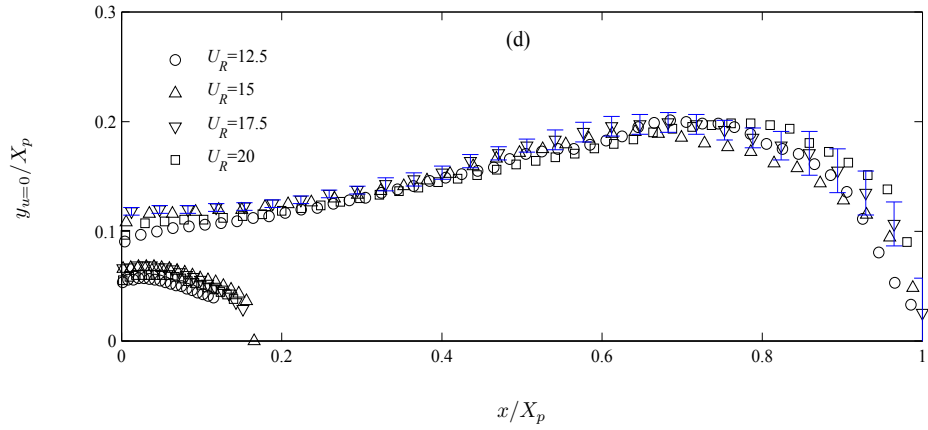
Figure 5-7: The normalized height of zero axial velocity versus normalized axial distance, a: offset ratio of 1.5, b: offset ratio of 2.5, c: offset ratio of 3.3, d: offset ratio of 4.3, **(**error bars are for U_R=17.5 but it is expected that error for other velocity ratios be similar).
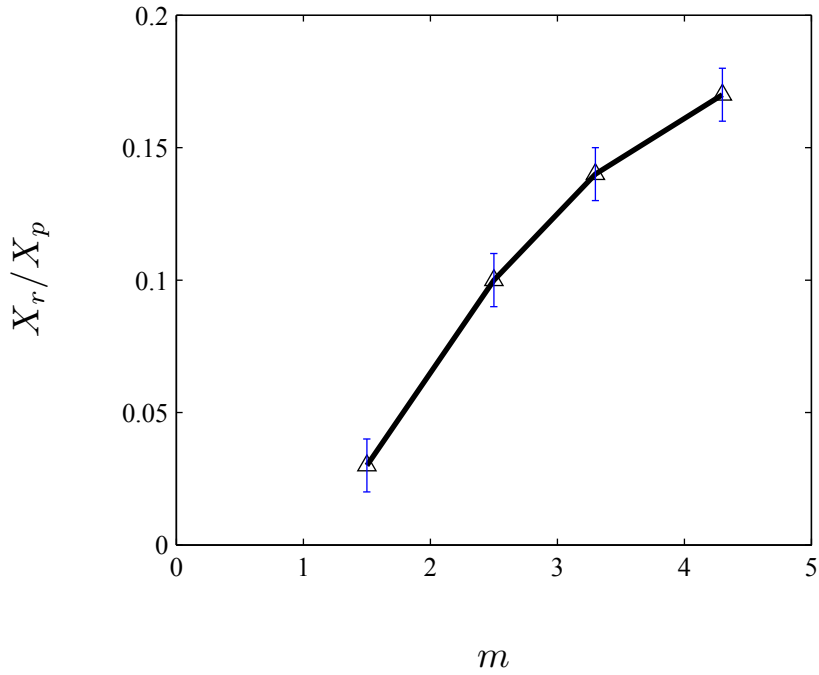
Figure 5-8: The normalized reattachment distance versus jet offset ratio.

The height at which the axial velocity of the jet becomes half of the local maximum velocity are called half velocity width ($y_{1/2}$) and are shown in Figures 5-9a to 5-9d for both the top side and the bottom side of the offset jets. In the top side, the half velocity width show linear variation versus axial distance in the range of $0.3 < x/X_p < 0.7$. A linear fit is proposed for each case in the form of:

$$y_{1/2}/X_p = a(x/X_p) + b \qquad\qquad (4)$$

and the coefficients are listed in table 5-2.

Table 5-2: The coefficients of the linear fit for the half velocity width.

m	1.5	2.5	3.3	4.3
a	0.04± 0.001	0.04± 0.001	0.045± 0.0015	0.06± 0.002
b	0.02± 0.003	0.04± 0.005	0.06± 0.006	0.09± 0.006

The half velocity width is an indicator for the spreading rate of the jet flow. Higher slope means faster spreading of the jet. As Table 5-2 shows, increasing the offset causes a rise in the half velocity width slopes. The slopes of 1.5m and 2.5m offset jets are the same as the half width slope of a generic wall jet in counter-flow [23] which means at these cases the jet forward momentum spreading are almost similar to each other. This was proven before as the jet penetration lengths were close for these cases, see Fig. 5-3. For m=3.3 and m=4.3, the slope increases 15% and 50% compared to 0.04 slope of 1.5m and 2.5m offset jets. This is due to greater interaction of the counter-flow with the offset jets as the gap between the jet and the wall increases.

In the lower side of the offset jets, due to the Coanda effect, the half velocity width has a curvature toward the wall which is more visible in the case of m=4.3.
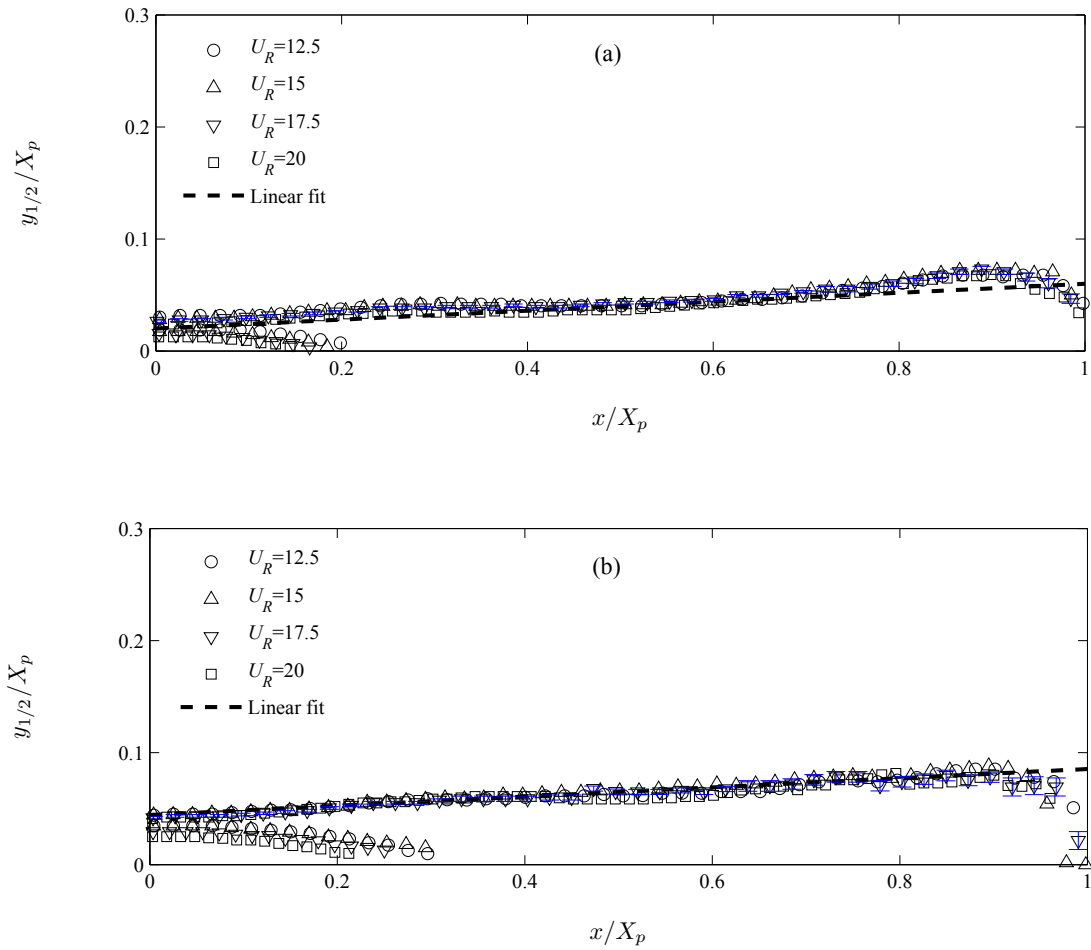
Figure 5-9 (a, b), for caption see facing page.
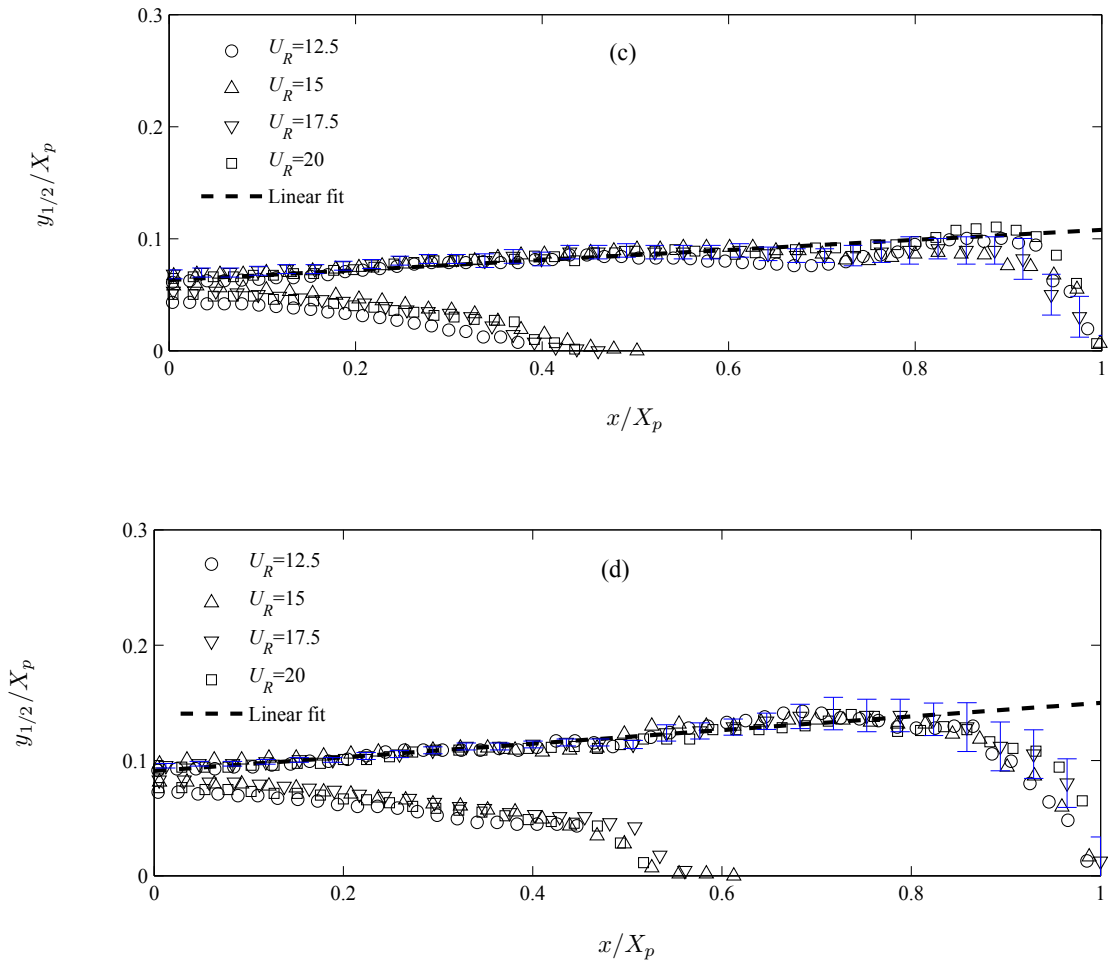
Figure 5-9: The normalized half velocity width versus normalized axial distance, a: offset ratio of 1.5, b: offset ratio of 2.5, c: offset ratio of 3.3, d: offset ratio of 4.3, (error bars are for U_R=17.5 but it is expected that error for other velocity ratios be similar).

Axial velocity profiles for the offset jets in counter-flow are normalized using the local scales of the flow. Figures 5-10a to 5-10d show the normalized profiles using the maximum velocity (u_m) and the half velocity width ($y_{1/2}$) in the upper jet body as the scaling factors. As Figure 5-10a shows for the 1.5m offset jet, the normalized velocity profiles show some degree of self-similarity in the range of 0.4<x/X_p<0.7. The Verhoff velocity profile for wall jets [25] is fitted to the data in the range of self-similarity (see Fig. 5-10a). For a wall jet in counter-flow as previously observed [23], the axial range of self-similarity for velocity profiles was 0.25<x/X_p<0.8. This range becomes narrower for the m=2.5 offset jet. As Figure 5-10b shows only for 0.6<x/X_p<0.7 the profiles collapse on each other and reveal the behavior of a wall jet. For m=3.3 and m=4.3 no self-similarity was observed for velocity profiles and the velocity fields do not reveal the characteristics of the generic wall jets (see Figs.5-10c and 5-10d). This indicates that the flow of an offset jet in an oppositely moving ambient flow does not behave like an established wall jet flow when the offset ratio is high. Clearly, the existence of the stagnation region at the jet downstream limits the similarity between offset jets and wall jets.
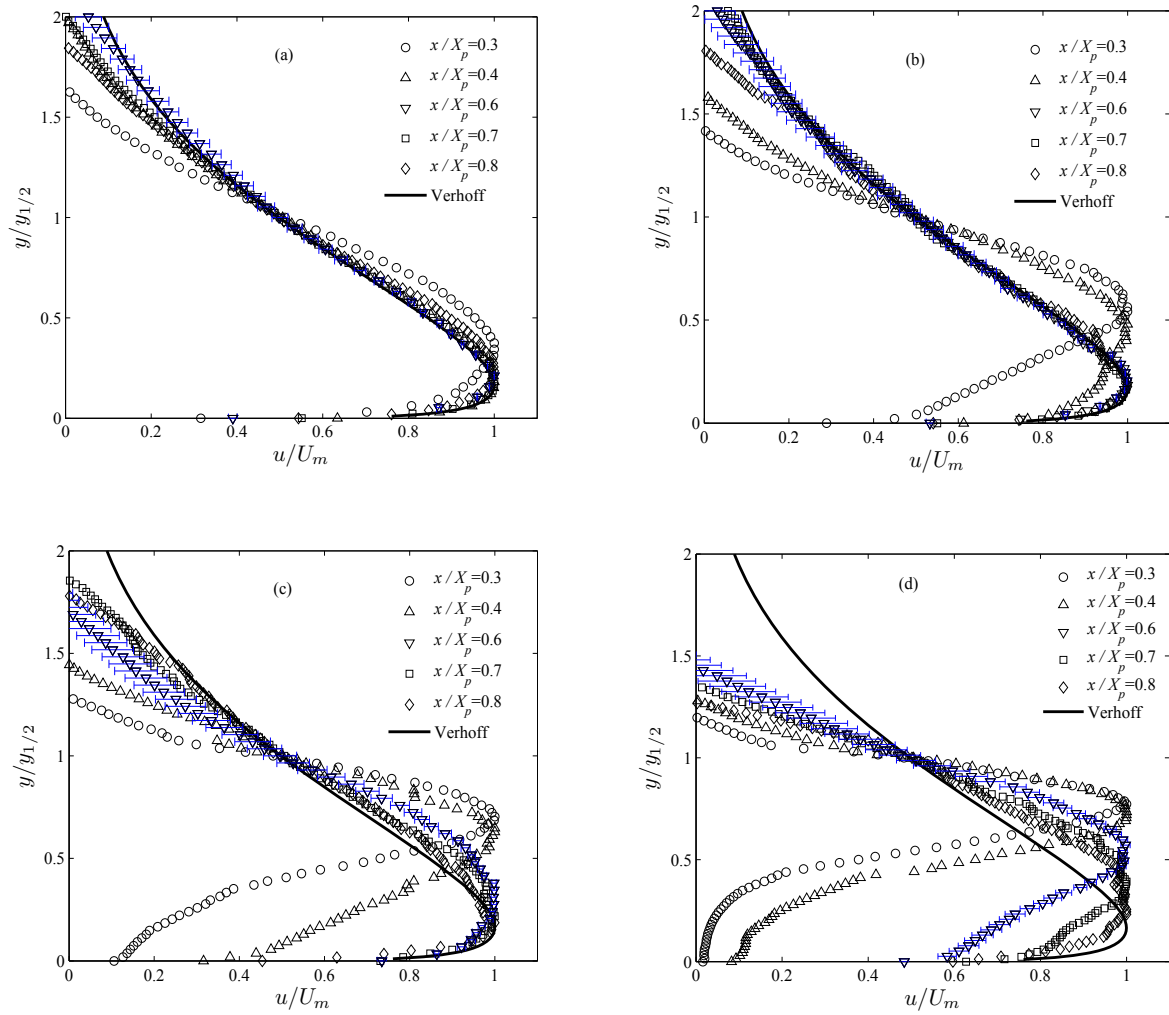
Figure 5-10: The normalized velocity profiles at different axial distance from the jet exit plane (a: offset ratio of 1.5, b: offset ratio of 2.5, c: offset ratio of 3.3, d: offset ratio of 4.3). The symbols o, $\triangledown$, Δ, $\triangleright$, $\diamondsuit$ represent x/X_p = 0.3, 0.4, 0.6, 0.7, and 0.8. Thick line shows the Verhoff velocity profile for a generic wall jet.

5.3.2   Vortical structures

One important characteristic of jets in counter-flow is the formation of large vortical structures. The streamline patterns of the mean flow clearly show a large recirculation region in the jet stagnation area (see Fig. 5-2). Generally, creation of vortices is the typical feature of all turbulent jet flows, but, when there is a counter flow interaction, strong shear between the jet and the ambient flow provides more input energy to the vortices. As a result, sustained swirling regions occurs in the flow. This feature was studied at the early stages of turbojet engine development, to be used as an aerodynamic flame holder in the combustion chambers and after-burners [11, 12].

The strong vortices resulting from the interaction of the jet and counter-flow have great impact on mixing of the jet and the ambient. Figures 5-6 and 5-9 show how y_{u_m} and $y_{1/2}$ have a significant rise at $0.8 < x/X_p < 1$ where the mean flow shows a big recirculation region. The vortices are also responsible for random oscillation of the jet in the counter-flow which is another means for enhancing the mixing. The vortical structures induce strong velocity fluctuations in both magnitude and direction which lead to random movement of macroscopic fluid elements.

As Kline and Robinson [26] described, "A vortex exists when instantaneous streamlines mapped onto a plane normal to the core exhibit a roughly circular or spiral pattern, when viewed in a reference frame moving with the centre of the vortex core". In simple flows with low shear, identifying the vortices is relatively easy. In fact, it is possible to observe the vortices and their physical characteristics by identifying isolated regions with a high amount of vorticity in comparison with nearby regions. However, as discussed by Adrian

et al. [27] in complex flow fields, vortices are usually masked by regions of high shear and the vorticity field analysis can not reveal their characteristics.

The Galilean transformation can be used to identify vortices in flows by subtracting the advection velocity of each vortex from the velocity field. However, since the vortices have various translational velocities depending on the local situation of the flow field, this method is not very effective in observing all the vortices in the flow.

The critical point analysis of the velocity gradient tensor is a popular method used to identify vortices in high shear flows. This method is based on the definition of a vortex proposed by Kline and Robinson [26]. A general discussion about using this method in finding the topology of three dimensional large structures in flow fields is reported by Chong et al. [28]. They showed that the solution trajectories of the fluid elements have spiral movement or closed circular shapes if the characteristics equation of the velocity gradient tensor had imaginary roots. This method has been applied widely as an effective tool for identifying vortical structures in velocity fields from PIV studies [29]. In this study, the 2D velocity gradient tensor was obtained for the offset jets in counter-flow. Following Vollmers [30], the discriminant of the characteristics equation of the 2D velocity gradient tensor is:

$$\Delta = (\partial u/\partial x + \partial v/\partial y)^2 - 4[(\partial u/\partial x)\,(\partial v/\partial y) - (\partial u/\partial y\,)(\partial v/\partial x)] \tag{5}$$

Using the above method, the areas with negative discriminant (imaginary eigenvalues) represent vortices in the flow. The swirling direction of the vortical structures can be found by analyzing the vorticity sign at those locations. Positive vorticity shows the

positive swirl direction and negative vorticity at the location of a vortex indicates that its swirl direction is negative.

Figure 5-11a show the instantaneous velocity vectors of a typical realization of the velocity field of the offset jet in counter-flow at U_R=17.5 and m=2.5. To keep the vector field clearer, a coarser grid resolution is selected to show only 4% of the available data points. As it is seen from Figure 5-11a, this vector field shows only one counter-clockwise vortex near the wall region at an axial distance of $65D$ from the jet exit plane. Assuming the advection velocity of all vortices is equal to the mean flow velocity and applying Galilean transformation more vortices are revealed as shown in Fig. 5-11b. In this scenario three vortices are clearly visible after the stagnation area at $x/D>65$. However, in the Galilean transformation if two times the mean velocity field was subtracted from the instantaneous velocity field it can show a new pattern of vortices in the flow that were hidden in the high shear region before the stagnation area, see Fig. 5-11c. As it was mentioned before, the exact advection velocity of each vortex should be known and subtracted from the flow field in order to discern all vortices of the flow by using Galilean transformation. Another way would be to apply this method with a range of various velocity subtraction from the flow. It can finally reveal all vortex patterns that exist in the flow, but, is not an efficient process.

Figure 5-11d, shows the vortical structures of the flow for the same instantaneous velocity field after using the critical point analysis. The red areas represent positive (counter-clockwise) vortices and the blue ones show the negative vortices (clockwise). As it is seen, in addition to the captured vortices with the two trials of Galilean

transformations, many new vortices are presented in the flow that were not visible in

Figs. 5-11a to 5-11c.
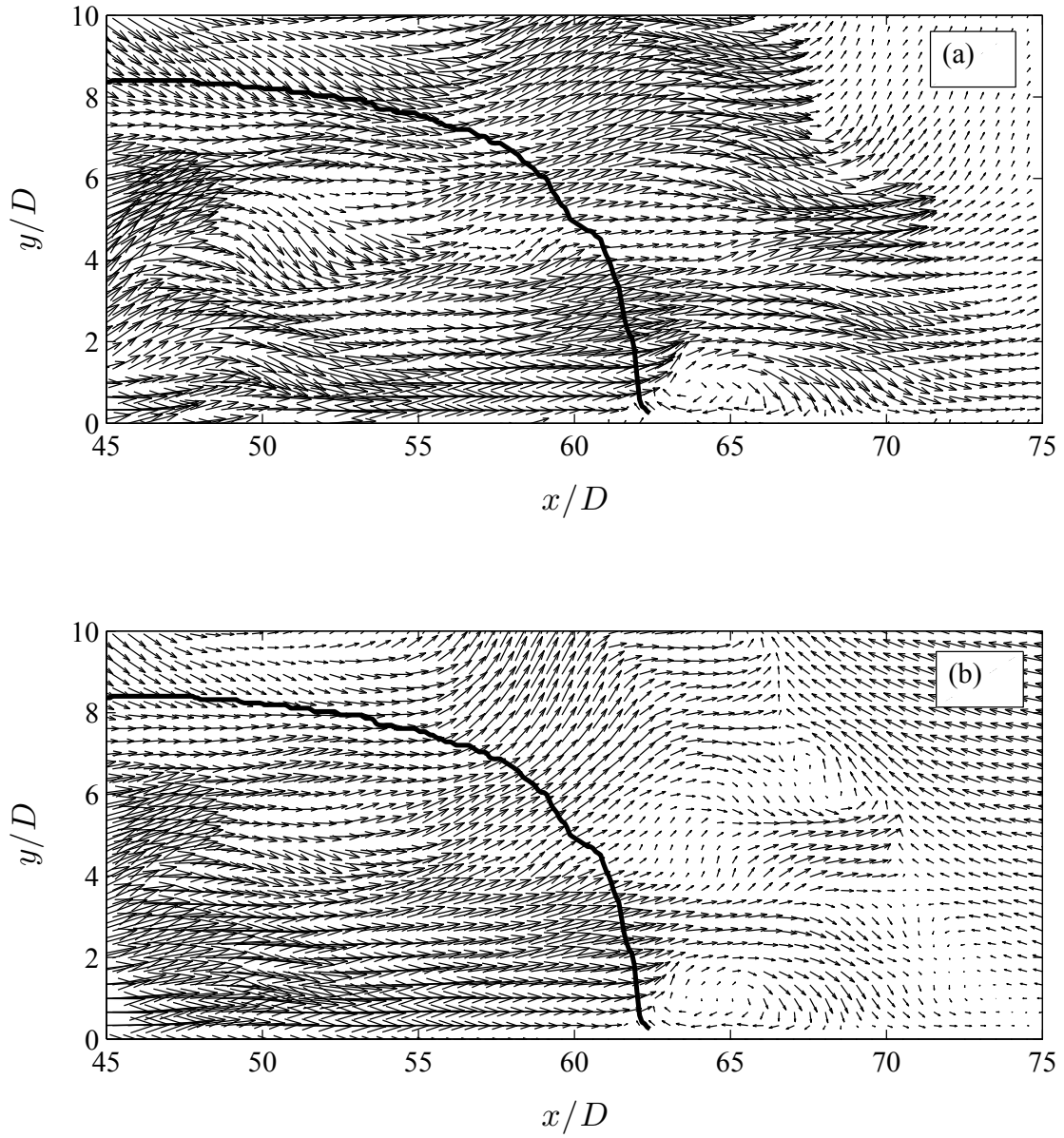
Figure 5-11 (a, b), for caption see facing page.
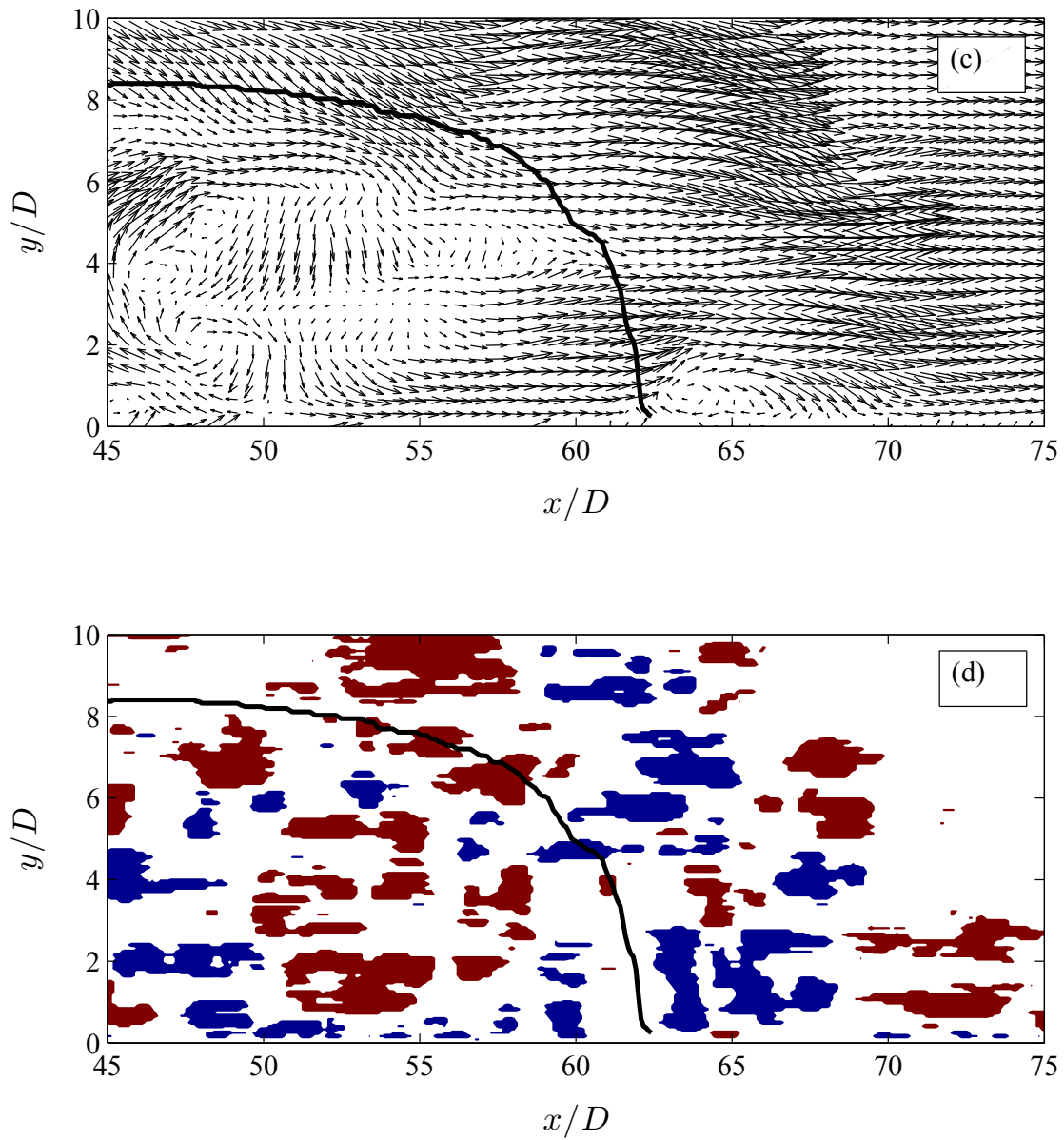
Figure 5-11: The instantaneous realization of the flow at the stagnation area, (a): original vector field, (b): vector field after subtracting mean velocity, (c): vector field after subtracting two times the mean velocity, (d): vortical structures captured via critical point analysis. Thick line shows the loci of zero axial velocity.

Figures 5-12a to 5-12d show instantaneous realizations of the flow, the vortices, and the streamline schematics of the offset jets in counter-flow at U_R=17.5 and offset ratios of 1.5 to 4.3. The thick black curve shows the location of zero axial velocity of the mean flow ($y_{u=0}$) and the dashed line shows the position of maximum local velocity (y_{u_m}). These particular selected realizations have the minimum instantaneous penetration among all 1000 samples of flow at each case.

The patterns of streamlines and the existence of vortical structures at different sizes and shapes indicate that as expected the offset jets in counter-flow have large regions with high turbulence during penetration into the counter-flow. In the initial region of the jet development, the shear forces create positive and negative vortices at the top and the bottom height of maximum velocity (dashed line), respectively. These vortical structures penetrate into the oncoming ambient flow, grow in size and finally reach to zero advection velocity as they approach the stagnation area. Then, they gain negative axial momentum from the counter-flow and return back. A portion of positive vortices roll back on each other and combine together to provide a very large recirculation zone. The near wall negative vortices construct a layer between the positive vortices generated by the jet and those vortices in the turbulent boundary layer of the flat plate. Some of these vortices return back to the jet due to entrainment. The interaction of these structures with the jet provides high amplitude random fluctuation in the flow that in some cases like m=4.3 offset jet provides 50% change in the instantaneous penetration length, see Fig. 5-12d. These vortices induce high velocity fluctuations that are able to change the bulk velocity vector of the jet toward wall normal direction or force the jet to move in another

plane rather than the symmetry plane. These random motions enhance the jet and counter-flow mixing and provides other vortices that sustains the jet chaotic motion.

At the stagnation region where the advection velocity of the flow is very low, the vortices generated by the jet and those produced by the boundary layer of the counter-flow have a very large time scale to evolve slowly and mix the jet flow with the counter-flow. The strongest vortex entrains the fluid from its surrounding area to itself. Generally the large recirculation region produced by accumulation of the jet positive vortices entrain the surrounding flow, see Figures 5-12a, b, and d. Figure 5-12c shows a different mode of vortex interaction in which the negative vortices produced by the jet make a large negative swirling region that drags the counter-flow to itself. Then it is followed by large regions of positive vortices that circulate the flow in counter-clockwise direction.
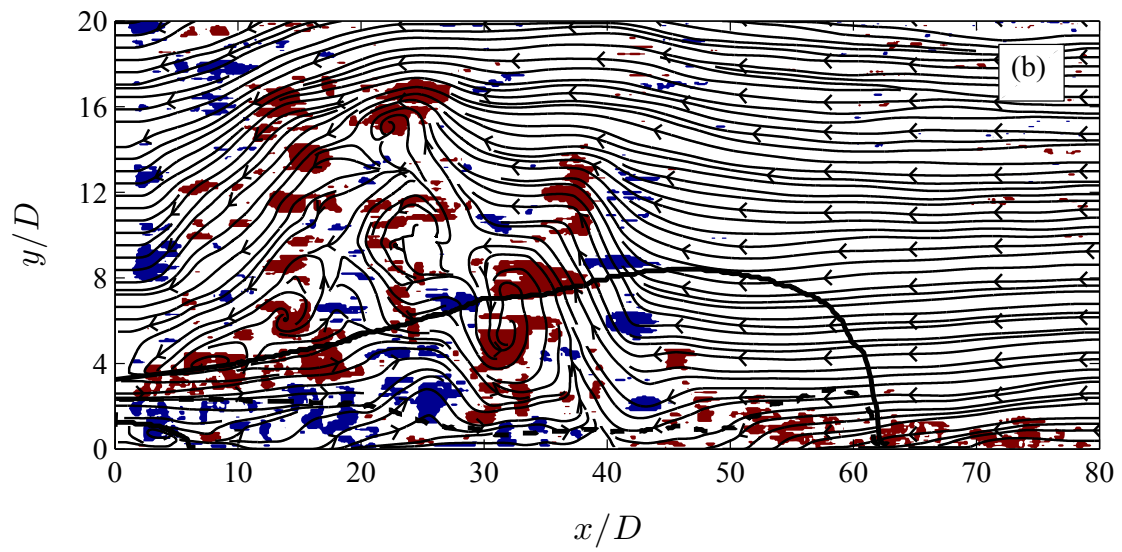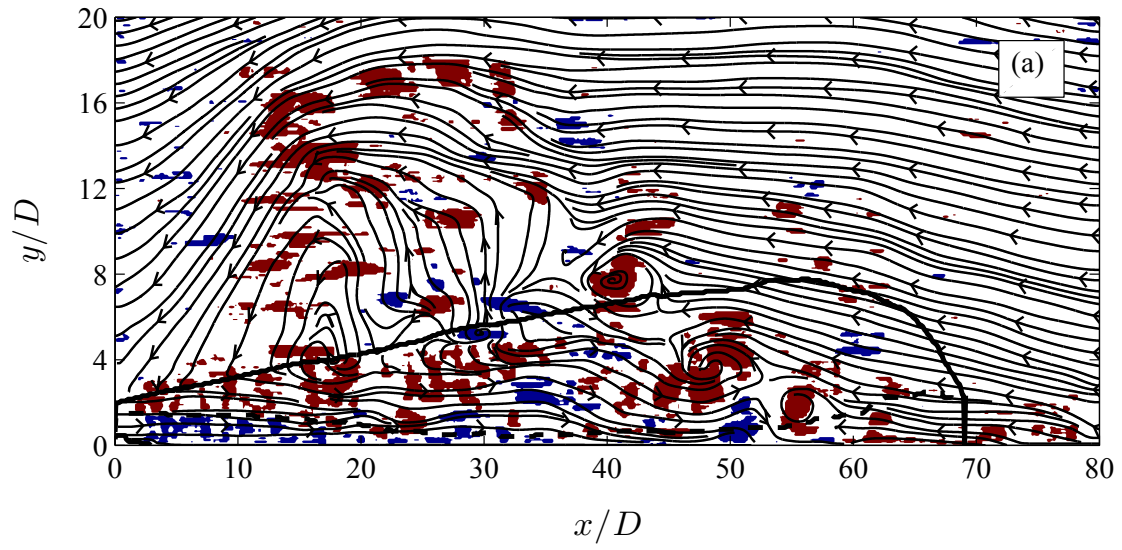
Figure 5-12 (a, b), for caption see facing page.
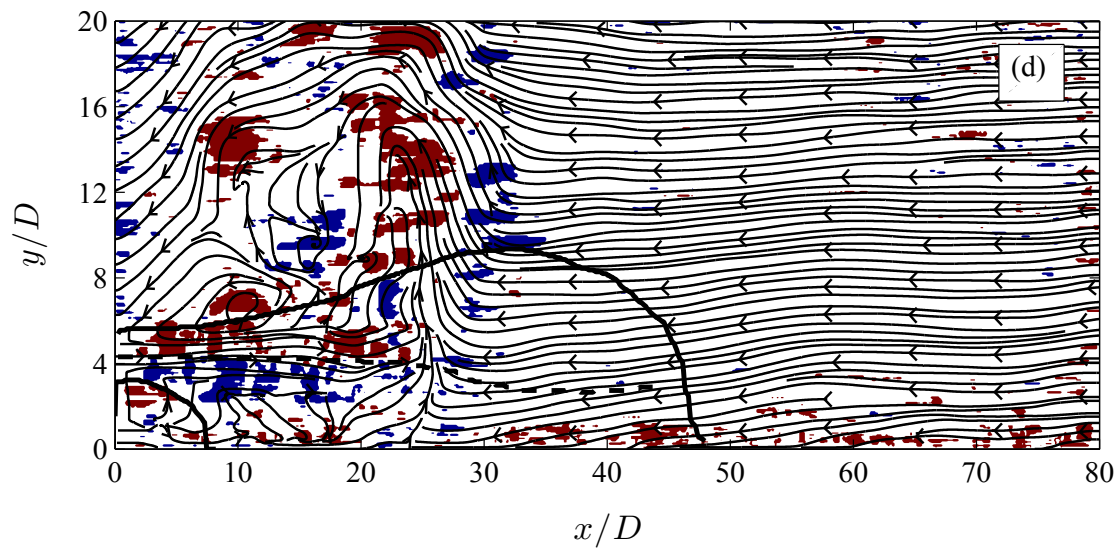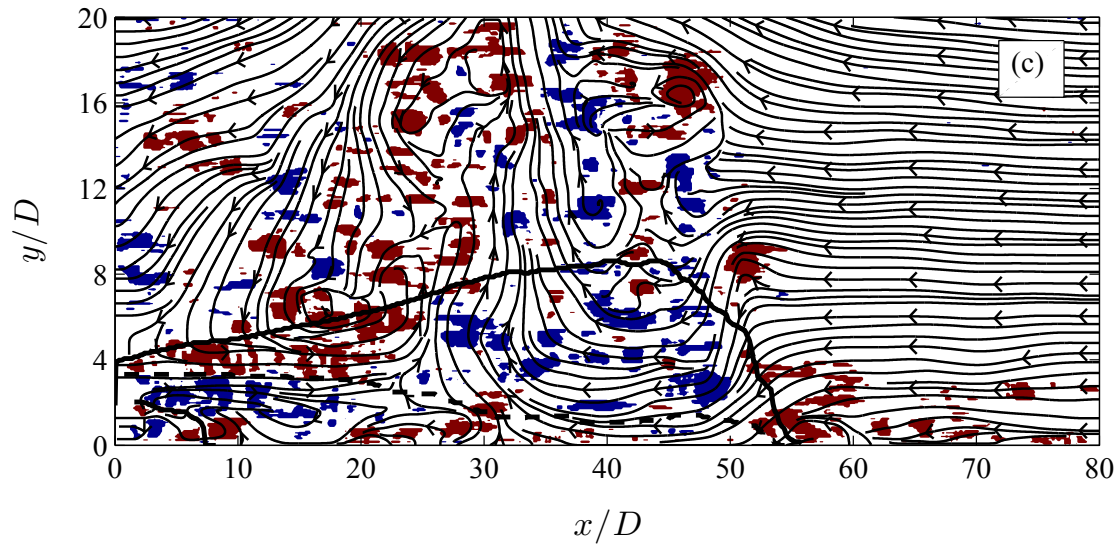
Figure 5-12: The instantaneous realization of the flow with minimum penetration along with vortical structures and instantaneous streamlines. Thick line and dashed line represent the height of zero axial velocity and maximum velocity (a: offset ratio of 1.5, b: offset ratio of 2.5, c: offset ratio of 3.3, d: offset ratio of 4.3).

To investigate the effect of offset distance on the interaction of the vortical structures in the flow, the population density of the positive and negative vortices was analyzed. This parameter is obtained by counting the number of vortices passing through each point divided by 1000 which was the total number of realizations of the flow that analyzed for each case. The results are shown in Figure 5-13 for various offset configurations at the jet to counter-flow velocity ratio of U_R=17.5. The thick black curve shows the location of zero axial velocity of the mean flow ($y_{u=0}$) and the dashed line indicates the position of maximum mean local velocity (y_{u_m}) at each case.

As expected, the population density (N) of negative vortices are higher close to the wall in the areas beneath the y_{u_m} line (the jet's inner layer). Conversely, the positive vortices are located mostly in the regions above the height of maximum velocity (the jet's outer layer). It is clearly visible from Figure 5-13 that increasing the offset ratio increases the region where positive and negative vortices mix together. For instance, at m=1.5 the negative vortices move near the wall and in the stagnation region they rise from the wall to occupy more space. At this point, they overlap with positive vortices produced by the outer layer of the jet and the vortices created by the turbulent boundary layer of the flat plate. As the offset distance increases, the overlap region of the positive and negative vortices extends to a larger space rather than just in the stagnation zone. This phenomenon proves that increasing the offset ratio increases the instability and random fluctuations of the jet and provides better mixing for the flow. In fact, increasing the jet distance from the wall provides more room for interaction of the counter-flow with the jet and enhances the random fluctuation of the flow.
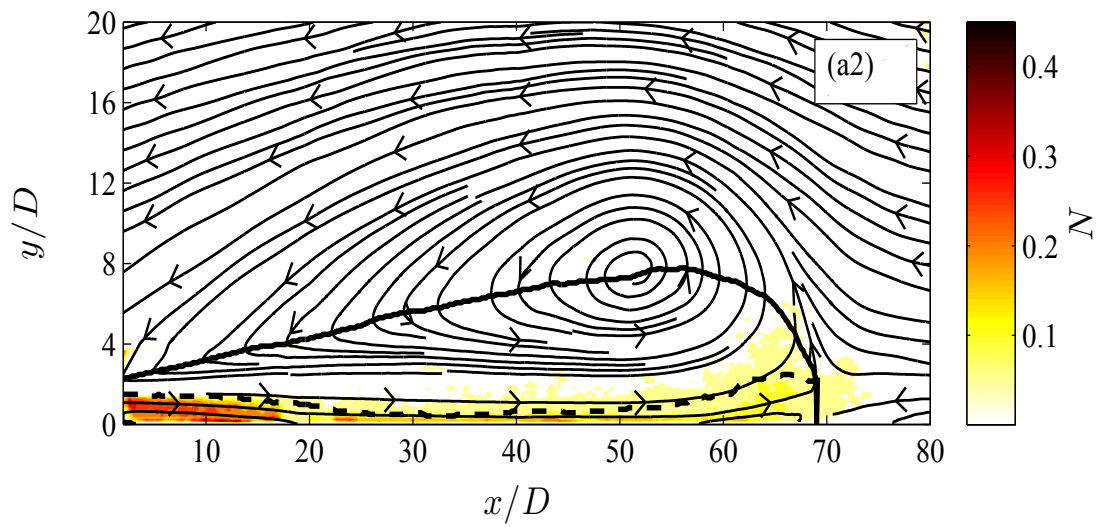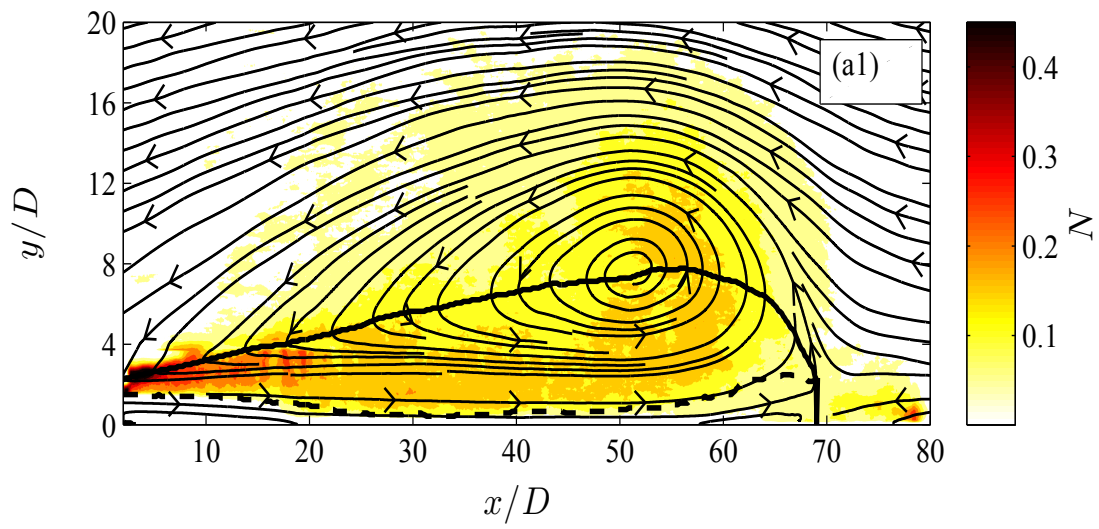
Figure 5-13 (a1, a2), for caption see facing page.
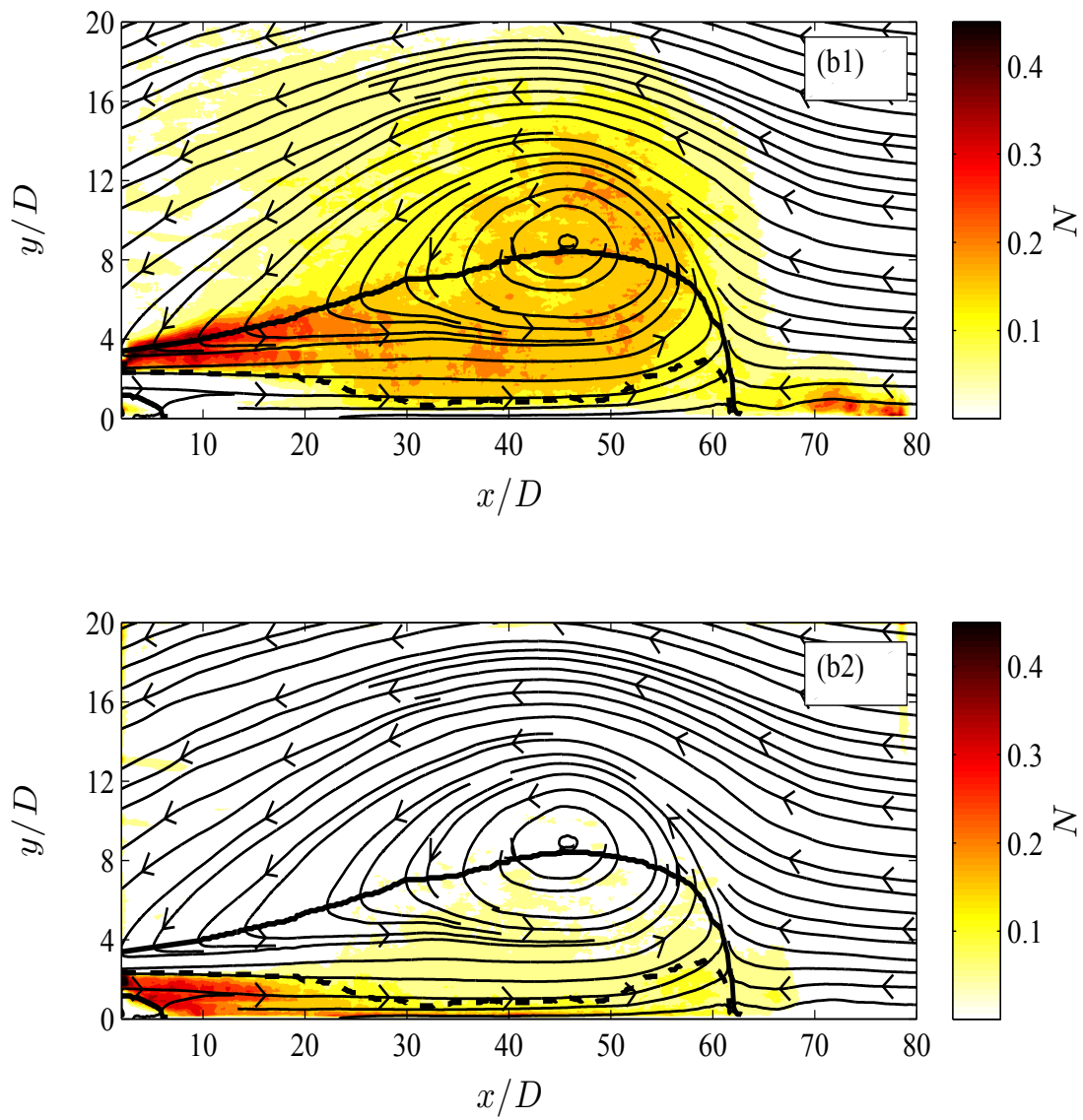
Figure 5-13 (b1, b2), for caption see facing page.
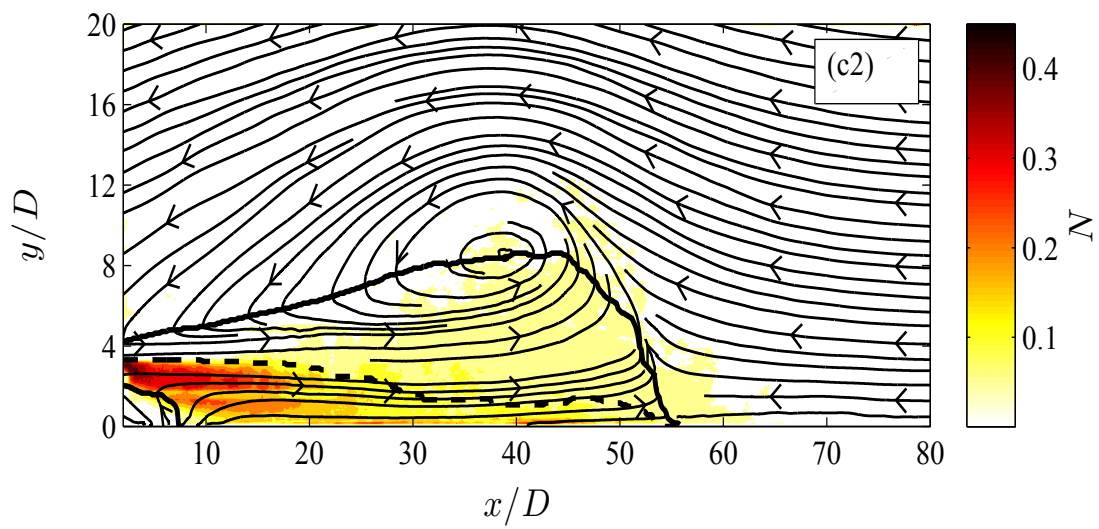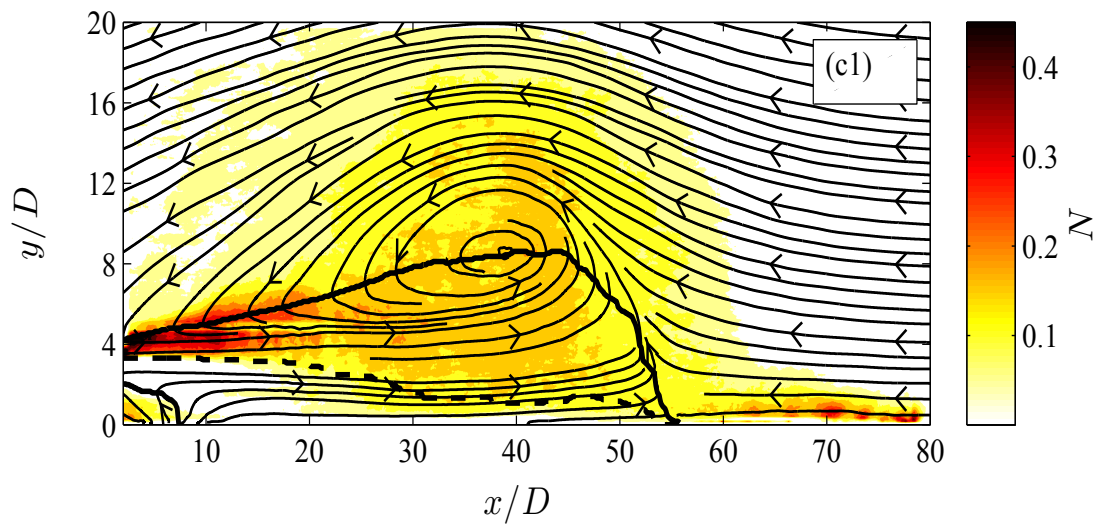
Figure 5-13 (c1, c2), for caption see facing page.
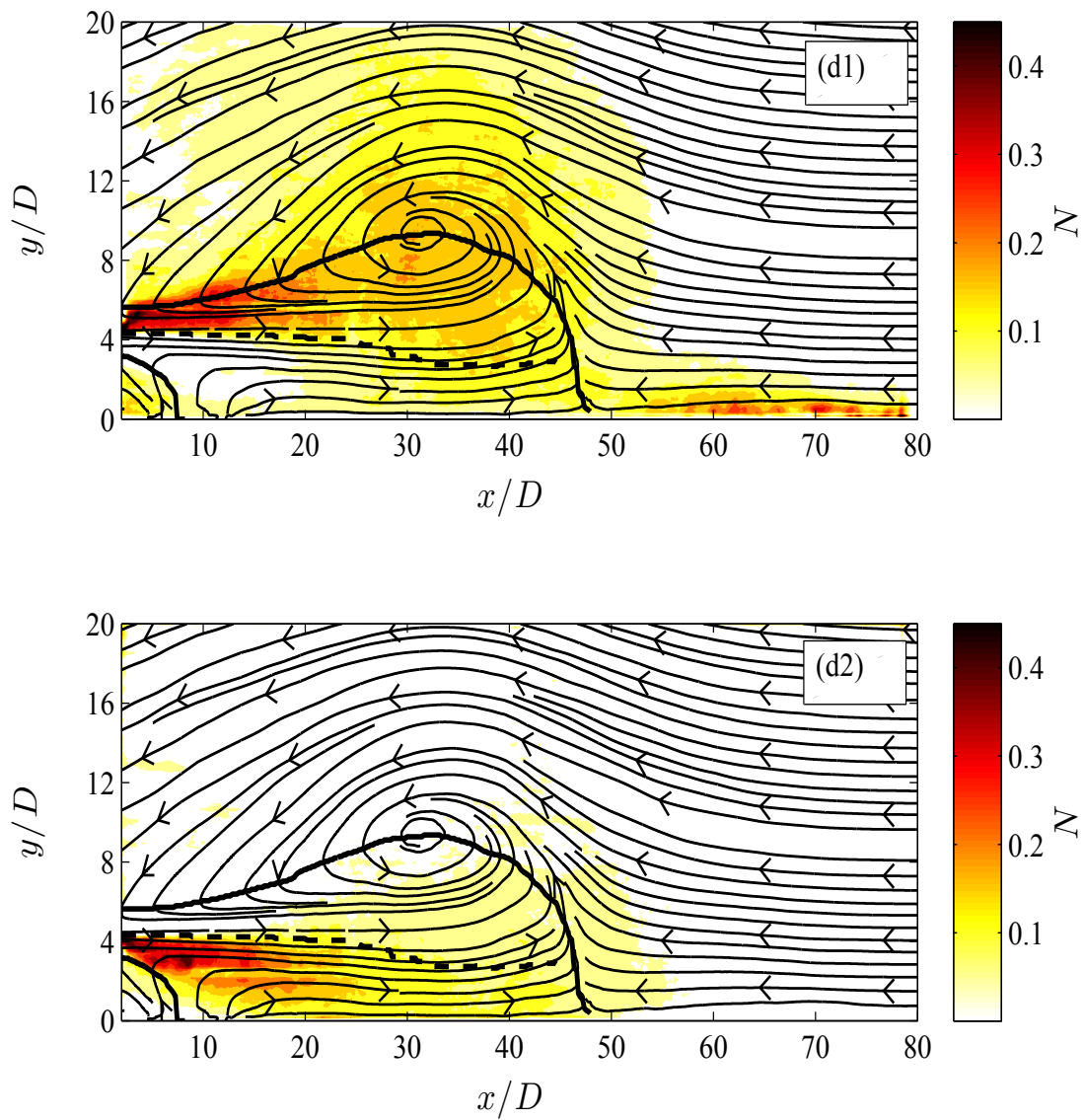
Figure 5-13: The population density of positive and negative vortical structures and mean flow streamlines. (a: offset ratio of 1.5, b: offset ratio of 2.5, c: offset ratio of 3.3, d: offset ratio of 4.3. Indices 1 and 2 represents data for positive and negative vortices, respectively). Thick line and dashed line represent the height of zero axial velocity and maximum velocity.

In order to understand the effect of offset ratio on the turbulent structures of the flow field, velocity correlations were studied. Two-point velocity correlation functions have been used widely in turbulent flow analysis to investigate the average shape and size of vortical structures in turbulent boundary layers [30, 31]. In this study the normalized spatial velocity correlation functions at a reference point (x_r, y_r) in the jet symmetry plane is evaluated in the form of:

$$R_{uu} = \frac{\overline{u'(x_r, y_r)u'(x_r + \Delta x, y_r + \Delta y)}}{\overline{u'^2(x_r, y_r)}} \qquad (7)$$

where u' is fluctuating velocity component in the streamwise direction obtained by subtracting the mean axial velocity field from the instantaneous one and Δx and Δy are distances from the reference point.

Figure 5-14 shows the correlation contours of R_{uu} at a reference point selected on $\bar{u} = 0$ line at 60% of the jet penetration distance for U_R=17.5 and at offset ratios of 1.5, 2.5, 3.3, and 4.3.

It is seen from Fig. 5-14 that the high correlated regions of horizontal velocity fluctuations become larger as the offset ratio increases. This is clearly obvious for regions in which R_{uu}> 0.8. This means that the turbulent structures become more energetic as the offset ratio increases. The energy of these structures comes from the mean flow. Therefore, the offset ratio increasing has a direct impact on the enhancement of the turbulent kinetic energy (TKE) of the flow. The other observation from Fig. 5-14 is the

larger extension of the correlation contours in axial direction. This implies that the turbulent structures of the flow are elongated in horizontal direction.
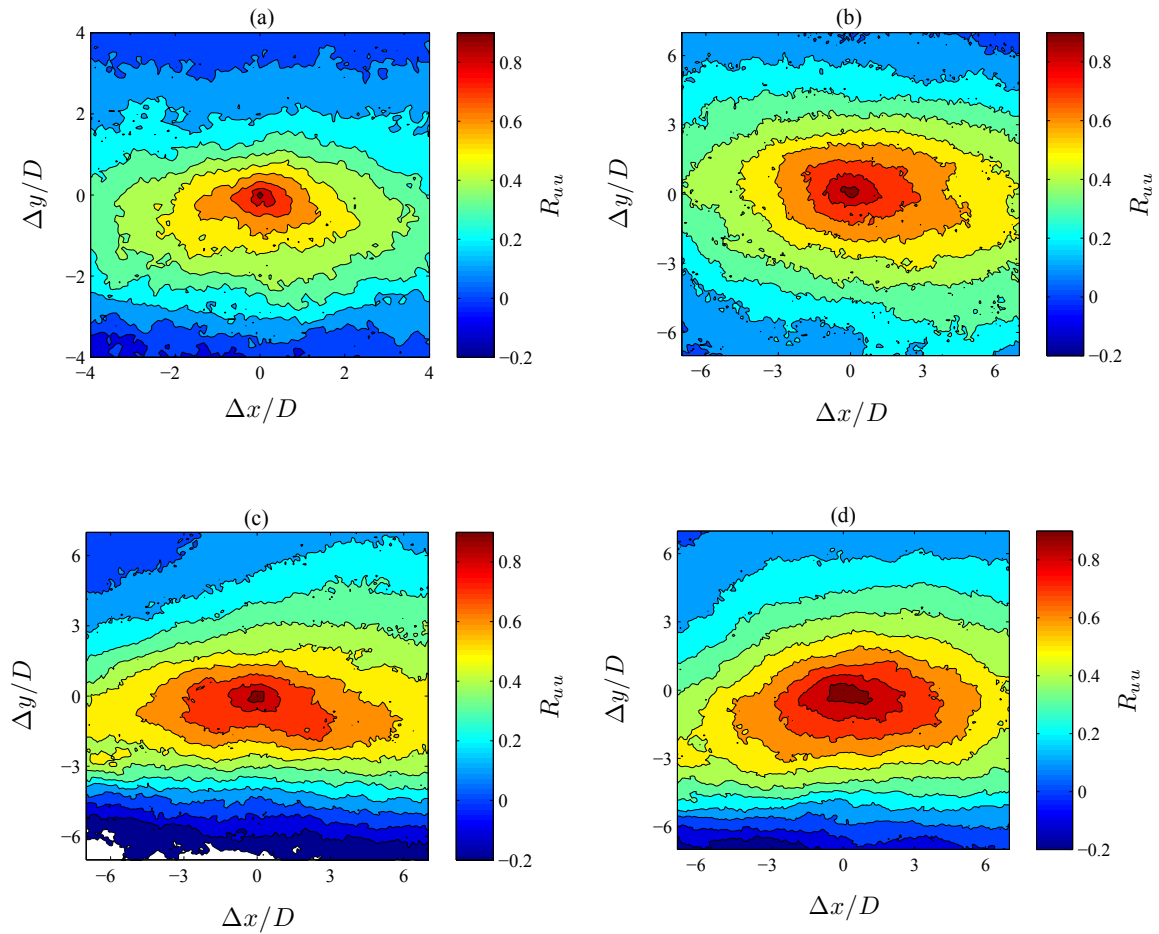
Figure 5-14: The auto correlation contours of axial velocity fluctuations at a reference point located at the loci of zero axial velocity and x/X_p=0.6 (a: offset ratio of 1.5, b: offset ratio of 2.5, c: offset ratio of 3.3, d: offset ratio of 4.3).

5.3.3   Turbulence statistics

The interaction of the jets with oncoming ambient flows creates strong turbulence and fluctuations in the flow that has great impact on increasing the mixing of the jet and the surrounding flow. At the stagnation zone the jet and counter-flow reach zero advection velocity and vortical structures of the flow play the major role in mixing. Turbulence statistics in these types of stagnating flows has not been reported in the literature. In this section the turbulence statistics of offset jets in counter-flow are studied. This information can provide valuable insights for designing engineering devices that use this flow configuration for increasing mixing and turbulence.

The Reynolds stresses of the offset jets in counter-flow in the symmetry plane at U_R=17.5 and jet Reynolds number of Re_j= 7.1×10^3 are shown in Figures 5-15 to 5-17 along with the streamline patterns. The counter-flow velocity is used to normalize these statistics. Figure 5-15 shows $\overline{u'^2}$ velocity fluctuations for offset ratios of 1.5 to 4.3. As seen from Fig. 5-15a for m=1.5 at the stagnation area and axial positions of 60<x/D<70 the streamwise velocity fluctuations show a local maxima. This area is the overlap region of positive and negative vortices at the stagnating zone such as Figures 5-13a1 and 5-13a2 show. The negative vortices that possess higher vorticity because of higher velocity gradients near the wall, have an important role in the stagnation area to enhance the velocity fluctuations in the flow. The same phenomenon is seen at Fig. 5-15b when the offset ratio is 2.5. As the offset ratio increases to m=3.3 and m=4.3, the overlap area of these vortices increases, which enhances the mixing and provides relatively uniform contours of velocity fluctuations in the stagnation region. Furthermore, the counter-flow interaction and its entrainment increases due to higher offset ratios which provides more

energy for the turbulent structures. It amplifies the level of velocity fluctuations for the whole zone of the stagnation area. For instance, the level of $\overline{u'^2}/U_0^2$ at a certain point located at the loci of u=0 and y/D=2 are 0.5, 0.7, 1.2, and 1.4 for offset ratios of 1.5, 2.5, 3.3, and 4.3, respectively. It clearly shows the amplifying effect of offset ratio on turbulence of the jets in counter-flow.

The normalized $\overline{v'^2}$ fluctuations are shown in Fig. 5-16 and they have lower values compared to axial velocity fluctuations. The normalized wall normal velocity fluctuations shrink as they approach to the stagnation area. Moreover, the offset ratio increases the magnitude of wall normal velocity fluctuations as well.

The contours of Reynolds shear stresses $(\overline{u'v'})$ are shown in Figures 5-17a to 5-17d for the same situation. The normalized $\overline{u'v'}$ contours for offset ratios of 1.5 and 2.5 at axial distances lower than $0.8X_p$ starts from negative values near the wall similar to a generic wall jet in counter-flow as shown before [23]. Then, they rise monotonically to a maximum value at height of $y/D = 4$ following with a decline as the height increases toward the edge of the free stream. At the stagnation zone a local increase in shear stresses happens due to the interaction of vortices as mentioned before. At offset ratios of 3.3 and 4.3 as Figures 5-17c and 5-17d show, the shear stress contours show a totally different behavior. The contours reveal two distinct and almost equal regions of negative and positive stresses similar to Reynolds shear stress of a free jet. The reason is that at m=3.3 and m=4.3 the offset jets do not reach to a state of fully developed wall jet because they need more distance to attach the side wall and their shorter penetration does not allow them to do so.
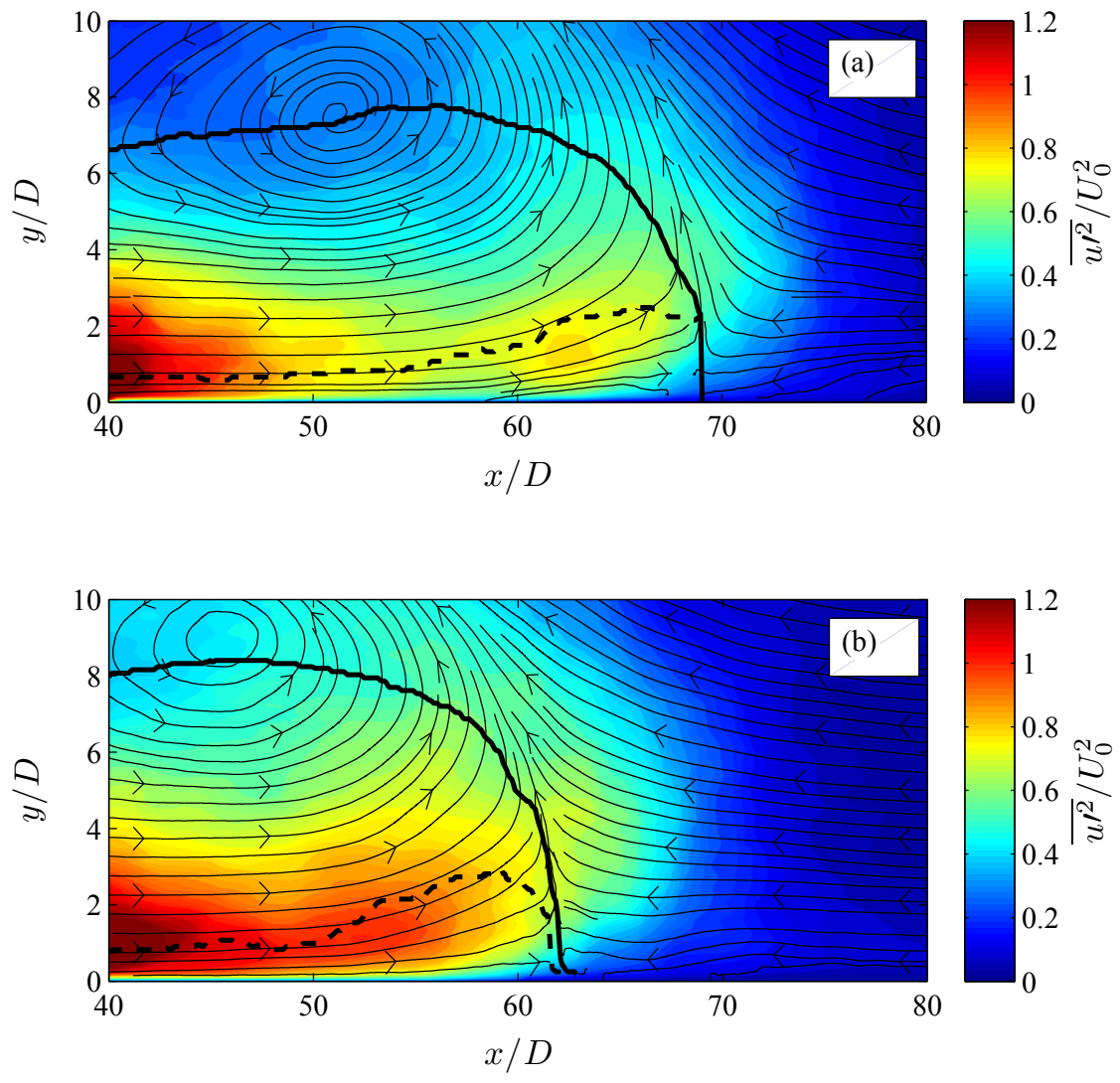
Figure 5-15 (a, b), for caption see facing page.
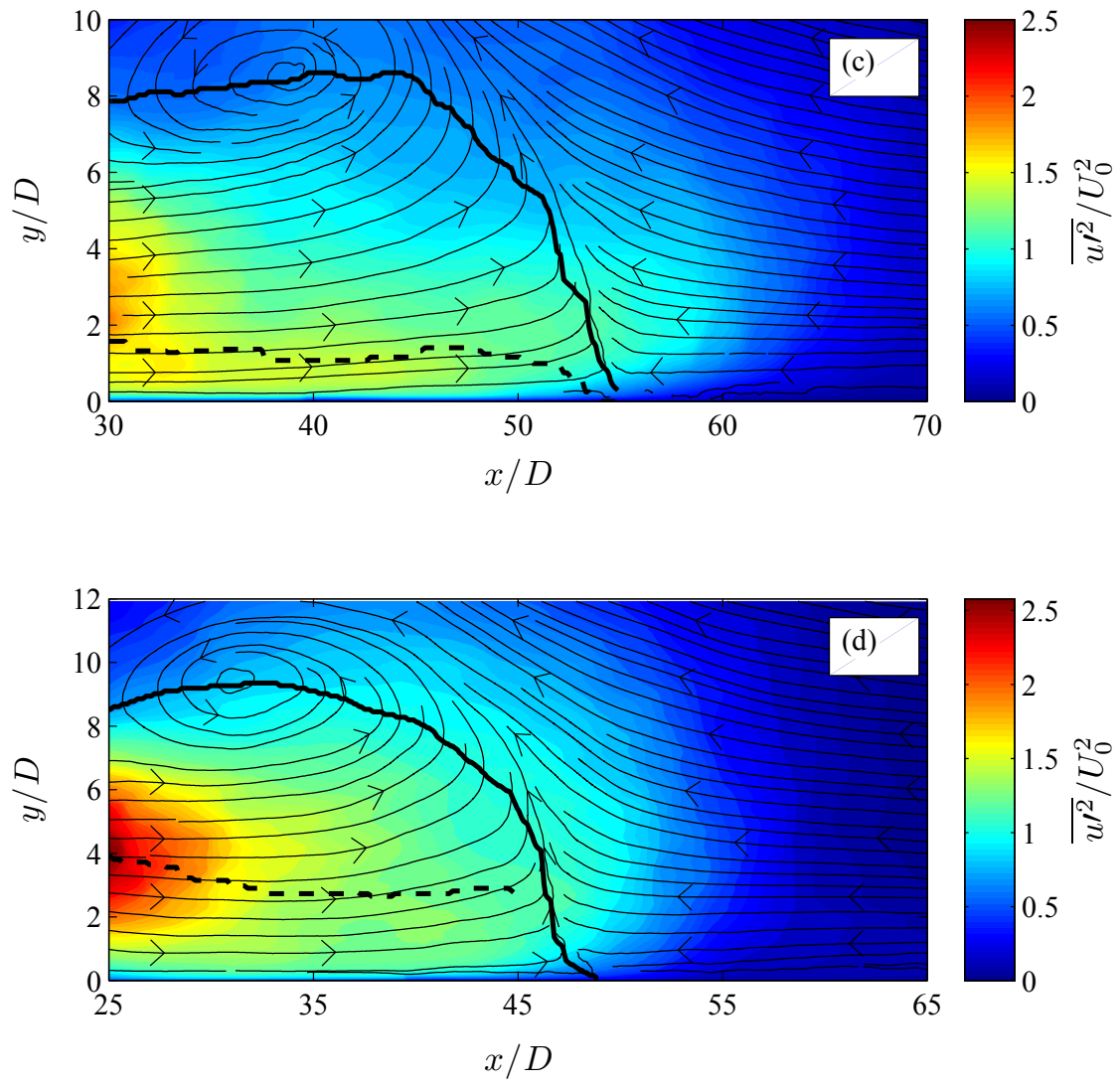
Figure 5-15: The normalized contours of streamwise Reynolds stress and mean flow streamlines. (a: offset ratio of 1.5, b: offset ratio of 2.5, c: offset ratio of 3.3, d: offset ratio of 4.3). Thick line and dashed line represent the height of zero axial velocity and maximum velocity.
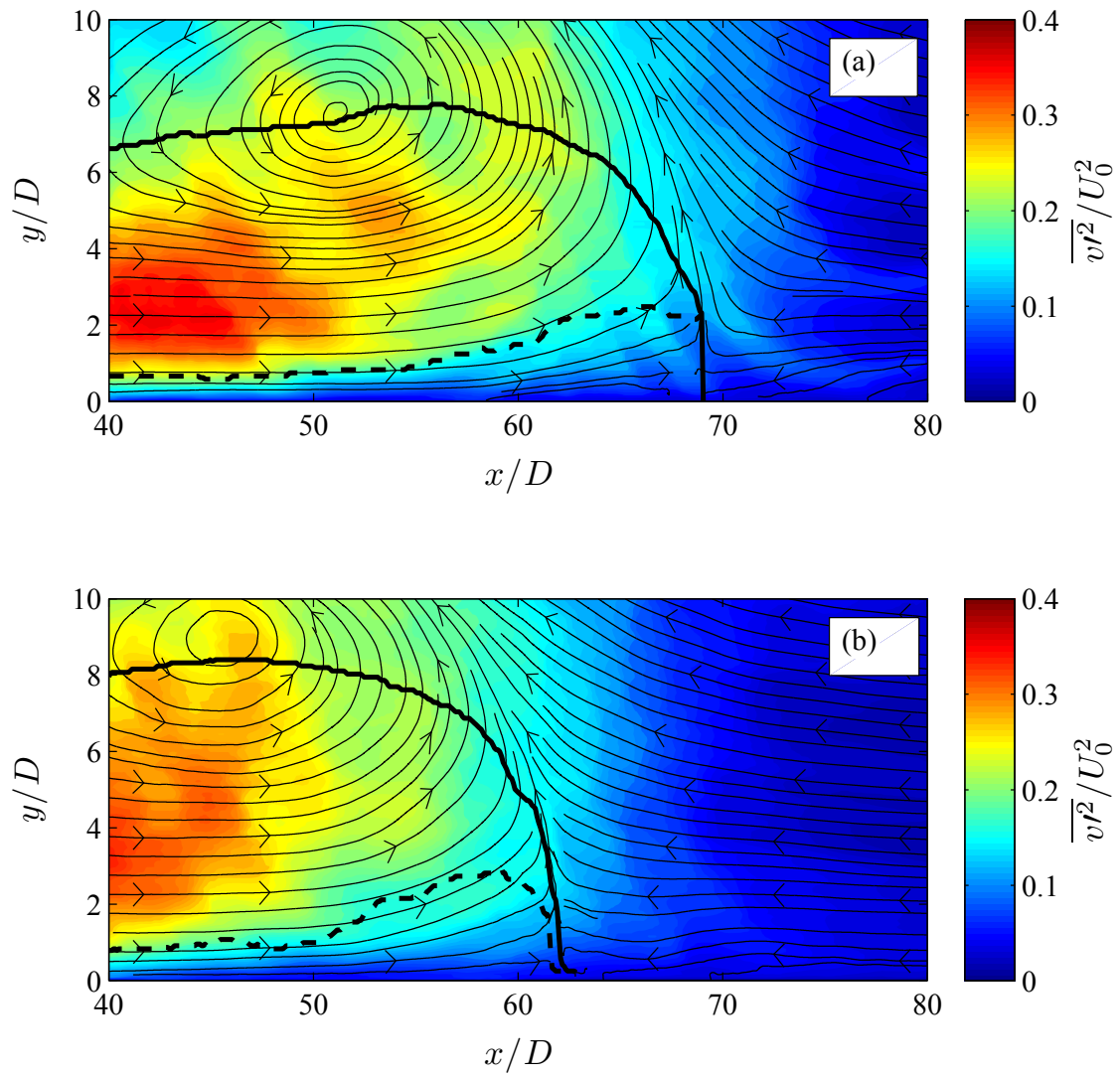
Figure 5-16 (a, b), for caption see facing page.
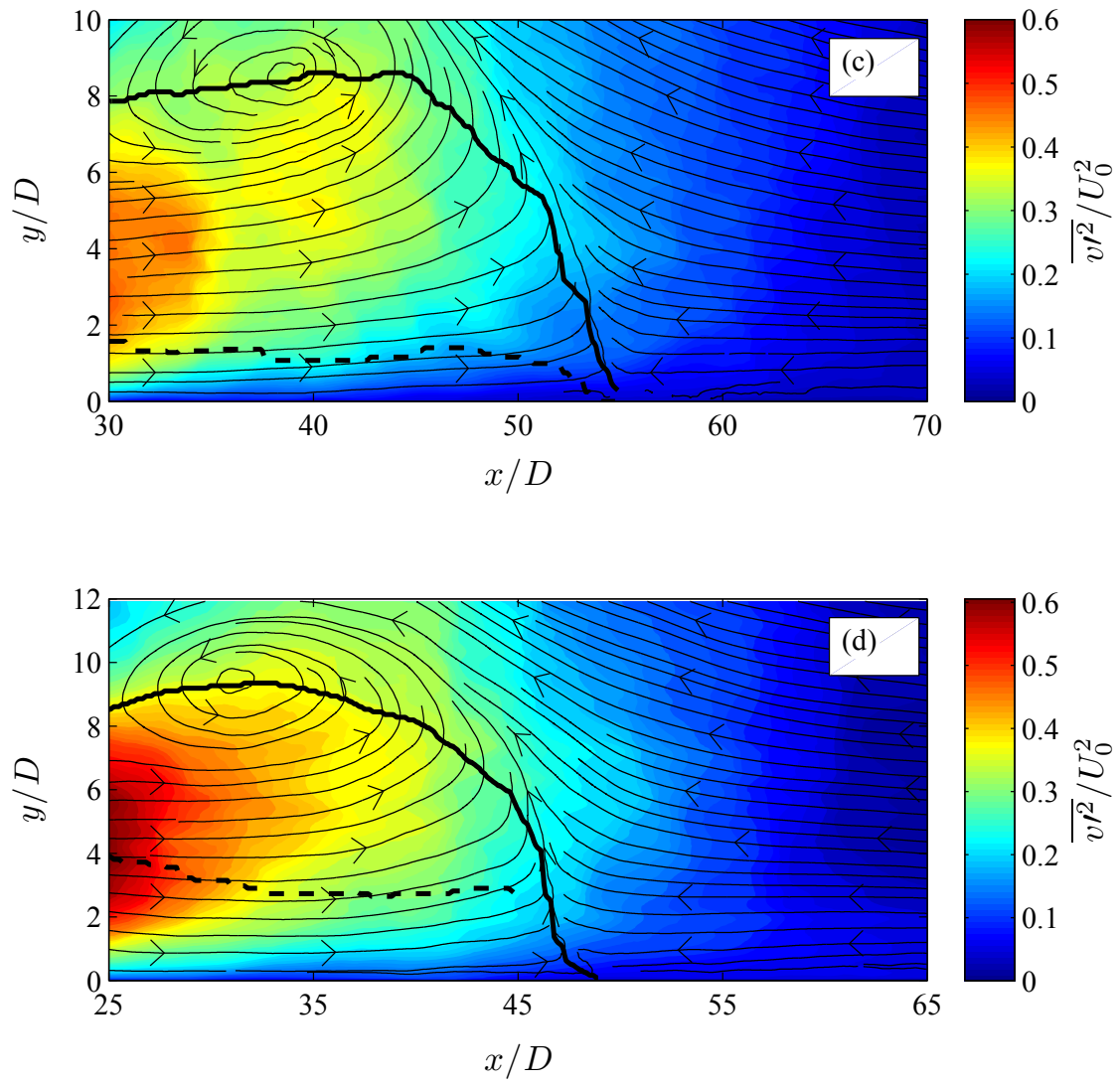
Figure 5-16: The normalized contours of wall normal Reynolds stress and mean flow streamlines. (a: offset ratio of 1.5, b: offset ratio of 2.5, c: offset ratio of 3.3, d: offset ratio of 4.3). Thick line and dashed line represent the height of zero axial velocity and maximum velocity.
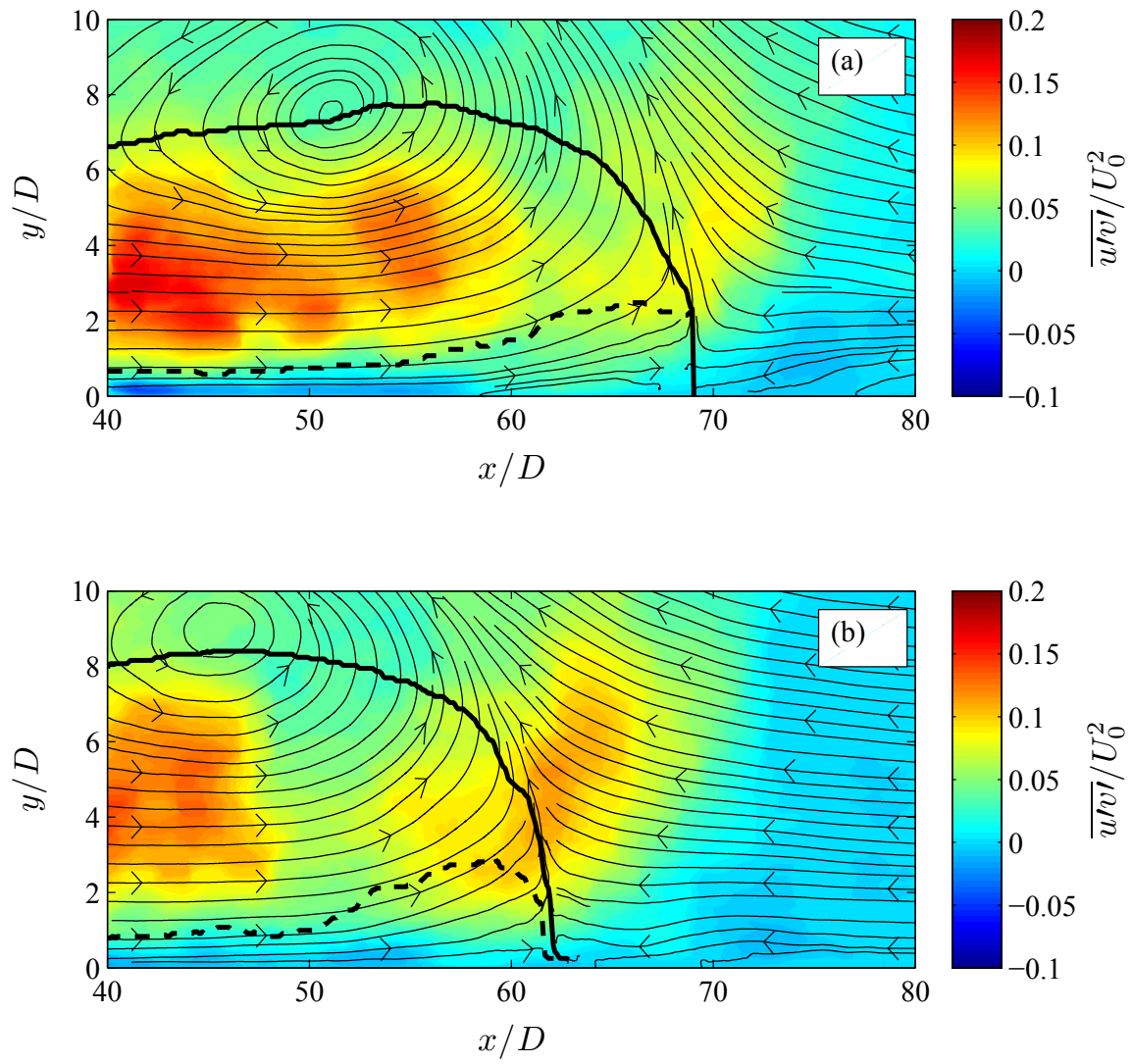
Figure 5-17 (a, b), for caption see facing page.
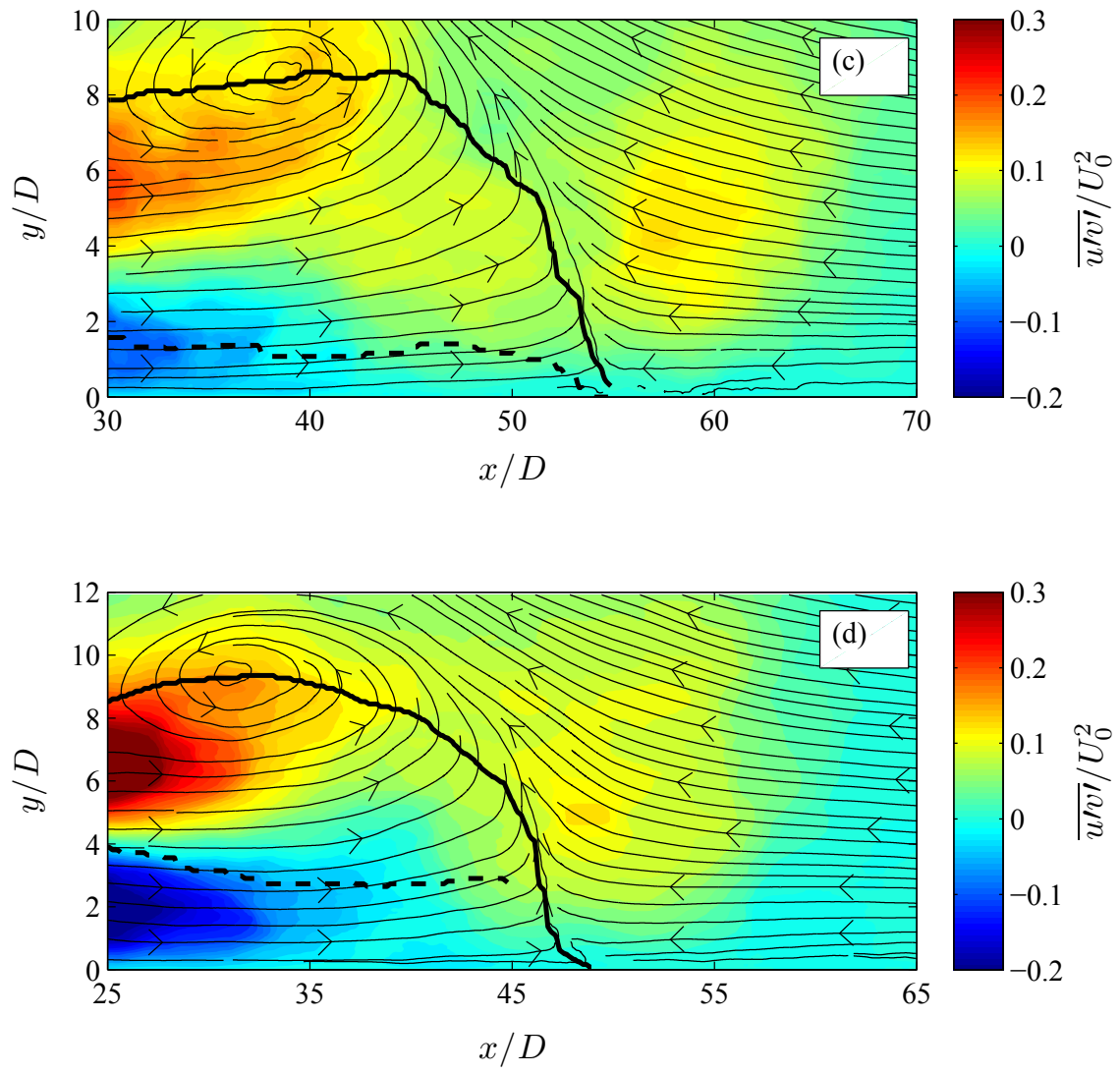
Figure 5-17: The normalized contours of Reynolds shear stress and mean flow streamlines. (a: offset ratio of 1.5, b: offset ratio of 2.5, c: offset ratio of 3.3, d: offset ratio of 4.3). Thick line and dashed line represent the height of zero axial velocity and maximum velocity.

153

Figure 5-18 shows the profiles of $\overline{u'^2}$ Reynolds stresses normalized with the jet local

maximum velocity (U_m) at several axial distances from the jet exit plane at U_R=17.5 and

offset ratios of 1.5 to 4.3. It is observed that for m=1.5 there is apparent self-similarity in

the range of 0.4<x/X_p<0.7. Beyond this range the profiles do not show a unique behavior

since the turbulent flow field is not fully established yet. Above x/X_p=0.7 the profiles

show very high values since the normalizing factor in the denominator (U_m) goes to zero

approaching the stagnation area (see for example the stress values for x/X_p=0.9 at Figure

5-18a). The streamwise Reynolds stress profiles at m=1.5 offset jet show two peaks at

$y/y_{1/2}$=0.2 and $y/y_{1/2}$=0.5. The first peak is larger and its value is around 0.25 which is

almost 30% larger than the value previously reported for a generic wall jet in counter-

flow [23]. The reason is generation of more turbulence in the flow as the jet offset

distance increases.

Figures 5-18b to 5-18c clearly show that as the offset ratio increases, the values of

streamwise Reynolds stresses rise dramatically. Moreover, the profiles completely lose

their self-similarity at higher offset ratios.

The stresses in the wall normal direction normalized with local maximum velocity are

shown in Figure 5-19. These profiles monotonically rise from zero at wall region and

show a maxima at $y/y_{1/2}$=0.7. For m=1.5, the data collapse on each other only for the

limited range of 0.4<x/X_p<0.6 (see Fig. 5-19a). As the offset distance increases, these

profiles show higher values and more deviation from each other. For instance at x/X_p=0.6

the maximum value of the wall normal Reynolds stress is $\overline{v'^2}/U_m^2 = 0.05$ when m=1.5

while this value for the case which offset ratio is 4.3 is equal to 0.2, showing 4 times growth.

The normalized profiles of Reynolds shear stresses $(\overline{u'v'}/U_m^2)$ are shown in Figure 5-20. At m=1.5, similar to the generic wall jet in counter-flow [23], the profiles begin from negative values of about -0.01 very close to the wall and change sign at around $y/y_{1/2}$=0.07. The maximum value of shear stresses is almost equal to 0.03 and happens at $y/y_{1/2}$=0.7. When the offset ratio is 2.5, because the jet needs more distance to reach to a developed wall jet, the shear stress profiles at the initial stage of the jet development $(x/X_p<0.5)$ shows a continuous decline and reaches -0.025 at $y/y_{1/2}$=0.25. Then it increases gradually to zero at $y/y_{1/2}$=0.5 and continues its rise toward $y/y_{1/2}$=1 and later it approaches to zero as the height increases. This is more visible at offset ratios of 3.3 and 4.3, see Figs. 5-20c and 5-20d. The increase in offset ratio enhances the magnitudes of shear stresses and the profiles do not reveal self-similarity. The turbulence fields do not reach to a fully developed situation and the local variables of the flow cannot represent a universal scaling of the flow.
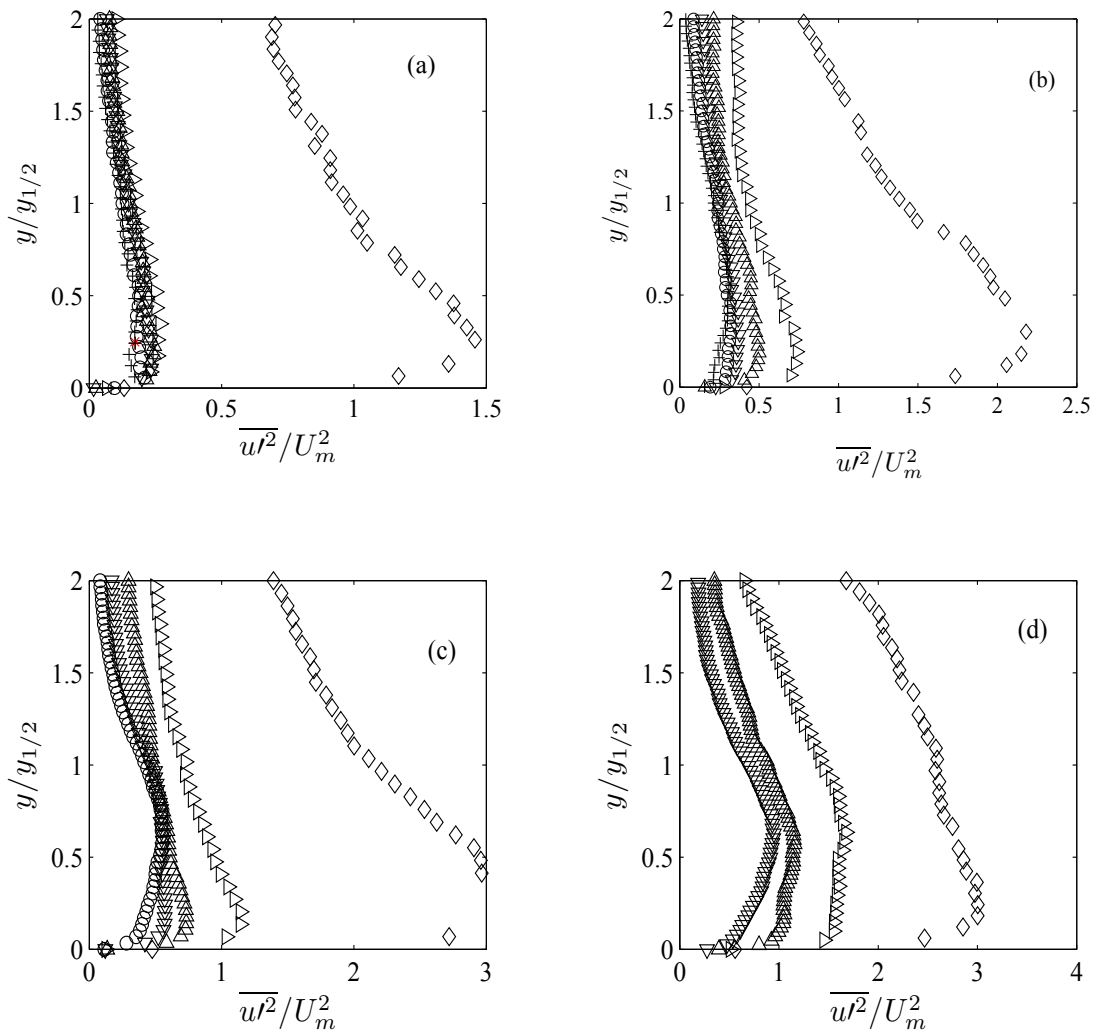
Figure 5-18: The normalized profiles of streamwise Reynolds stress (a: offset ratio of 1.5, b: offset ratio of 2.5, c: offset ratio of 3.3, d: offset ratio of 4.3). The symbols $+$, o, ∇,Δ, $\triangleright$,$\diamond$ represent x/X_p = 0.4 to 0.9 with steps equal to 0.1.
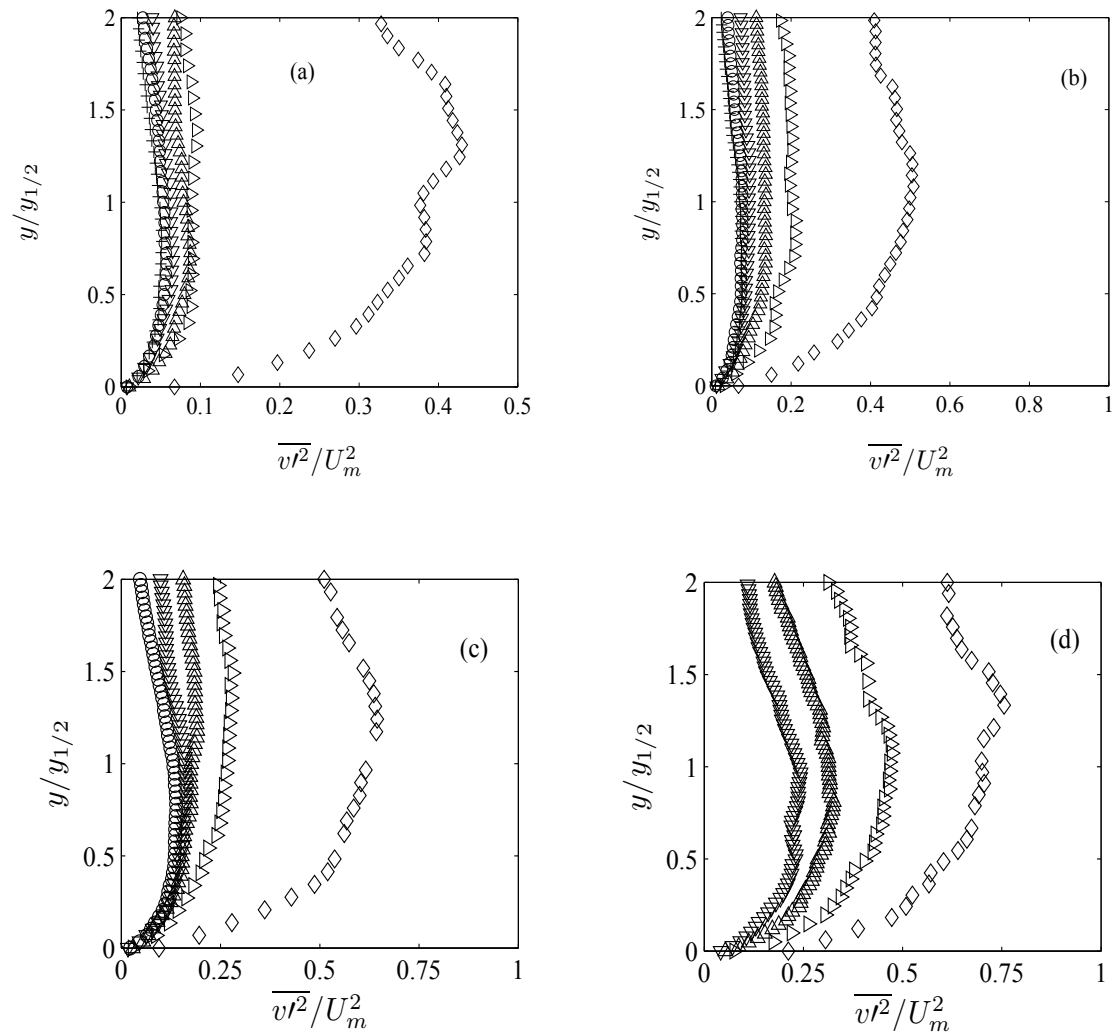
Figure 5-19: The normalized profiles of wall normal Reynolds stress (a: offset ratio of 1.5, b: offset ratio of 2.5, c: offset ratio of 3.3, d: offset ratio of 4.3). The symbols are similar to Fig. 5-18.
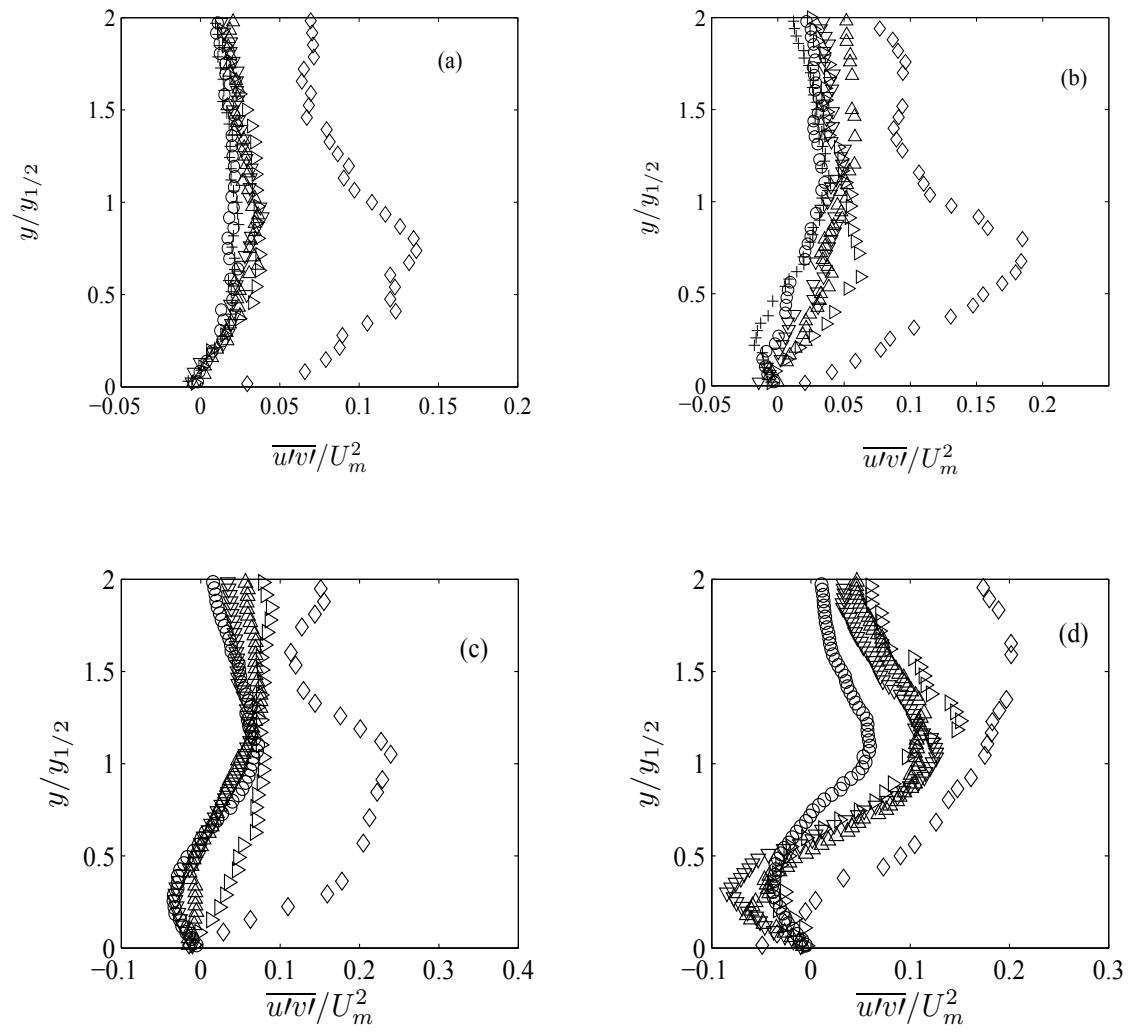
Figure 5-20: The normalized profiles of Reynolds shear stress (a: offset ratio of 1.5, b: offset ratio of 2.5, c: offset ratio of 3.3, d: offset ratio of 4.3). The symbols are similar to Fig. 5-18.

5.4   Summary

A series of experiments were conducted in a water channel to investigate the flow field of offset jets in a uniform counter-flow. The jet to counter-flow velocity ratio (U_R) was changed from 2.5 to 20. In addition, the jet offset distance from the side wall was varied in the range of 1.5 $<m<$ 4.3. The results revealed that:

1) All jets in counter-flow show a large recirculation region at the end of jet penetration that shows their high mixing capabilities. The jets show large amplitude random motions in both the axial and the wall normal direction and the amplitude of oscillation increases as the offset ratio increases (e.g. from $0.25X_p$ for m=1.5 to 0.5 X_p for m=4.3).

2) The penetration lengths of offset jets in counter-flow for U_R<7.5 are in between that of the wall jet and free jet flows in opposite ambient current. By increasing U_R, the penetration of 1.5m and 2.5m offset jets approach the penetration distance of a wall jet in counter-flow. The m=4.3 offset jet penetration gets closer to the penetration of free jet in counter-flow. The penetration of 3.3m offset jet remains in the middle of the penetration of wall jets and free jets in counter-flow.

3) The offset distance from the wall affects the amount of ambient flow entrainment to the jet, thus can change the penetration length of the jets in counter-flow. As the offset ratio increases, the counter-flow entrainment from the bottom side of the jet body increases.

4) The maximum velocity decay profiles demonstrate self-similarity for x/X_p> 0.15. Increasing the offset ratio increases the velocity decay rate. This is due to higher entrainment of the ambient flow into the jet as the offset ratio increases. Moreover,

increasing the jet offset distance causes a rise in the slope of the jets' half velocity width. The slopes of 1.5m and 2.5m offset jets are the same as the half width slope of a generic wall jet in counter-flow, but, for m=3.3 and m=4.3, the slope increases 12.5% and 50% compared to 0.04 slope for 1.5m and 2.5m offset jets.

5) The normalized velocity profiles of 1.5m offset jet show self-similarity in the range of 0.4$<x/X_p<$0.7, showing the characteristics of a wall jet velocity profile. For m=2.5, self-similarity of velocity profiles only exists for 0.6$<x/X_p<$0.7. When m=3.3 and m=4.3, no self-similarity was observed for velocity profiles and the velocity fields do not reveal the characteristics of the generic wall jets.

6) The interaction of the jet and counter-flow makes large scale vortical structures in the flow. In the stagnation zone the positive and negative vortices that are generated by the jet reach zero advection velocity, then roll back on each other and make large scale swirling regions. A portion of these structures return into the jet via entrainment and induce large velocity fluctuations in the flow that deviate the jet from its original path. This process makes large amplitude random oscillation of the jet in counter-flow.

7) As the jet offset distance increases, the auto correlation of velocity fluctuations becomes larger. It means that the turbulent structures of the flow become larger and gain more energy from the flow.

8) The velocity fluctuations show a local maxima at the stagnation region where the positive and negative vortices of the jet and counter-flow interact with each other. As the offset ratio increases the flow provides relatively uniform distribution of velocity fluctuations in the stagnation zone and the level of velocity fluctuations rises. Moreover,

the triple products of velocity fluctuations show higher values as the jet offset distance increases. This means that as the jets in counter-flow gets more distance from the sidewall, the turbulent transport in the flow field rises.

References

[1] Miozzi, M., F. Lalli, and G. P. Romano. "Experimental investigation of a free-surface turbulent jet with Coanda effect," Experiments in Fluids 49, no. 1 (2010): 341-353.

[2] NOZAKI, Tsutomu, Keiji HATTA, Masahiro NAKASHIMA, and Hirohisa MATSUMURA. "Reattachment flow issuing from a finite width nozzle." Bulletin of JSME 22, no. 165 (1979): 340-347.

[3] NOZAKI, Tsutomu, Keiji HATTA, Norihide SATO, and Hirohisa MATSUMURA. "Reattachment Flow Issuing from a Finite Width Nozzle: Report 2, Effects of Initial Turbulence Intensity." Bulletin of JSME 24, no. 188 (1981): 363-369.

[4] Pelfrey, J. R. R., and J. A. Liburdy. "Mean flow characteristics of a turbulent offset jet." *Journal of Fluids Engineering* 108, no. 1 (1986): 82-88.

[5] Pelfrey, J. R. R., and J. A. Liburdy. "Effect of curvature on the turbulence of a two-dimensional jet." Experiments in Fluids 4, no. 3 (1986): 143-149.

[6] Yoon, Soon Hyun, Kyung Chun Kim, DaeSeong Kim, and MyungKyoon Chung. "Comparative study of a turbulent wall-attaching offset jet and a plane wall jet." KSME Journal 7, no. 2 (1993): 101-112.

 [7] Nasr, A., and J. C. S. Lai. "A turbulent plane offset jet with small offset ratio." Experiments in Fluids 24, no. 1 (1998): 47-57.

[8] Nasr, A., and J. C. S. Lai. "Comparison of flow characteristics in the near field of two parallel plane jets and an offset plane jet." Physics of Fluids (1994-present) 9, no. 10 (1997): 2919-2931.

[9] Agelin-Chaab, M., and M. F. Tachie. "Characteristics of Turbulent Three-Dimensional Offset Jets." *Journal of Fluids Engineering* 133, no. 5 (2011): 051203.

[10] Agelin-Chaab, M., and M. F. Tachie. "Characteristics and structure of turbulent 3D offset jets." International Journal of Heat and Fluid Flow 32, no. 3 (2011): 608-620.

[11] Sekundov, A. N. "The propagation of a turbulent jet in an opposing stream." Turbulent jets of air, plasma and real gas (1969): 99-109.

[12] McDannel, M. D., P. R. Peterson, and G. S. Samuelsen. "Species concentration and temperature measurements in a lean, premixed flow stabilized by a reverse jet." Combustion Science and Technology 28, no. 5-6 (1982): 211-224.

[13] Peck, R.E. "Aerodynamics of a round jet in a counter-flowing wind," *Journal of Aircraft* 18, (1981): 61-62.

[14] Beltaos, S. and Rajaratnam, N. "Circular Turbulent Jet in an Opposing Infinite Stream." Proc. First Canadian Hydraulics Conference, Edmonton, AB, (1973): 220-237.

[15] Morgan, William D., Brian J. Brinkworth, and Gordon V. Evans. "Upstream penetration of an enclosed counterflowing jet." Industrial & Engineering Chemistry Fundamentals 15, no. 2 (1976): 125-127.

[16] Lam, K. M., and H. C. Chan. "Round jet in ambient counterflowing stream." *Journal of Hydraulic Engineering* 123, no. 10 (1997): 895-903.

[17] Chan, C. H. C., and K. M. Lam. "Centerline velocity decay of a circular jet in a counterflowing stream." Physics of Fluids 10, no. 3 (1998): 637-644.

[18] Tsunoda, H., and M. Saruta. "Planar laser-induced fluorescence study on the diffusion field of a round jet in a uniform counter-flow." *Journal of Turbulence* 4, no. 1 (2003): 1-12.

[19] Yoda, M., and H. E. Fiedler. "The round jet in a uniform counterflow: flow visualization and mean concentration measurements." Experiments in Fluids 21, no. 6 (1996): 427-436.

[20] Torres, Luis A., Mohammad Mahmoudi, Brian A. Fleck, David J. Wilson, and David Nobes. "Mean concentration field of a jet in a uniform counterflow." *Journal of Fluids Engineering* 134, no. 1 (2012): 014502.

[21] Balachandar, R., L. Robillard, and A. S. Ramamurthy. "Some characteristics of counter flowing wall jets." *Journal of Fluids Engineering* 114, no. 4 (1992): 554-558.

[22] Tanaka, E., Y. Inoue, and S. Yamashita. "An experimental study on the two-dimensional opposed wall jet in a turbulent boundary layer: Change in the flow pattern with velocity ratio." Experiments in Fluids 17, no. 4 (1994): 238-245.

[23] Mahmoudi, M., and Fleck, B. "Experimental measurement of the velocity field of round wall jet in counter-flow." to be published at the ASCE *journal of Hydraulic Engineering.*

[24] Mahmoudi, M., Nobes, D., and Fleck, B. "An experiment design for measuring the velocity field of a round wall jet in counter-flow." International Journal of Mechanical Engineering and Mechatronics, Vol. 2, (2014): 23-32.

[25] Verhoff, August. The Two-dimensional, Turbulent Wall Jet With and Without an External Free Stream. No. 626. PRINCETON UNIV NJ, 1963.

[26] Kline, S. J., and S. K. Robinson. "Quasi-coherent structures in the turbulent boundary layer. I-Status report on a community-wide summary of the data." Near-Wall Turbulence 1 (1990): 200-217.

[27] Adrian, R. J., K. T. Christensen, and Z-C. Liu. "Analysis and interpretation of instantaneous turbulent velocity fields." Experiments in Fluids 29, no. 3 (2000): 275-290.

[28] Chong, M. S., A. Eo Perry, and B. J. Cantwell. "A general classification of three dimensional flow fields." Physics of Fluids A: Fluid Dynamics (1989-1993) 2, no. 5 (1990): 765-777.

[29] Volino, R. J., M. P. Schultz, and K. A. Flack. "Turbulence structure in rough-and smooth-wall boundary layers." *Journal of Fluid Mechanics* 592 (2007): 263-293.

[30] Vollmers, Heinrich. "Detection of vortices and quantitative evaluation of their main parameters from experimental velocity data." Measurement Science and Technology 12, no. 8 (2001): 1199.

[31] Nakagawa, Shinji, and Thomas J. Hanratty. "Particle image velocimetry measurements of flow over a wavy wall." Physics of Fluids 13, no. 11 (2001): 3504-3507.

Chapter 6: Conclusion and recommendations

6.1   Conclusion

The velocity field of 3D round jets in counter-flow in the proximity of a solid wall were analyzed experimentally using PIV. The jet to counter-flow velocity ratio were changed from 2.5 to 25 and the jet offset ratio were set to five different values from 0.5 (generic wall jet) to 4.3. The study was focused on the penetration length, mean flow velocity and length scales, vortical structures in the flow, and the turbulence statistics. A summary of findings in this research is provided as:

1- In all jets in counter-flow situation, the jet penetrates into the ambient flow, loses its forward momentum and reaches to zero advection velocity. Then it returns back with the counter-flow. The jet shows large amplitude random oscillations in both axial and wall normal direction. The maximum amplitudes of oscillation ranges from 20% of mean penetration length for the case of generic wall jet to 50% of mean penetration length when the jet offset ratio is 4.3. The stream line patterns of the mean flow shows large recirculation region close to the jet stagnation zone.

2- The variation of the mean penetration length of the flush mounted jet in counter-flow versus jet to counter-flow velocity ratio has a power law relation in the form of:

$$X_p/D = 14U_R^{0.53}$$

3- The penetration length of the generic round wall jet configuration is larger than that of a free round jet in counter-flow and lower than the penetration of 2D slot wall jets with the same velocity ratio. The wall jet in counter-flow is more stable than a free jet in counter-flow since its interaction with the ambient flow is banned in the wall side. As a result, it is encountered with lower entrainment of negative momentum from the ambient and penetrates more than a free jet in counter-flow. Compare to a 2D slot wall jet, the 3D wall jets in counter-flow show lower penetration because of their momentum distribution in wall normal direction. For three dimensional wall jets wall normal momentum spreading is 5.5 times more than axial direction.

4- Offset jets in general have lower mean penetration in counter-flow compare to flush mounted wall jets. As the jet distance from the wall increases, its penetration approaches to that of a free jet in counter-flow. When the jet offset ratio increases, the jet random oscillation amplitudes rise. The jets attach to the side wall due to the Coanda effect if they could extend enough in the axial direction before reaching to stagnation. However, they separate from the wall easier than a generic wall jet due to their lower near wall momentum. In addition to ambient entrainment increase due to their higher random oscillations, the gap between the jet and the wall provides room for more counter-flow entrainment. It reduces the jets forward momentum faster. Therefore, their penetration decreases as the offset ratio increases.

However, this general trend is a function of velocity ratio as well. At high enough velocity ratios, the jet attachment to the side wall is strong and limits the jet oscillation

and counter-flow entrainment from the offset region. In this situation the penetration of the offset jet becomes almost equal to that of a flush mounted wall jet in counter-flow. At this study, for offset ratios of 1.5 and 2.5 the jet penetration became equal to the penetration of a generic wall jet in counter-flow at velocity ratios of U_R=7.5 and U_R=12.5, respectively.

5- Rising the offset ratio increases the jet velocity decay rate due to higher entrainment of the ambient flow into the jet. Moreover, the slope of the jets half velocity width increases as the jet gets more distance from the wall. For U_R>12.5, the slopes of 1.5m and 2.5m offset jets are the same as the half width slope of a generic wall jet in counter-flow. But, For m=3.3 and m=4.3, the slope shows 12.5% and 50% rise compare to that of the 1.5m and 2.5m offset jets.

6- The critical point analysis of the velocity gradient tensor revealed the dynamics of the vortical structures in the flow. In the stagnation zone the positive and negative vortices that generated by the jet reach to zero advection velocity. They roll back on each other, merge together and make a large scale swirling region. A portion of these structures return in the jet via entrainment process and induce large velocity fluctuations in the flow that deviate the jet from its original path. This process makes large amplitude random oscillation of the jet in counter-flow.

7- As the jet offset distance increases, the auto correlation of velocity fluctuations becomes larger. This shows that the turbulent structures of the flow become stronger and gain more energy from the flow.

8- In the stagnation region where the positive and negative vortices of the jet and counter-flow have higher interaction with each other, the Reynolds stresses increase and show a local maxima. As the offset ratio increases the flow provides relatively uniform contours of stress in the stagnation zone and the level of velocity fluctuations rise. Moreover, the triple products of velocity fluctuations show higher values as the jet offset distance increases. This indicates that as the jets in counter-flow gets more distance from the side wall, the turbulent transport in the flow field rises.

6.2 Recommendations for future works

The velocity fields of offset jets in counter-flow are analyzed using PIV in the two dimensional plane passing through the jet centerline. The jet penetration, dynamics of vortical structures and the turbulence fluctuation fields are studied. There are still many things remained to understand the detail physics of this complex flow. Here are some recommendations for future research studies:

1- To understand more details of the velocity field, quantizing the entrainment process, and analyzing the interaction of vortical structures on the flow, it is recommended that this flow be analyzed in full three-dimensional space using more advanced techniques such as time resolved 3D-PIV.

2- The velocity field of the offset jets can provide some information about the mixing characteristics of the offset jets in counter-flow. The details of jet mixing is still remained as an important problem. It is recommended that the same tests were done using PLIF for investigating the scalar field distribution of the offset jets in counter-flow.

3- The wall surface roughness can play an important role in the jet penetration. Experiments can be performed to analyze the effects of surface finishing.

4- The heat transfer rate of the flow to the side wall is an interesting problem with numerous industrial applications in designing more efficient heat exchangers and HVAC systems. It is recommended that an experimental study starts to analyze the impact of counter-flowing offset jets on the heat transfer to the adjacent surface. The effect of jet to counter-flow velocity ratio and offset distance in providing controlling mechanism for adjusting the amount of heat transfer can be an interesting research topic.

Appendix 1: Uncertainty analysis

Error is the difference between the true value of a parameter and its measured quantity. Since the exact amount of the parameter is not known and is actually the subject of the study, it is only possible to estimate the error. All measurement systems and experimental analysis are faced with different error sources. However, all sources of errors can be categorized as bias errors (E_b) and random errors (E_r). Bias errors or system errors are those uncertainties in the measurement system that depends on the physics of the sensor or the mathematical process that the sensor conduct to calculate the output. This type of uncertainty is called accuracy, and the manufacturer of the sensor provides formulas or graphs to help the user to estimate the amount of bias error in the sensor output. Random errors have usually unknown sources and can be associated to the noise in the environment and the process of data acquisition. Increasing the number of samples can reduce the random error. The random error associated with the mean value of a measured quantity with 95% confidence limit can be evaluated as (Bendat and Piersol, 1980):

$$E_r = \frac{2\sigma}{\sqrt{N}} \qquad (1)$$

where σ is the standard deviation of the measured quantity and N is number of samples. The standard deviation of the N measured samples of V_i can be found as:

$$\sigma = \sqrt{\frac{1}{N-1}\sum_{i=1}^{N}(V_i - \bar{V})^2} \qquad (2)$$

$\bar{P}$ is the mean value of the measured V quantities:

$$\bar{V} = \frac{\sum_{i=1}^{N} V_i}{N} \qquad (3)$$

When the amount of bias error and random error were evaluated, the total error (E_t) can

be estimated as:

$$E_t = \sqrt{E_b^2 + E_r^2} \qquad (4)$$

PIV error sources

PIV finds the velocity vector field in the flow based on the inherent definition of velocity

which is the ratio of displacement vector (ΔX) over time (Δt).

$$V = \frac{\Delta X}{\Delta t} \qquad (5)$$

The PIV hardware and software can control the time component with order of magnitude

better accuracy compared to the displacement vector. Therefore, the main source of error

in PIV relates to identifying the displacement vector of the group of particles in the flow.

The bias errors related to calculating the displacement vector are particle seed density,

particle image diameter, dynamic range issues, spatial resolution and the size and shape

of the interrogation region, and the numerical errors of the cross correlation algorithms.

Some of the sources of random errors in PIV are camera and other electronic noise, non-

uniform illumination by the laser, and non-uniform light reflection from particles

(Timmins, 2011).

Different researchers (e.g. Timmins et al. (2012), Wilson and Smith (2013), Lavoie et al.

(2007)) tried to find empirical relations for PIV bias error variation versus the

aforementioned uncertainty sources that expressed above. The major basis for their effort was to measure a well-known flow field by means of a mature experimental technique such as hot wire anemometry (HWA) and measuring the same flow field with PIV. Then they found PIV errors at different conditions by comparing the results of the two measuring techniques and assuming that HWA gives the true values of velocities. Although this method provides qualitative behavior of PIV uncertainty variation versus error sources, it cannot provide a universal error estimation procedure to be applied at any kind of flow field with different turbulence characteristics, different geometries and different boundary conditions. Especially when the real scenario can have multiple error sources acting together, provides a challenging situation that makes the estimation of PIV uncertainty impossible based on those empirical relations.

For instance, Lavoie et al. (2007) provided a semi-empirical method to quantify the effects of finite spatial resolution of PIV measurements and proposed some correction methods for turbulent dissipation, structure functions, and turbulent kinetic energy. They studied grid turbulence flow since there are theoretical modelings available for these isotropic and homogeneous turbulent flows. They used wind tunnel testing, deployed a grid made of woven wires with diameter of 1.2 mm, and conduct their experiments at a Reynolds number of 3000 based on the mesh size and the free stream velocity. 1000 PIV images were recorded for their research. In addition, data from HWA were used in parallel with PIV to compare the PIV output with the HWA results. They provided empirical relations and graphs to correct PIV results based on HWA.

In this research the velocity profiles of the three-dimensional wall jet in quiescent flow is measured and compared with the widely accepted wall jet velocity profile reported by

Verhoff (1963). In Figure 1, the triangles show the experimental data for the wall jet at

Rej = 10,000 and at x/D = 40 and the thick line shows the Verhoff profile. As it is seen

from Fig. 1, the difference between the results of the experiment and the true value of

velocities is as low as 2%. Therefore, the bias error in the PIV measurement system that

is used in this research is estimated to be at the maximum level of 2%.
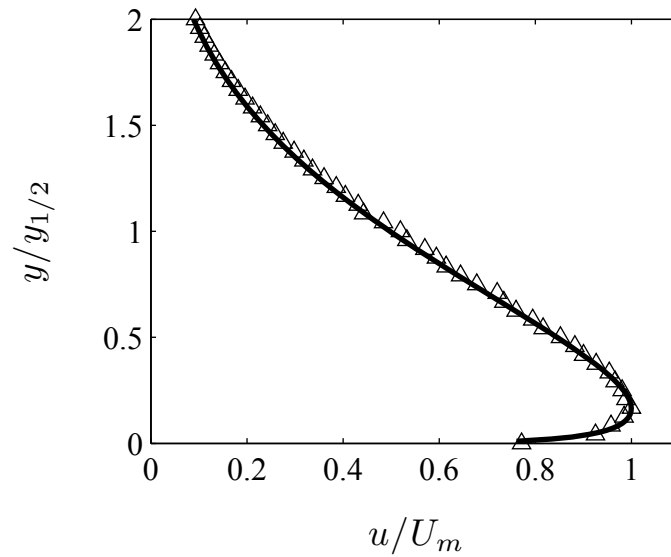
Figure 1: Comparison of experimental data and the Verhoff (1963) velocity profile for wall jet.

Some samples of error bar distribution for the reported parameters in this study are shown

in the original text. Both the bias error and random error are imposed to the measured

velocity profiles and the error bars based on 95% confidence limits are evaluated and

showed at each point.

References

Abrahamsson, H., Johansson, B., and Lofdahl L. "The turbulence field of a fully developed three dimensional wall jet. "*Internal Rep. No. 97/1*, Department of Thermo and Fluid Dynamics, Chalmers Univ. of Tech., Goteborg, Sweden (1997).

Adrian, R. J., K. T. Christensen, and Z-C. Liu. "Analysis and interpretation of instantaneous turbulent velocity fields." Experiments in Fluids 29, no. 3 (2000): 275-290.

Agelin-Chaab, M., and M. F. Tachie. "Characteristics and structure of turbulent 3D offset jets." International Journal of Heat and Fluid Flow 32, no. 3 (2011): 608-620.

Agelin-Chaab, M., and M. F. Tachie. "Characteristics of Turbulent Three-Dimensional Offset Jets." *Journal of Fluids Engineering* 133, no. 5 (2011): 051203.

Agelin-Chaab, M., and M. F. Tachie. "Characteristics of Turbulent Three-Dimensional Wall Jets." *Journal of Fluids Engineering* 133, no. 2 (2011): 021201.

Agelin-Chaab, Martin. "Experimental study of three-dimensional offset jets and wall jets." PhD diss., University of Manitoba, 2010.

Arendt, J., H. A. Babcock, and J. C. Schuster. "Penetration of a jet into counter-flow." Proc. ASCE Journal 82 (1956): 8-11.

Balachandar, R., L. Robillard, and A. S. Ramamurthy. "Some characteristics of counter flowing wall jets." *Journal of Fluids Engineering* 114, no. 4 (1992): 554-558.

Beltaos, S. and Rajaratnam, N. "Circular Turbulent Jet in an Opposing Infinite Stream." Proc. First Canadian Hydraulics Conference, Edmonton, AB, (1973): 220-237.

Bendat, Julius S., and Allan G. Piersol. "Engineering applications of correlation and spectral analysis." New York, Wiley-Interscience, 1980. 315 p. 1 (1980).

Bernero, S., and H. E. Fiedler. "Application of particle image velocimetry and proper orthogonal decomposition to the study of a jet in a counter-flow." Experiments in Fluids 29, no. 1 (2000): S274-S281.

Bernero, S., and H. E. Fiedler. "Experimental investigations of a jet in counter-flow." In Advances in Turbulence VII, pp. 35-38. Springer Netherlands, 1998.

Bernero, Stefano, and Heinrich E. Fiedler. "Simultaneous PIV and LIF experiments on a round jet in counter-flow." In Proc. 1st Int. Symp. on Turbulence and Shear Flow Phenomena (Santa Barbara), pp. 1053-8. 1999.

Chan, C. H. C., and K. M. Lam. "Centerline velocity decay of a circular jet in a counter-flowing stream." Physics of Fluids 10, no. 3 (1998): 637-644.

Chong, M. S., A. Eo Perry, and B. J. Cantwell. "A general classification of three dimensional flow fields." Physics of Fluids A: Fluid Dynamics (1989-1993) 2, no. 5 (1990): 765-777.

Christensen, Kenneth T., and Yanhua Wu. "Characterization of vortex organization in the outer layer of wall turbulence." Proc. Fourth Intl Symp. On Turbulence and Shear Flow Phenomena, Williamsburg, Virginia, vol. 3, 1025-1030.

Christensen, Kenneth T., and Yanhua Wu. "Visualization and characterization of small-scale spanwise vortices in turbulent channel flow." *Journal of Visualization* 8, no. 2 (2005): 177-185.

Craft, T. J., and B. E. Launder. "On the spreading mechanism of the three-dimensional turbulent wall jet." *Journal of Fluid Mechanics* 435 (2001): 305-326.

Davis, M. R., and H. Winarto. "Jet diffusion from a circular nozzle above a solid plane." *Journal of Fluid Mechanics* 101, no. 01 (1980): 201-221.

E. Fillippi."La stabilizzazion della fiamma degliesorettori," L'aerotecnica, No. 1, (1958). Eriksson, J. G., R. I. Karlsson, and J. Persson. "An experimental study of a two-dimensional plane turbulent wall jet." Experiments in Fluids 25, no. 1 (1998): 50-60.

Fujisawa, Nobuyuki, and Hiroyuki Shirai. "Mean flow and turbulence characteristics of three-dimensional wall jet along plane surface." Japan Society of Aeronautical Space Sciences Transactions 32 (1989): 35-46.

Gad-el-Hak, M. "Flow Control: Passive, active and reactive flow management, 2000."

George, William K., Hans Abrahamsson, Jan Eriksson, Rolf I. Karlsson, Lennart Löfdahl, and Martin Wosnik. "A similarity theory for the turbulent plane wall jet without external stream." *Journal of Fluid Mechanics* 425 (2000): 367-411.

Han, G., M. De Zhou, and I. Wygnanski. "On streamwise vortices and their role in the development of a curved wall jet." Physics of Fluids (1994-present) 18, no. 9 (2006): 095104.

Kaplan, Wilfred. Ordinary Differential Equations. Reading, MA: Addison-Wesley, 1952.

Kline, S. J., and S. K. Robinson. "Quasi-coherent structures in the turbulent boundary layer. I-Status report on a community-wide summary of the data." Near-Wall Turbulence 1 (1990).

Konig, O. and Fiedler, H. E., 1991, "The Structure of Round Turbulent Jets in Counter-Flow: a Flow Visualization Study," Advances in turbulence 3, pp. 61-66.

Lam, K. M., and C. H. C. Chan. "Time-averaged mixing behavior of circular jet in counter-flow: Velocity and concentration measurements." *Journal of Hydraulic Engineering* 128, no. 9 (2002): 861-865.

Lam, K. M., and H. C. Chan. "Investigation of turbulent jets issuing into a counter-flowing stream using digital image processing." Experiments in Fluids 18, no. 3 (1995): 210-212.

Lam, K. M., and H. C. Chan. "Round jet in ambient counter-flowing stream." *Journal of Hydraulic Engineering* 123, no. 10 (1997): 895-903.

Lander, B. E., and Rodi, W., 1983, "The turbulent wall jet- Measurement and modeling," Ann. Rev. Fluid mech., 15, pp. 429-459.

Launder, B. E., and W. Rodi. "The turbulent wall jet." Progress in Aerospace Sciences 19 (1979): 81-128.

Lavoie, P., G. Avallone, F. De Gregorio, G. P. Romano, and R. A. Antonia. "Spatial resolution of PIV for the measurement of turbulence." Experiments in Fluids 43, no. 1 (2007): 39-51.

Law, Adrian Wing-Keung, and Herlina. "An experimental study on turbulent circular wall jets." *Journal of Hydraulic Engineering* 128, no. 2 (2002): 161-174.

Mahmoudi, M., and Fleck, B. "Experimental measurement of the velocity field of round wall jet in counter-flow." to be published at the ASCE *Journal of Hydraulic Engineering.*

Mahmoudi, M., Nobes, D., and Fleck, B. "An experiment design for measuring the velocity field of a round wall jet in counter-flow." International Journal of Mechanical Engineering and Mechatronics, Vol. 2, (2014): 23-32.

Mathieu, Jean, and Julian Scott. An introduction to turbulent flow. Cambridge University Press, 2000.

McDannel, M. D., P. R. Peterson, and G. S. Samuelsen. "Species concentration and temperature measurements in a lean, premixed flow stabilized by a reverse jet." Combustion Science and Technology 28, no. 5-6 (1982): 211-224.

Miozzi, M., F. Lalli, and G. P. Romano. "Experimental investigation of a free-surface turbulent jet with Coanda effect." Experiments in Fluids 49, no. 1 (2010): 341-353.

Morgan, William D., Brian J. Brinkworth, and Gordon V. Evans. "Upstream penetration of an enclosed counter-flowing jet." Industrial & Engineering Chemistry Fundamentals 15, no. 2 (1976): 125-127.

Nasr, A., and J. C. S. Lai. "A turbulent plane offset jet with small offset ratio." Experiments in Fluids 24, no. 1 (1998): 47-57.

Nasr, A., and J. C. S. Lai. "Comparison of flow characteristics in the near field of two parallel plane jets and an offset plane jet." Physics of Fluids (1994-present) 9, no. 10 (1997): 2919-2931.

NOZAKI, Tsutomu, Keiji HATTA, Masahiro NAKASHIMA, and Hirohisa MATSUMURA. "Reattachment flow issuing from a finite width nozzle." Bulletin of JSME 22, no. 165 (1979): 340-347.

NOZAKI, Tsutomu, Keiji HATTA, Norihide SATO, and Hirohisa MATSUMURA. "Reattachment Flow Issuing from a Finite Width Nozzle: Report 2, Effects of Initial Turbulence Intensity." Bulletin of JSME 24, no. 188 (1981): 363-369.

Or, C.M., Lam, K.M., Liu, P., (2011). "Potential core lengths of round jets in stagnant and moving environments" *Journal of Hydro-Environment Research* 5, pp. 81-91.

Padmanabham, G., and BH Lakshmana Gowda. "Mean and turbulence characteristics of a class of three-dimensional wall jets—part 1: mean flow characteristics." *Journal of Fluids Engineering* 113, no. 4 (1991): 620-628.

Peck, R.E. "Aerodynamics of a round jet in a counter-flowing wind," *Journal of Aircraft* 18, (1981): 61-62.

Pelfrey, J. R. R., and J. A. Liburdy. "Effect of curvature on the turbulence of a two-dimensional jet." Experiments in Fluids 4, no. 3 (1986): 143-149.

Pelfrey, J. R. R., and J. A. Liburdy. "Mean flow characteristics of a turbulent offset jet." *Journal of fluids engineering* 108, no. 1 (1986): 82-88.

Raffel, M., Willert, C. E. and Kompenhaus, J., "Particle Image Velocimetry: A Practical Guide," Springer Verlag, 1998.

Saghravani, S. F., and A. S. Ramamurthy. "Penetration length of confined counter flowing free jets." *Journal of Hydraulic Engineering* 136, no. 3 (2010): 179-182.

Schilichting, H., "Boundary Layer Theory," McGraw-Hill, 4th edition, 1962.

Sekundov, A. N. "The propagation of a turbulent jet in an opposing stream." Turbulent jets of air, plasma and real gas (1969): 99-109.

Shang, J.S., 2002, "Validation of plasma injection for hypersonic blunt-body drag reduction," RTO AVT symposium on reduction of military vehicle acquisition time and cost through advanced modeling and virtual simulation, Paris, France, April 22-25.

Sun, H. "Development of three-dimensional turbulent wall jet. " PhD thesis, McMaster University, Hamilton, Canada. (2002).

Tachie, M., R. Balachandar, and D. Bergstrom. "Scaling the inner region of turbulent plane wall jets." Experiments in Fluids 33, no. 2 (2002): 351-354.

Tanaka, E., Y. Inoue, and S. Yamashita. "An experimental study on the two-dimensional opposed wall jet in a turbulent boundary layer: Change in the flow pattern with velocity ratio." Experiments in Fluids 17, no. 4 (1994): 238-245.

Timmins, Benjamin H., Brandon W. Wilson, Barton L. Smith, and Pavlos P. Vlachos. "A method for automatic estimation of instantaneous local uncertainty in particle image velocimetry measurements." Experiments in Fluids 53, no. 4 (2012): 1133-1147.

Torres, Luis A., Mohammad Mahmoudi, Brian A. Fleck, David J. Wilson, and David Nobes. "Mean concentration field of a jet in a uniform counter-flow." *Journal of Fluids Engineering* 134, no. 1 (2012): 014502.

Tsunoda, H., and M. Saruta. "Planar laser-induced fluorescence study on the diffusion field of a round jet in a uniform counter-flow." *Journal of Turbulence* 4, no. 1 (2003): 1-12.

Tsunoda, Hiroyuki, and Jun-Ichi Takei. "Statistical characteristics of the cross-sectional concentration field in a round counter jet." *Journal of Fluid Science and Technology* 1, no. 2 (2006): 105-113.

Verhoff, A., 1963, "The two-dimensional turbulent wall jet with and without an external stream," Rep. No. 626, Princeton University, Princeton, N.J.

Volchkov, E. P., V. P. Lebedev, M. I. Nizovtsev, and V. I. Terekhov. "Heat transfer in a channel with a counter-current wall jet injection." International journal of heat and mass transfer 38, no. 14 (1995): 2677-2687.

Volino, R. J., M. P. Schultz, and K. A. Flack. "Turbulence structure in rough-and smooth-wall boundary layers." *Journal of Fluid Mechanics* 592 (2007): 263-293.

Vollmers, Heinrich. "Detection of vortices and quantitative evaluation of their main parameters from experimental velocity data." Measurement Science and Technology 12, no. 8 (2001): 1199.

Wake, Brian E., Gregory Tillman, Stuart S. Ochs, and J. Scott Kearney. "Control of high-reynolds-number turbulent boundary layer separation using counter-flow fluid injection." In 3rd AIAA Flow Control Conference. 2006.

Wilson, Brandon M., and Barton L. Smith. "Uncertainty on PIV mean and fluctuating velocity due to bias and random errors." Measurement Science and Technology 24, no. 3 (2013): 035302.

Yoda, M., and H. E. Fiedler. "The round jet in a uniform counter-flow: flow visualization and mean concentration measurements." Experiments in Fluids 21, no. 6 (1996): 427-436.

Yoon, S. H., K. C. Kim, D. S. Kim, and M. K. Chung. "Effect of surface roughness on a turbulent wall-attaching offset jet." Experiments in Fluids 19, no. 1 (1995): 38-42.

Yoon, Soon Hyun, Kyung Chun Kim, DaeSeong Kim, and Myung Kyoon Chung. "Comparative study of a turbulent wall-attaching offset jet and a plane wall jet." KSME Journal 7, no. 2 (1993): 101-112.